Karlsruhe Institute of Technology

imec

Physikalisches Institut

Coherent Two-Qubit Control in Industrial Si/SiGe Spin Qubits

Viktor Adam, AG Wernsdorfer, Team Semiconductor

01 July 2025

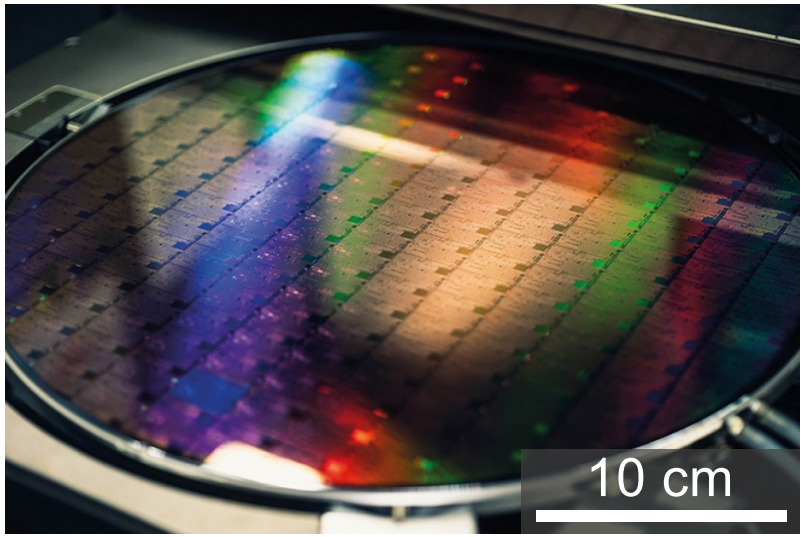

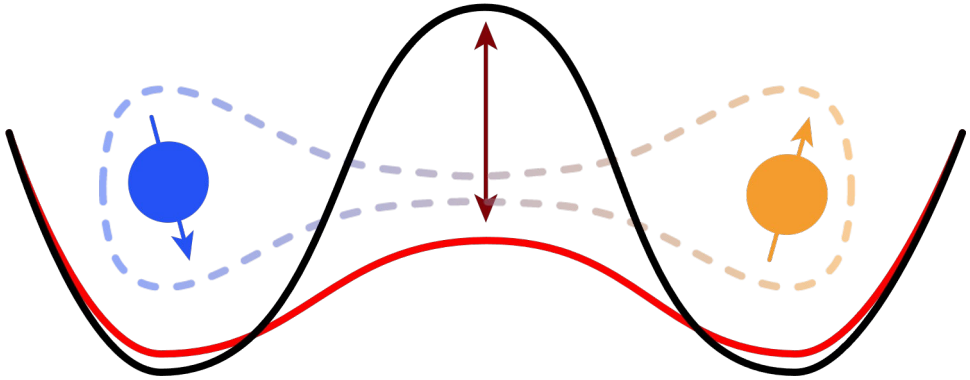

From MOSFET to spin qubit

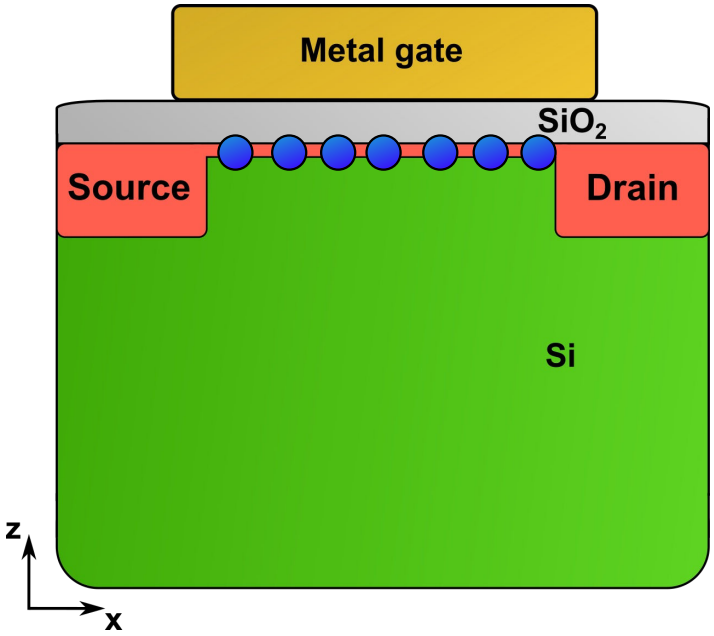

From MOSFET to spin qubit

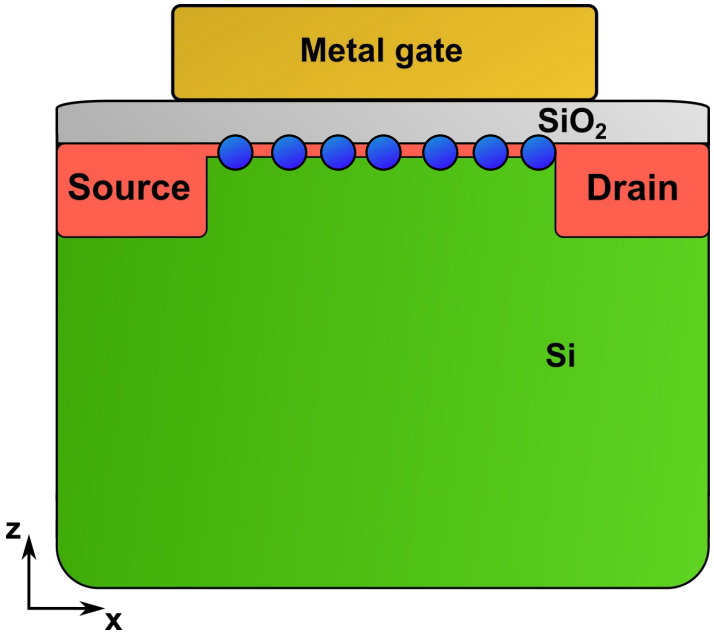

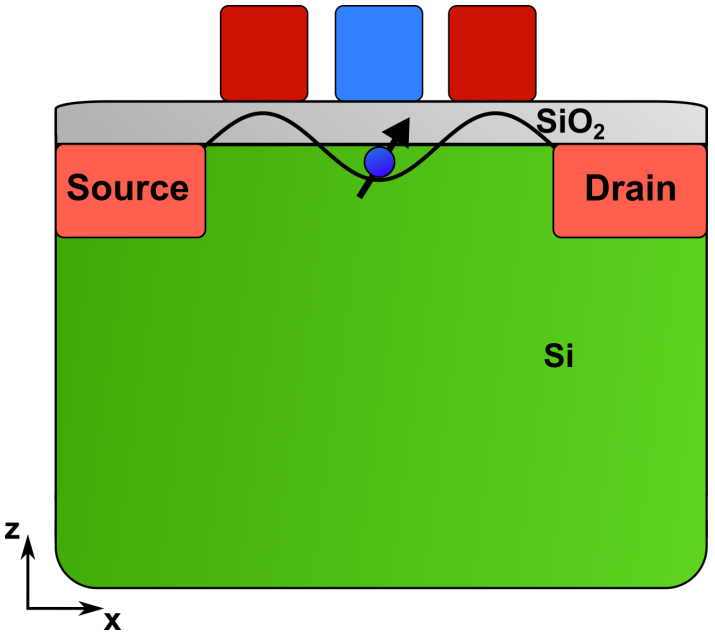

Loss-DiVincenzo qubit (1998)

Spin Qubit

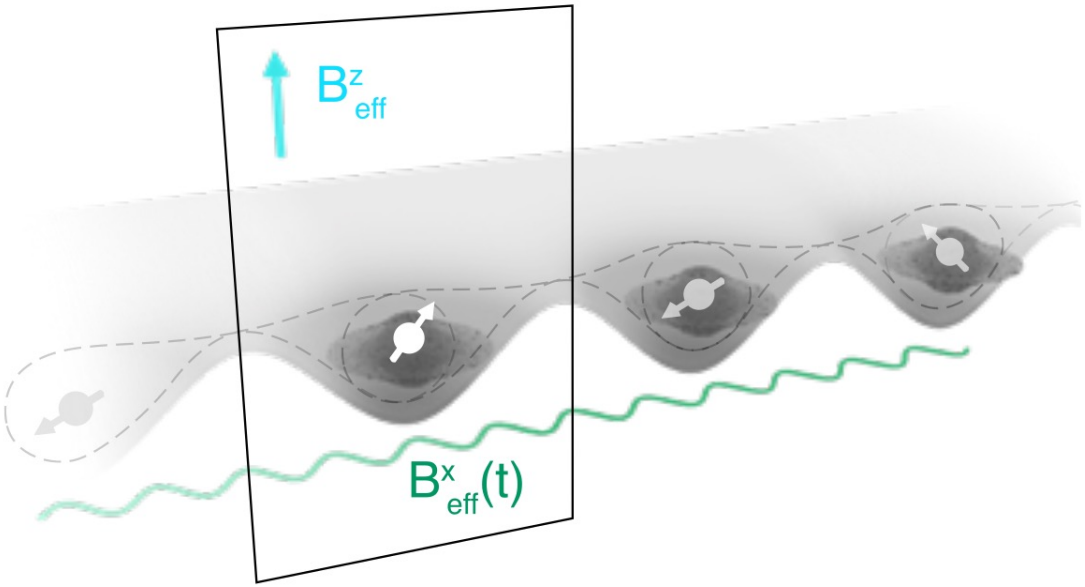

Bloch Sphere

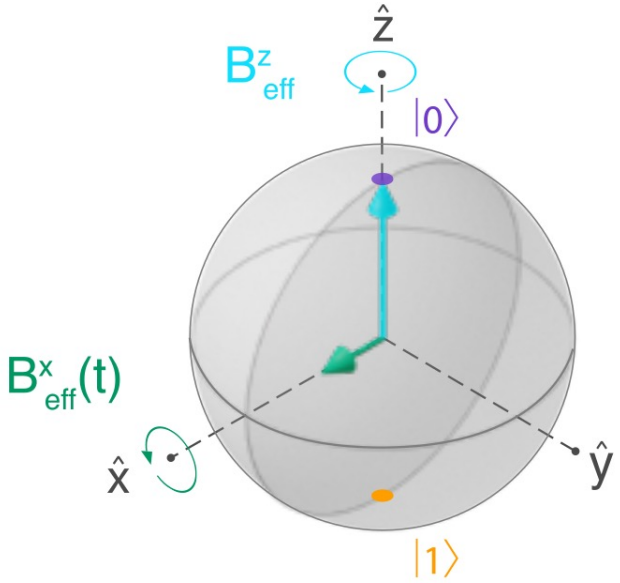

Loss and DiVincenzo, *Phys. Rev. A 57* (1998)

Loss-DiVincenzo qubit (1998)

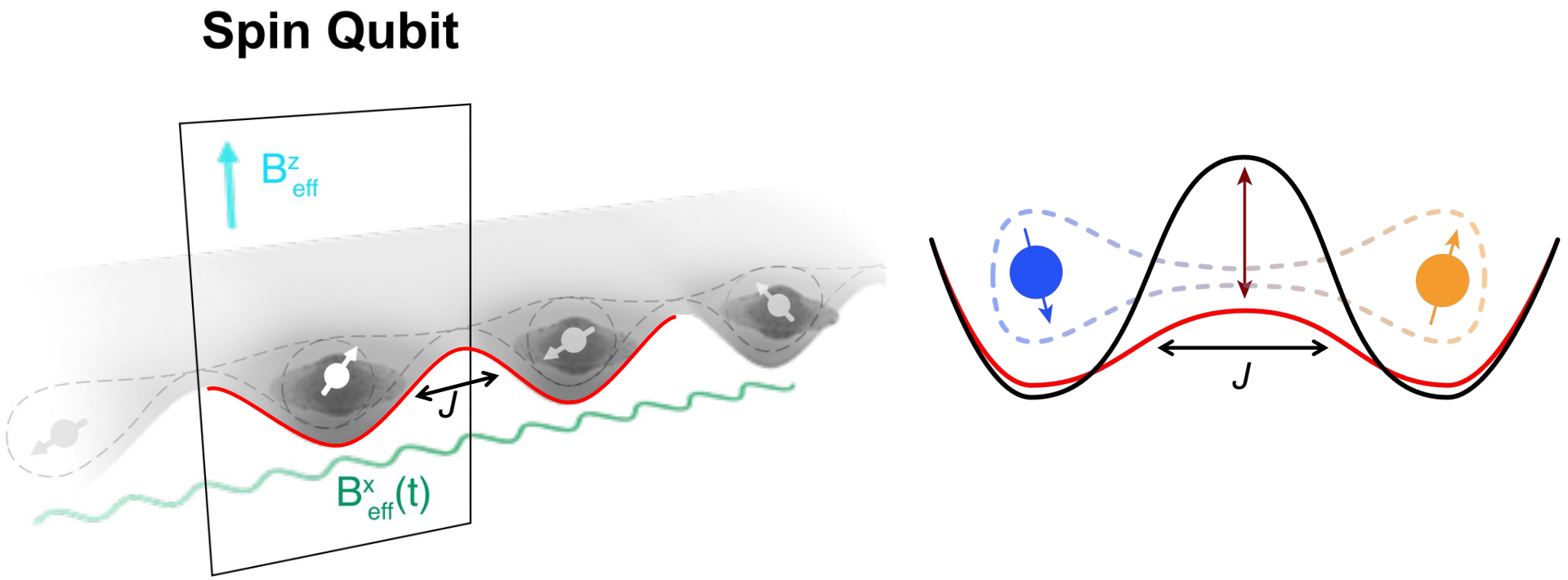

Loss and DiVincenzo, *Phys. Rev. A 57* (1998)

Large scale architecture

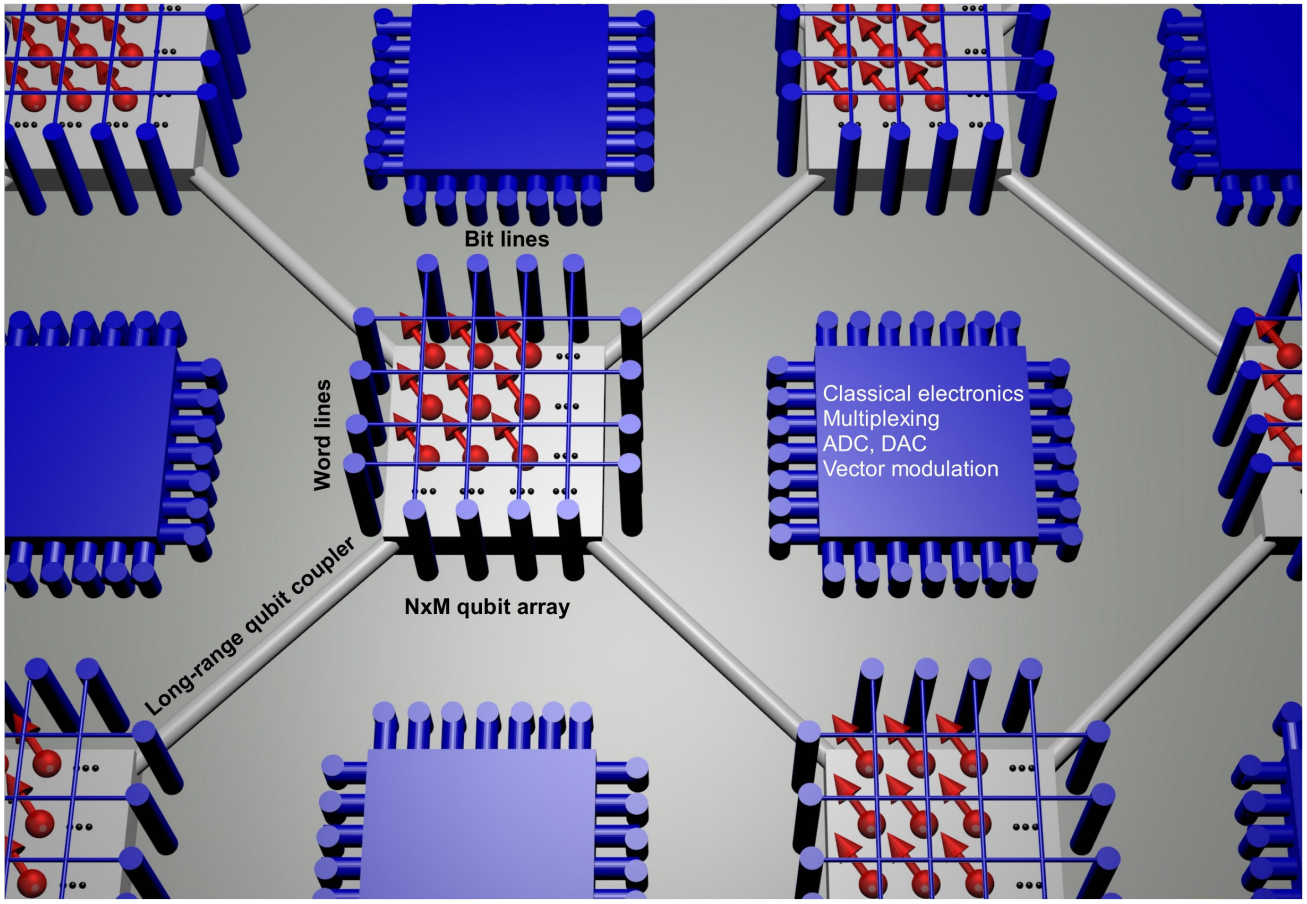

Universal quantum computer

Coupled qubit arrays

Long range coupler

Classical electronics

Vandersypen *et al., npj Quantum Inf* 3 (2017)

Large scale architecture

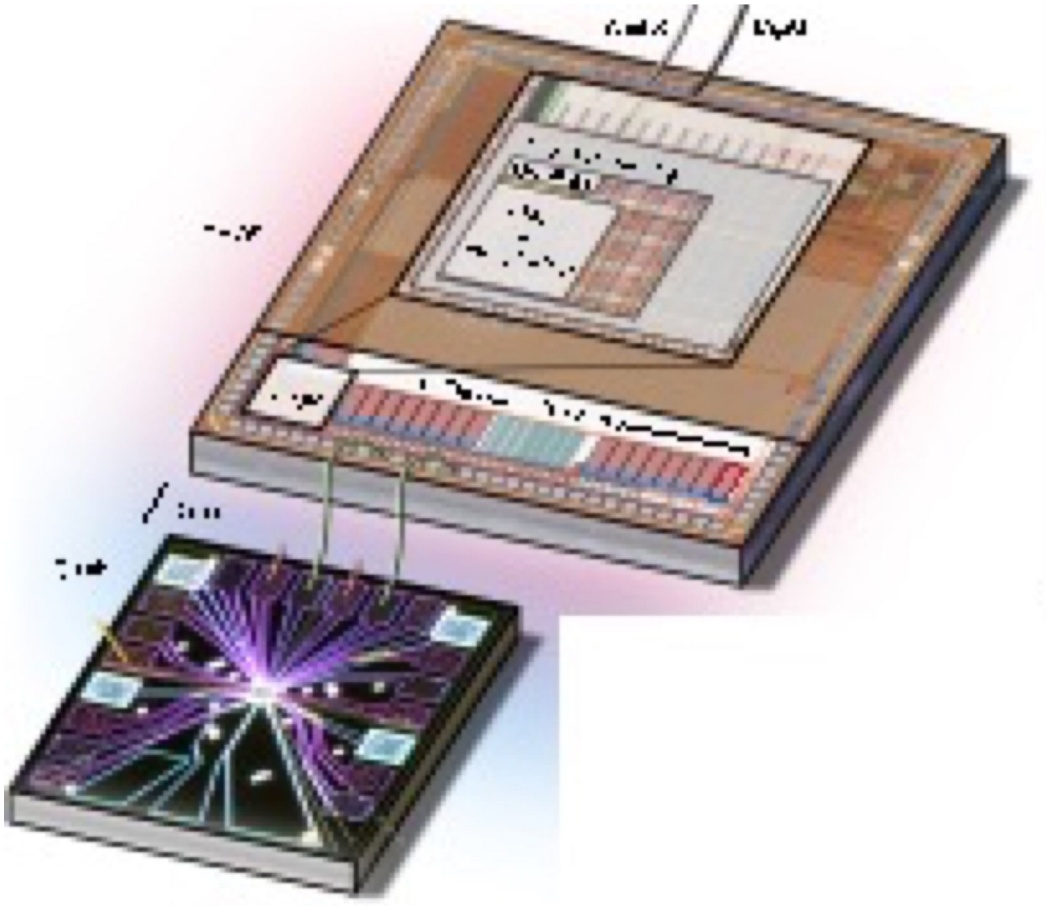

Bartee *et al., Nature* (2025)

Universal quantum computer

Coupled qubit arrays

Long range coupler

Classical electronics

Large scale architecture

Superconducting links

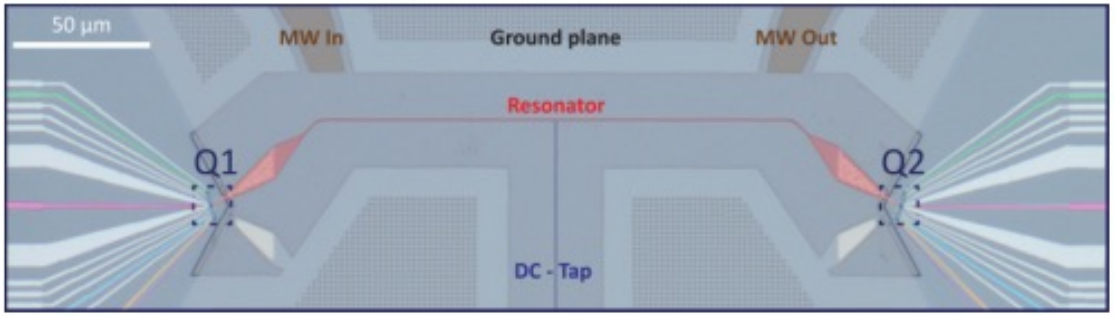

Dijkema *et al., Nat. Phys.* 21, 168–174 (2025)

Conveyor belt shuttling

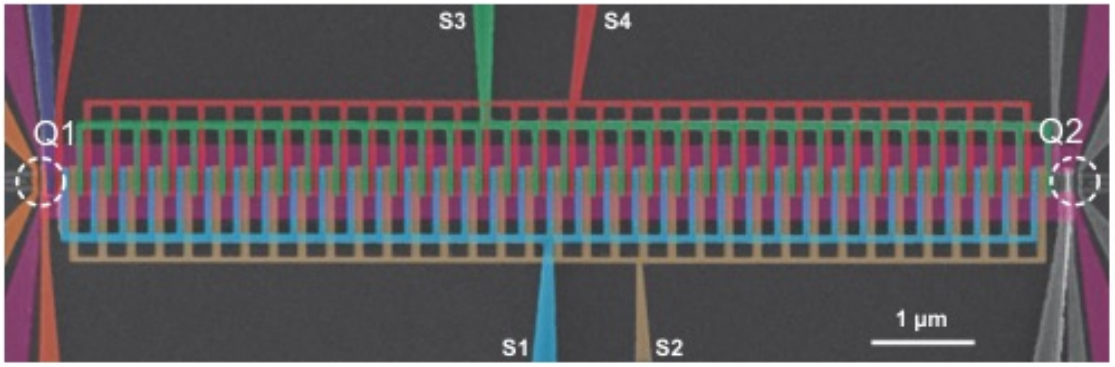

Xue *et al., Nat. Commun* 15, 2296 (2024)

Universal quantum computer

Coupled qubit arrays

Long range coupler

Classical electronics

Large scale architecture

A six qubit processor

Philips *et al., Nature* (2022)

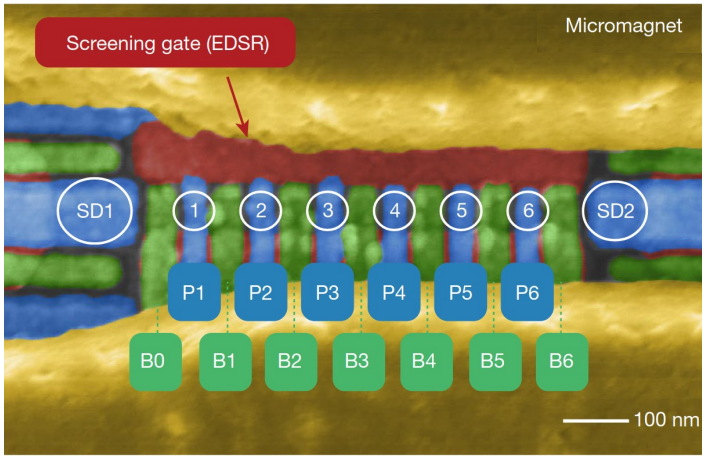

2D array

Hendrickx *et al., Nature* (2021)

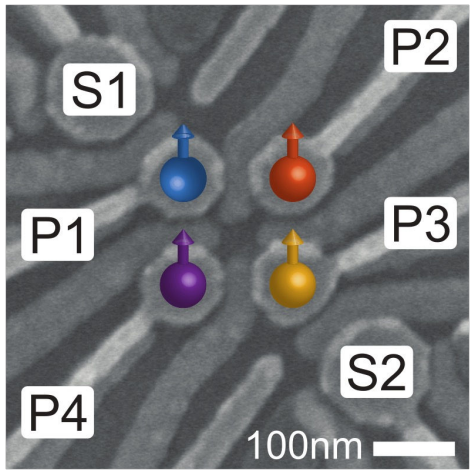

Universal quantum computer

Coupled qubit arrays

Long range coupler

Classical electronics

Si-based quantum computing roadmap

Academic prototypes

Large scale integration

QPU

Coupled qubit arrays

Long range coupler

Classical electronics

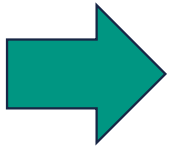

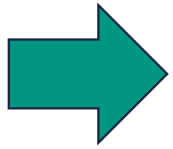

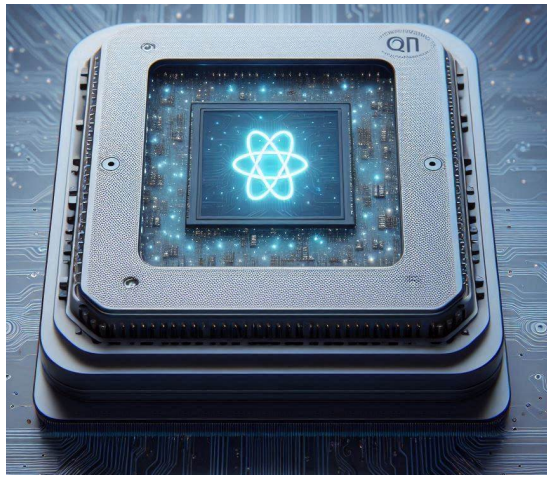

Universities

Intel, AMD and co.

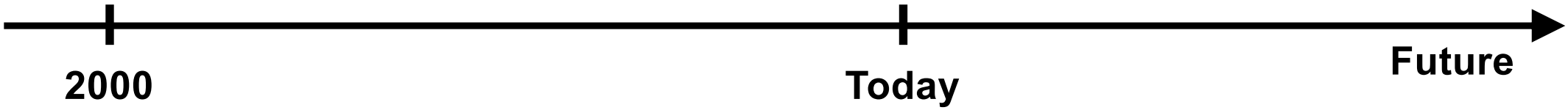

Si-based quantum computing roadmap

Academic prototypes

Large scale integration

QPU

Coupled qubit arrays

Long range coupler

Classical electronics

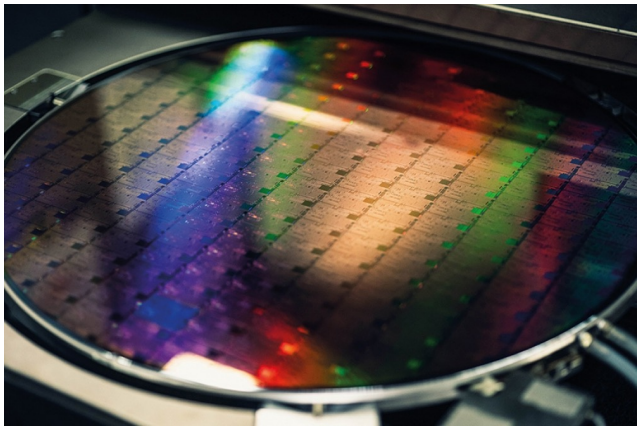

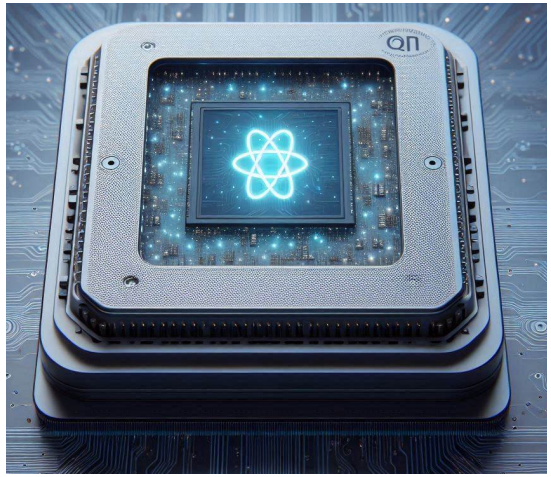

Universities

imec + collaboration partners

Intel, AMD and co.

2000

Today

Future

Interuniversity Microelectronics Centre

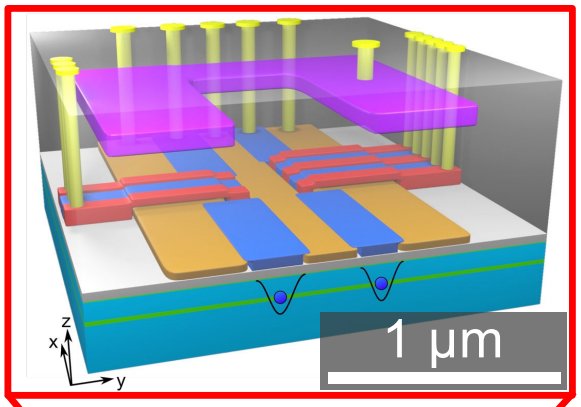

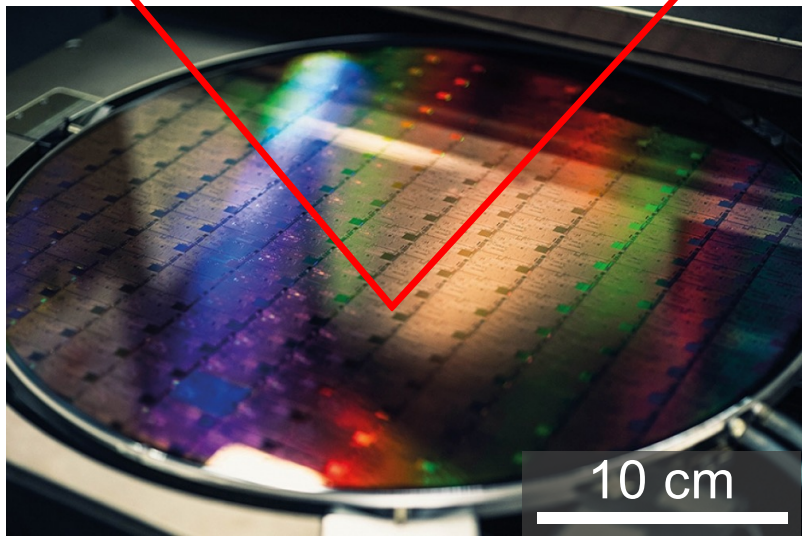

- Development of next-generation technologies
- First to produce spin qubit devices fully industrially

Two-qubit Si/SiGe device from imec

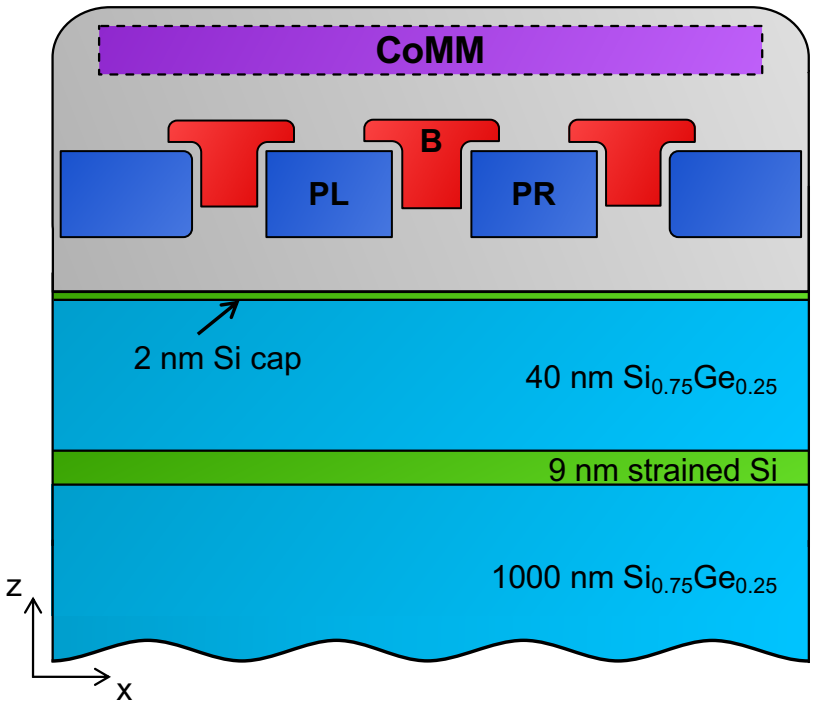

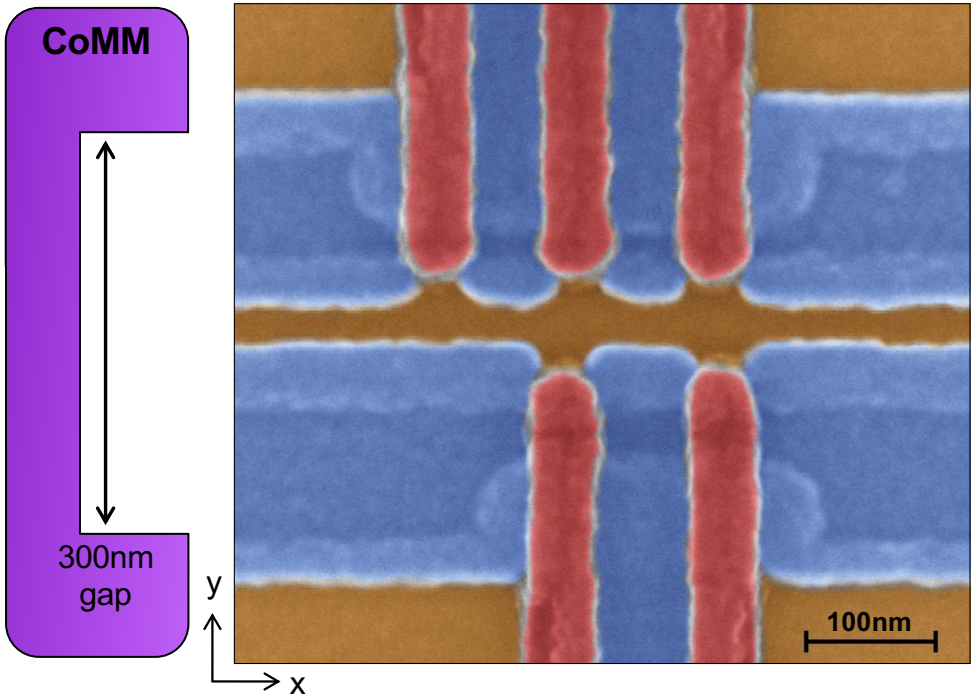

Two-qubit Si/SiGe device from imec

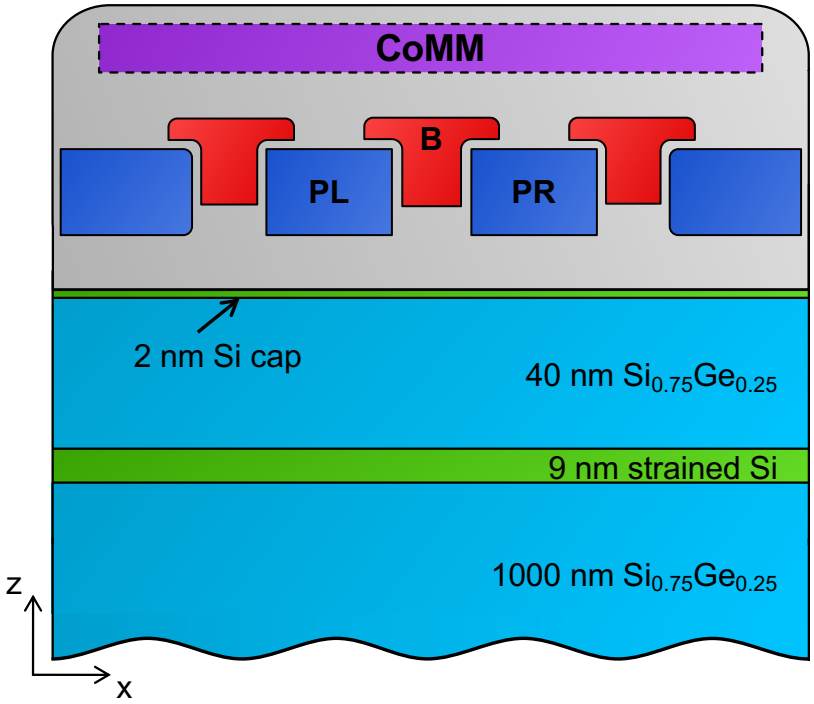

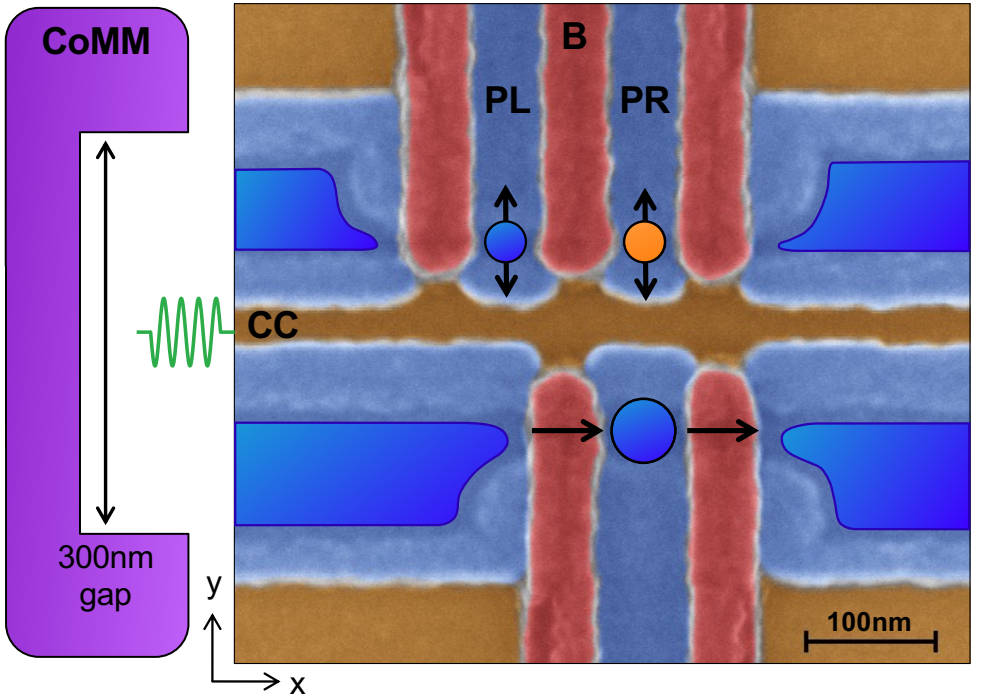

Double dot potential

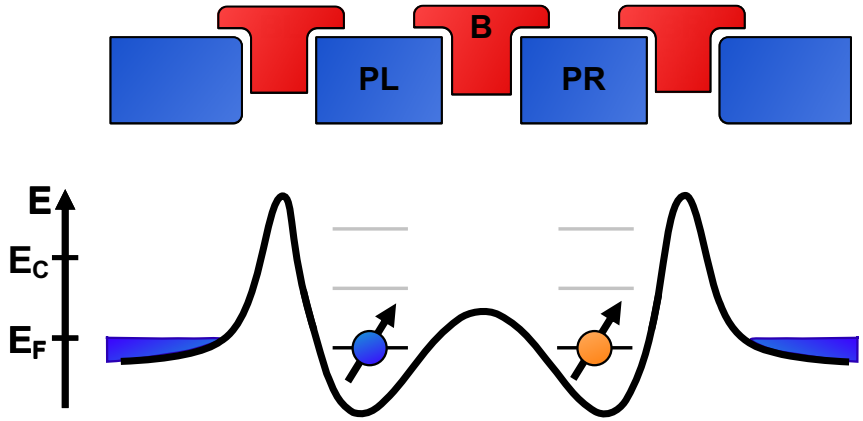

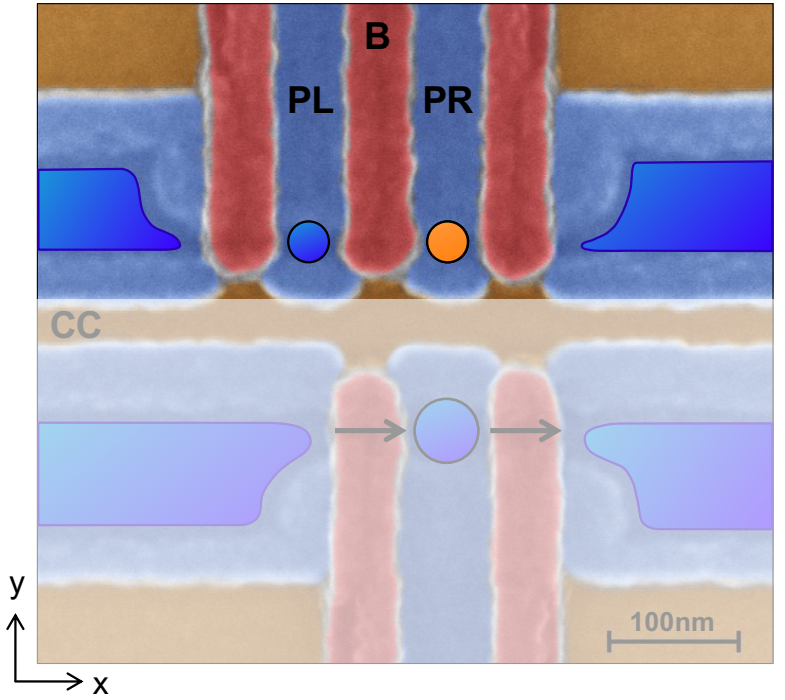

Charge sensing

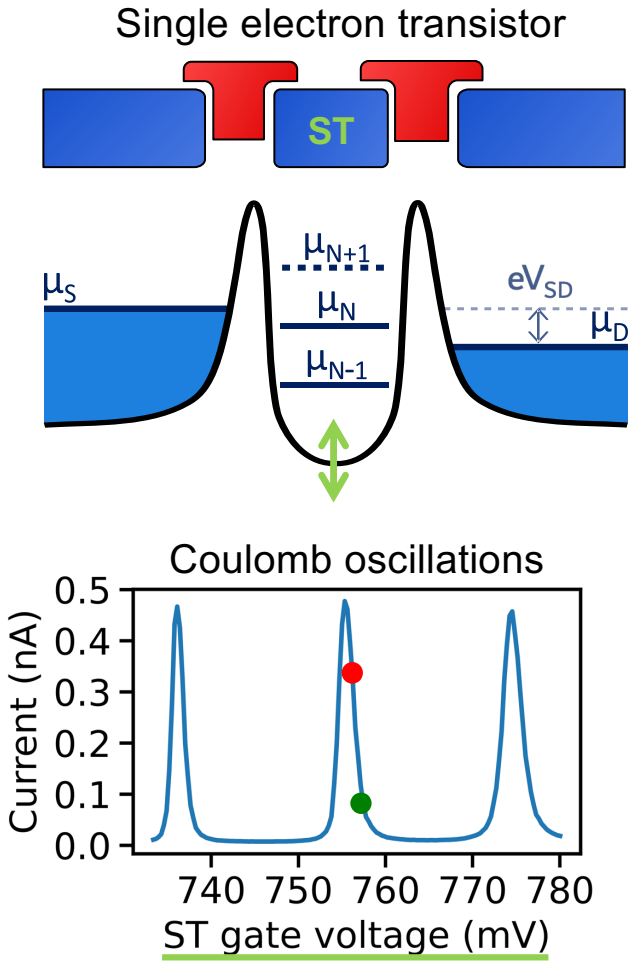

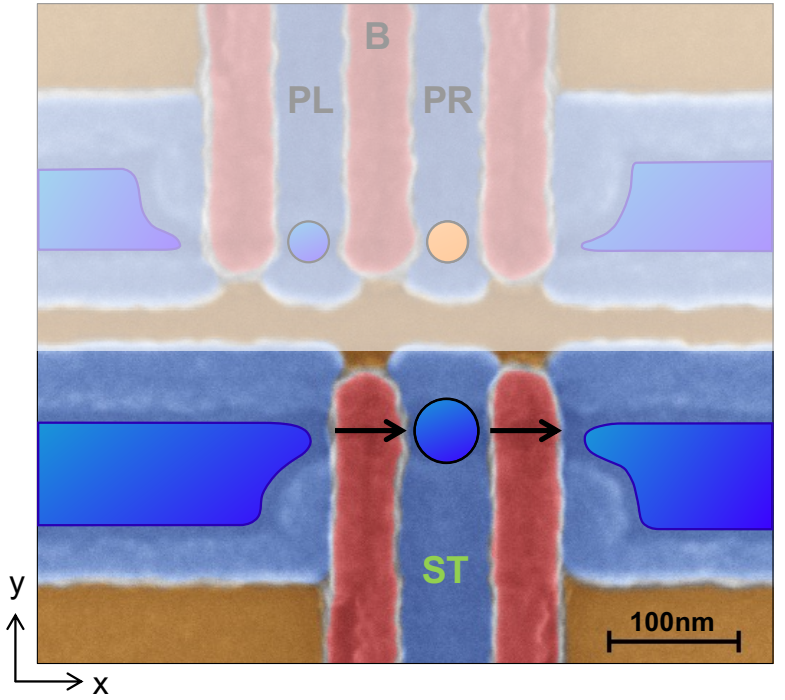

Charge stability diagram

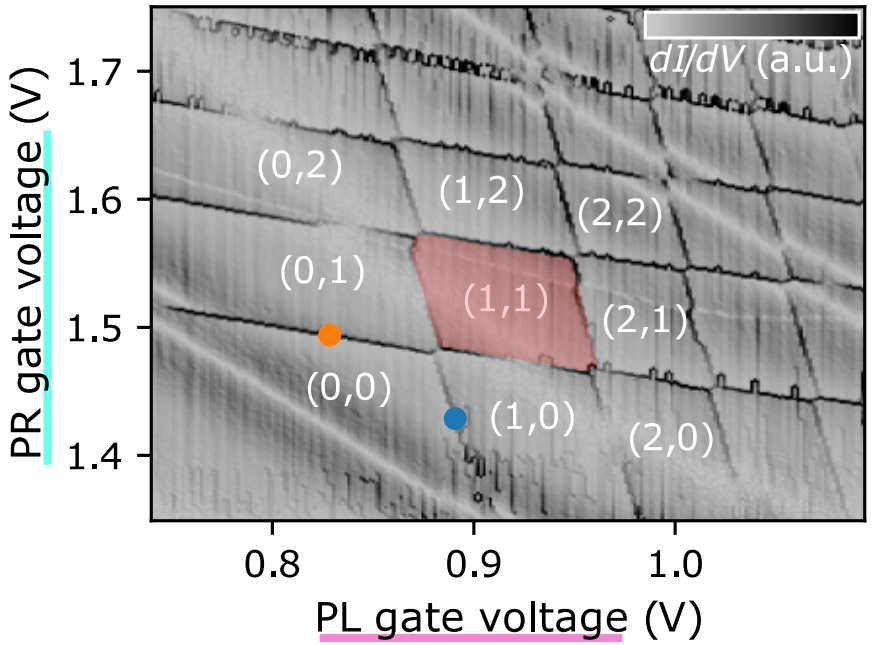

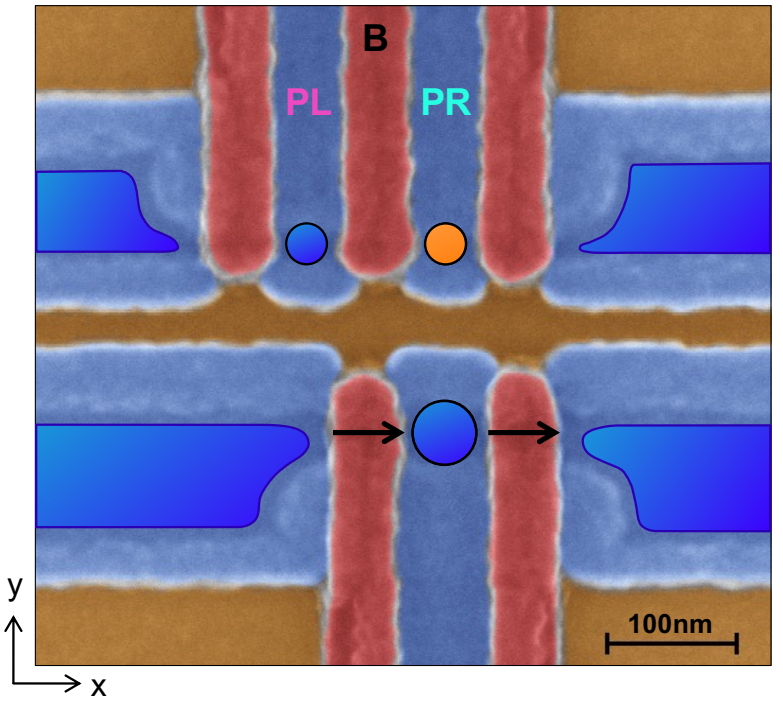

Spin to charge conversion

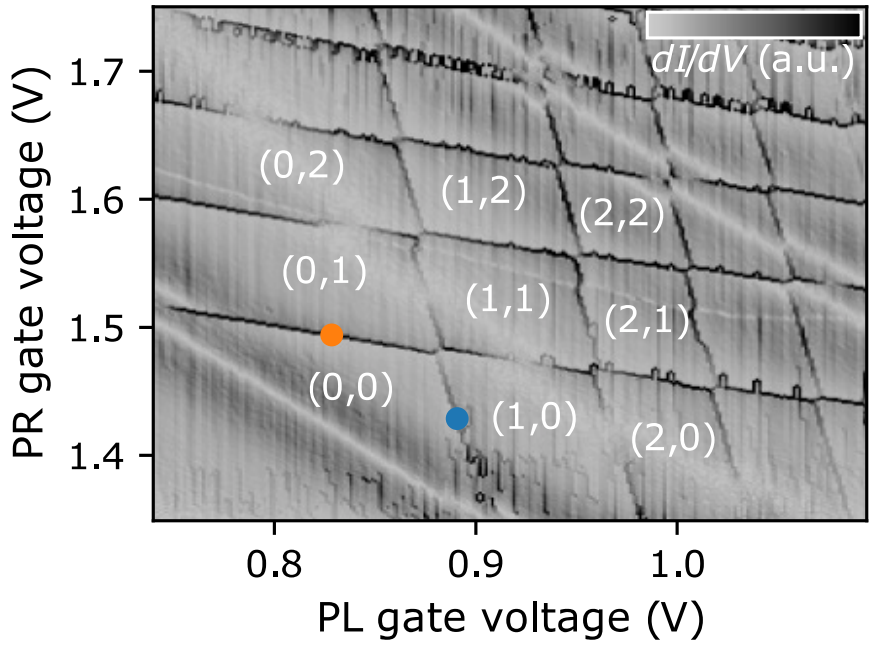

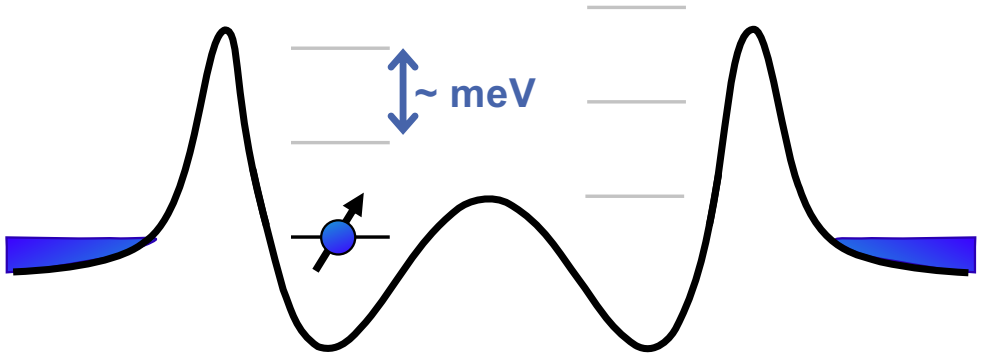

Spin to charge conversion

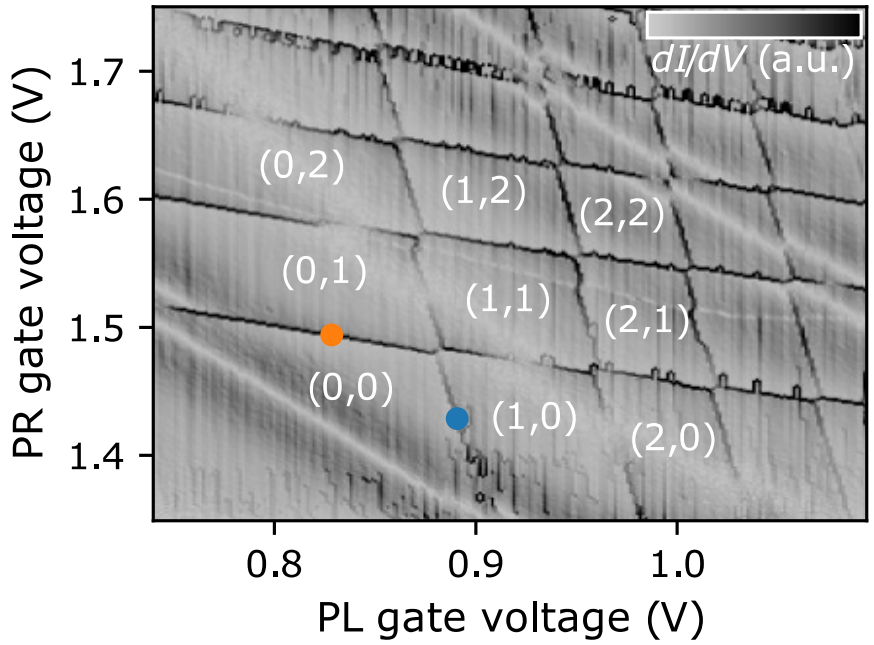

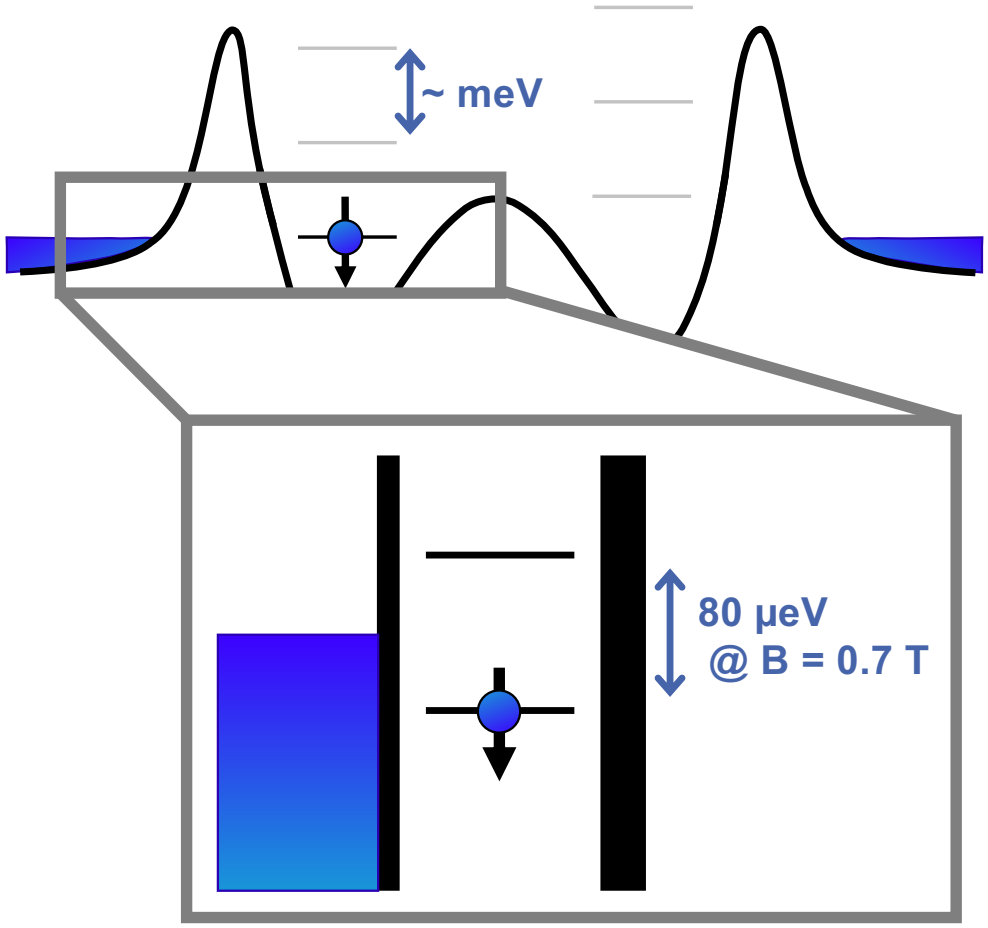

Spin to charge conversion

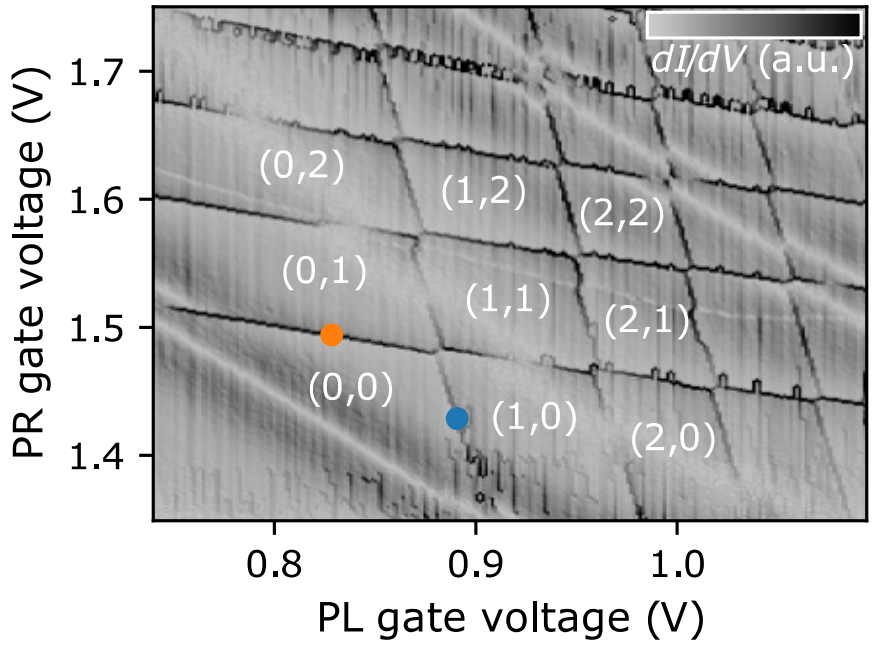

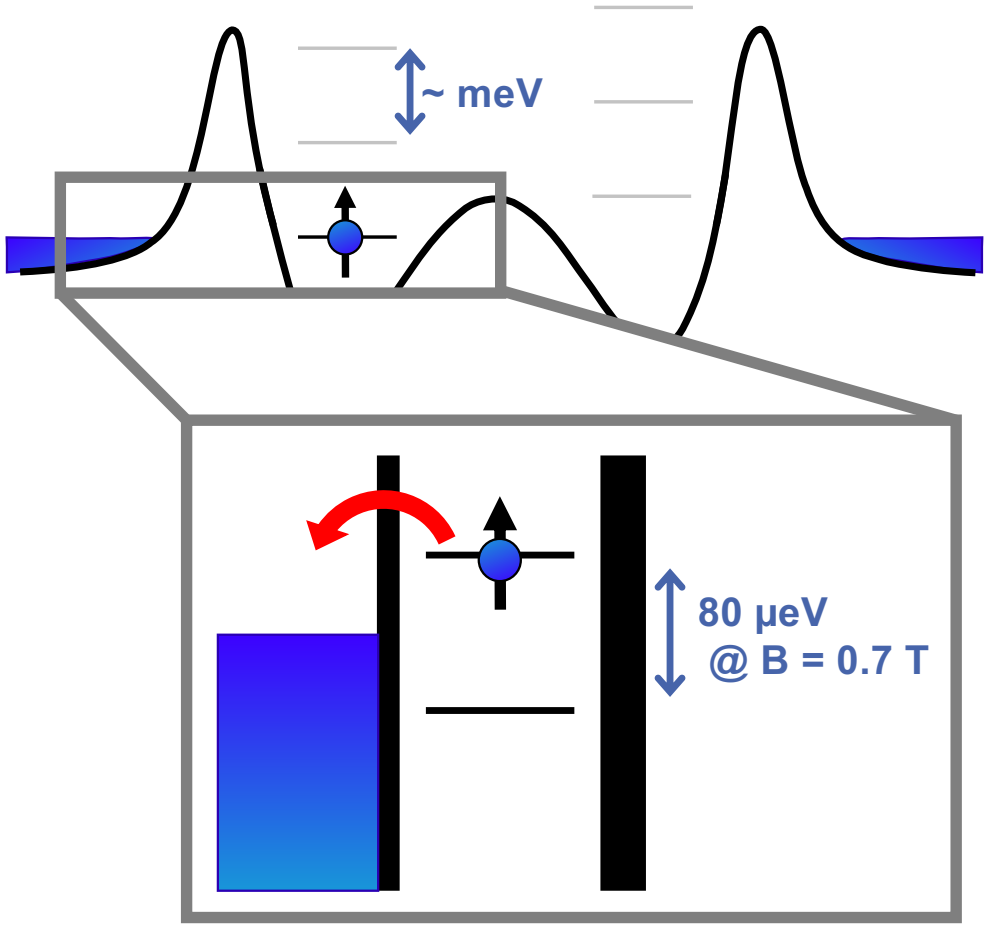

Electric dipole spin resonance (EDSR) qubit manipulation

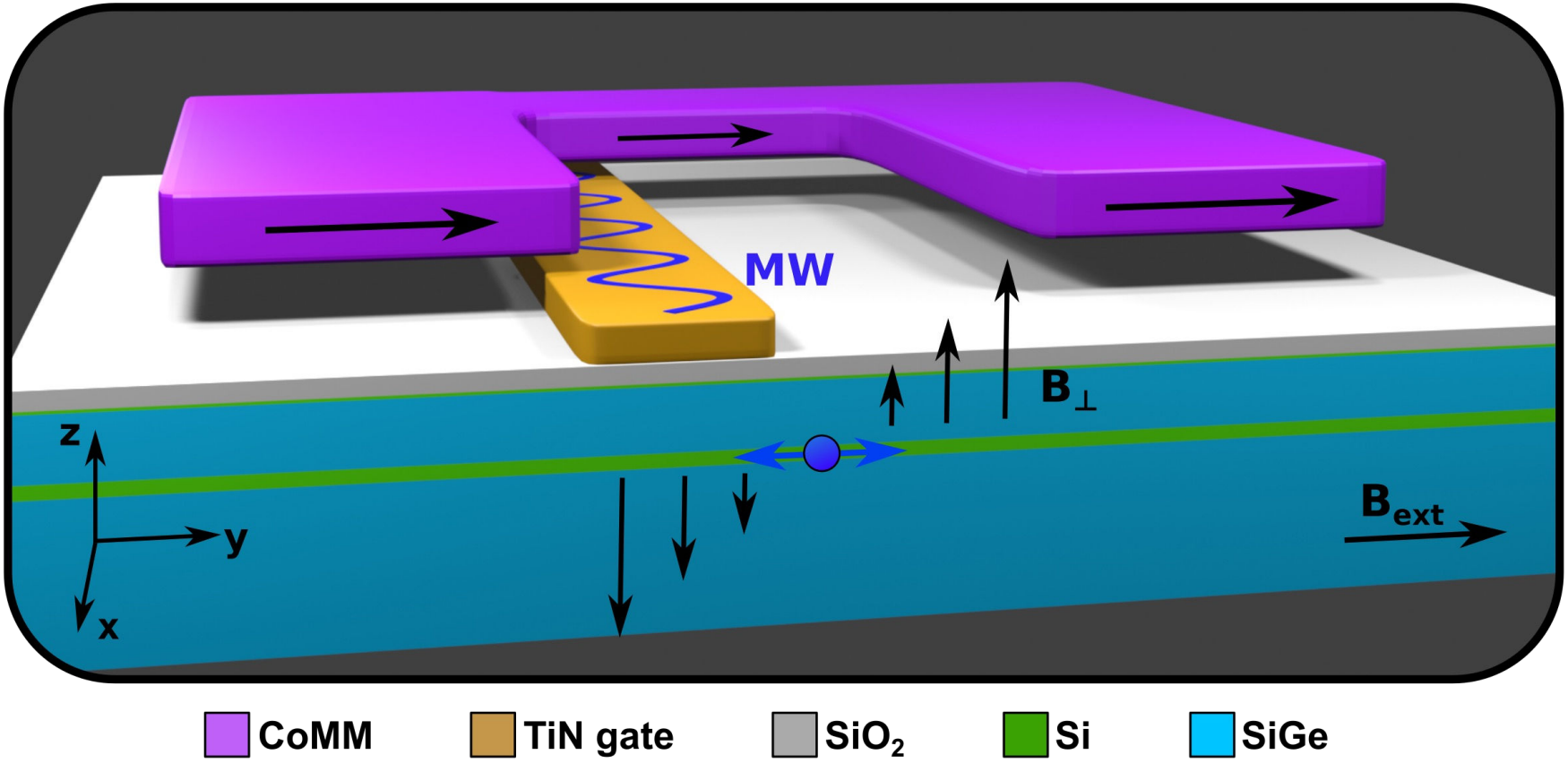

Electric dipole spin resonance (EDSR) qubit manipulation

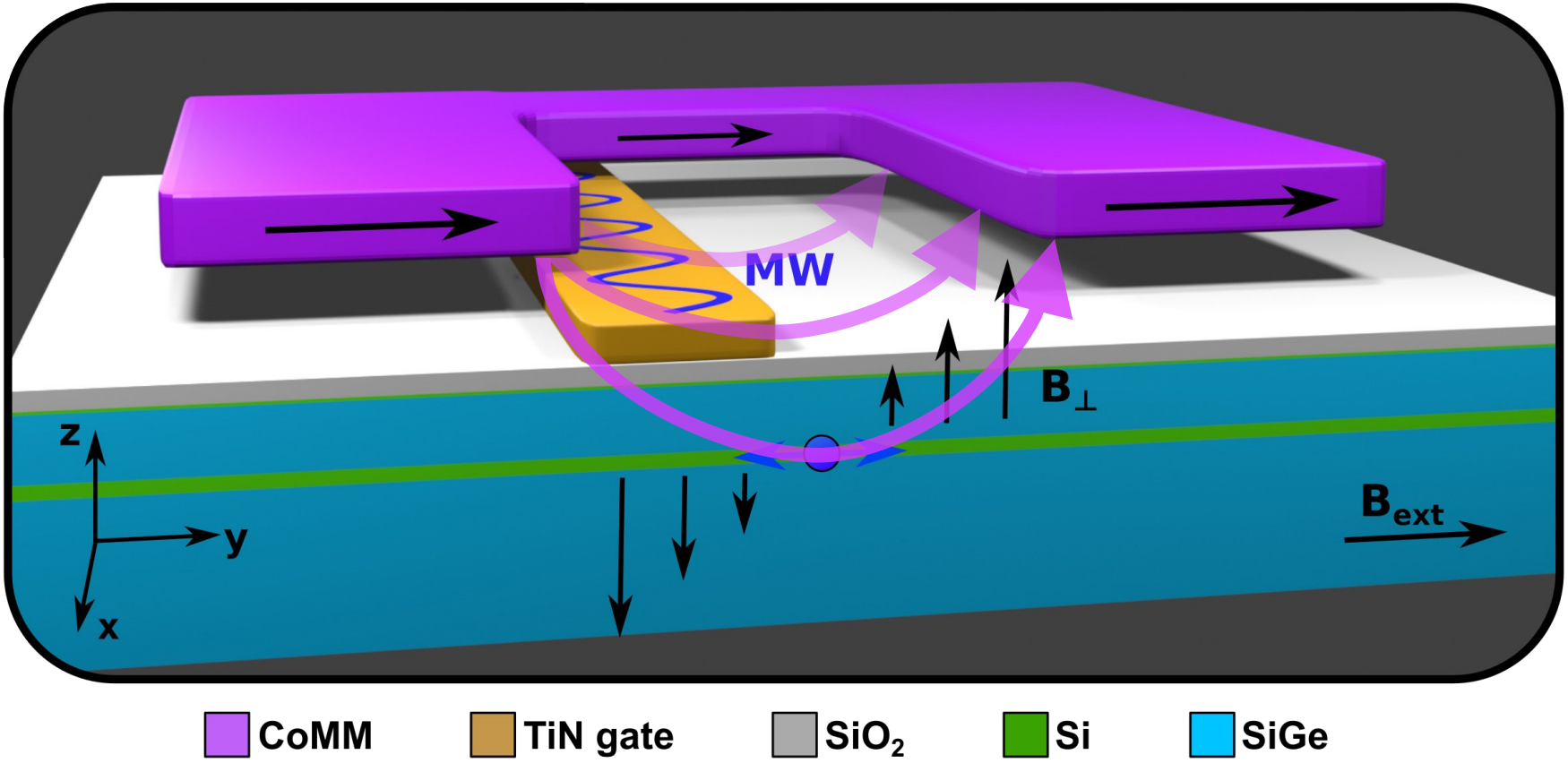

Electric dipole spin resonance (EDSR) qubit manipulation

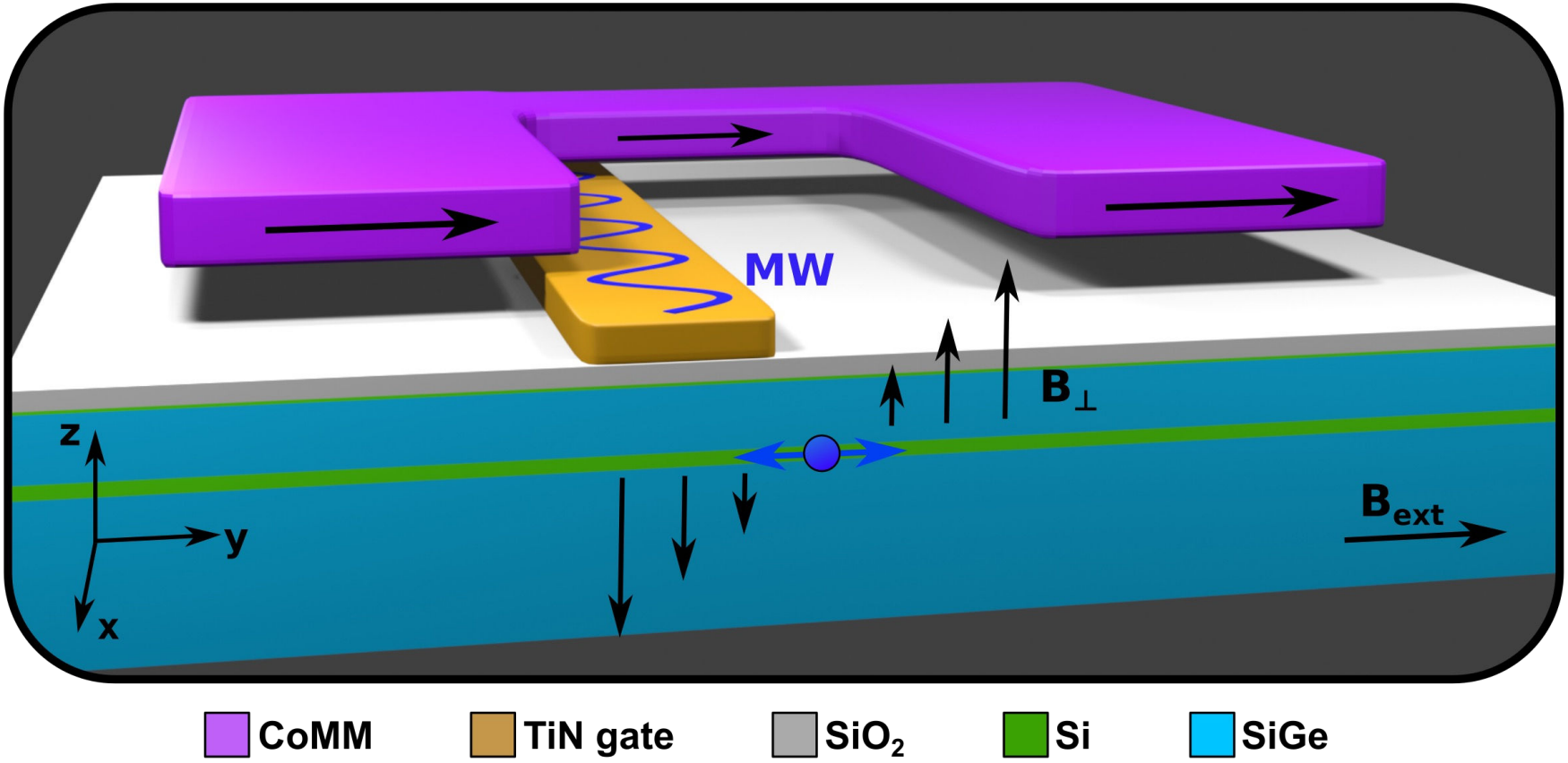

Two individually addressable spin qubits

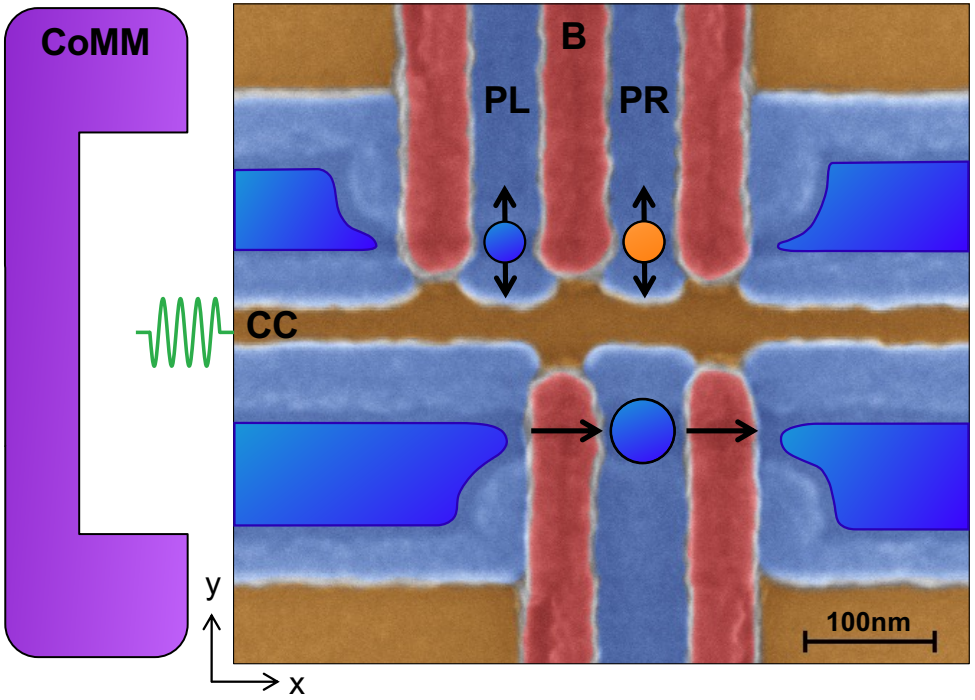

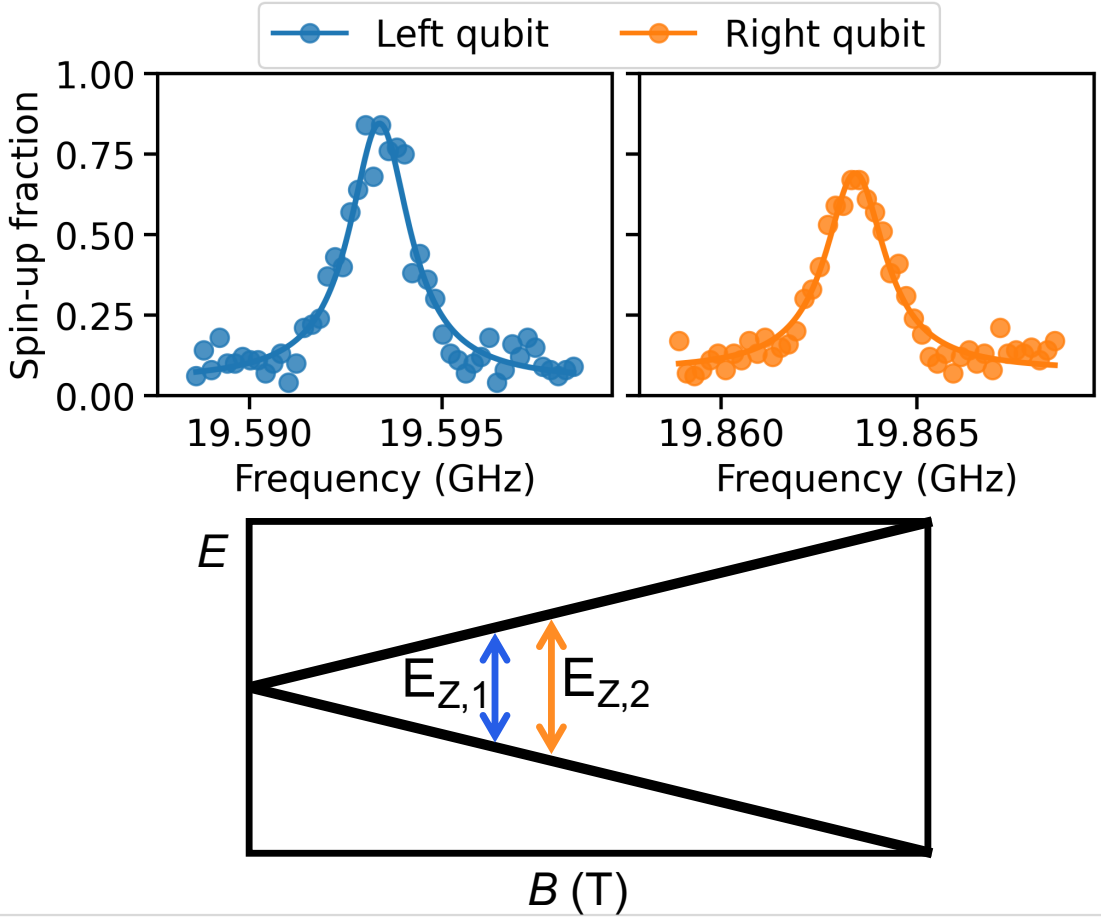

Single qubit operations

Rabi

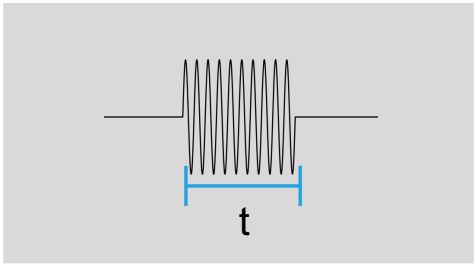

Ramsey

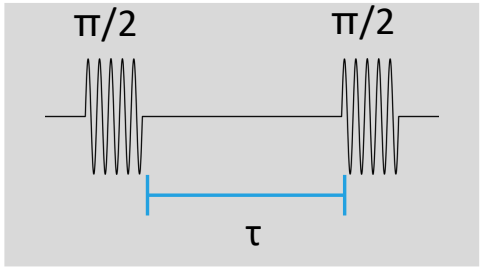

Spin-Echo

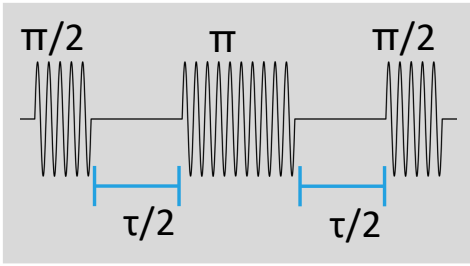

Single qubit operations

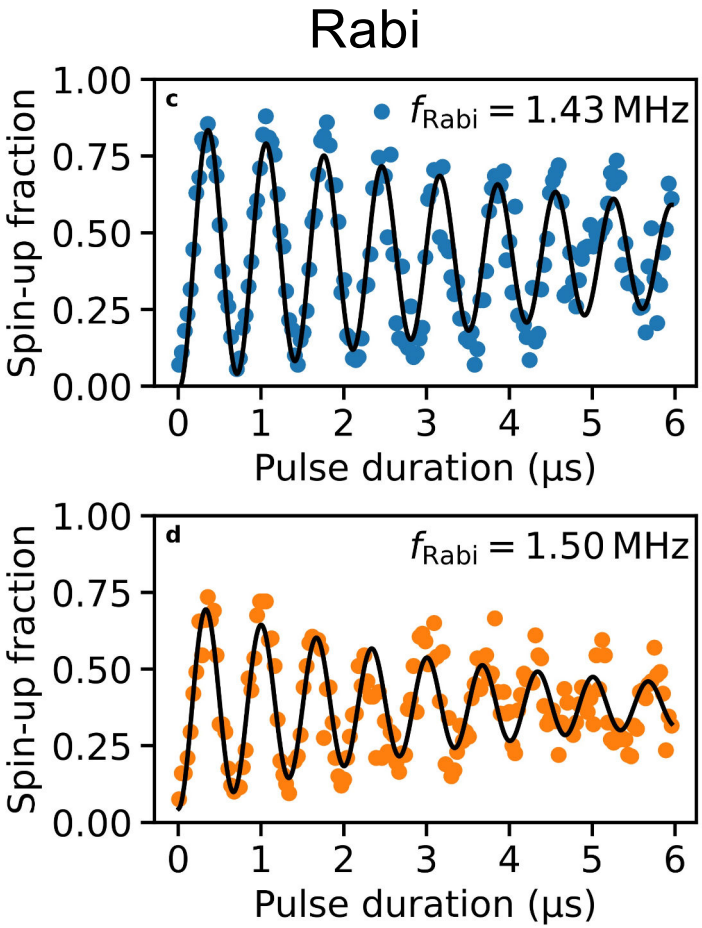

Left qubit — Fit — Right qubit

Single qubit operations

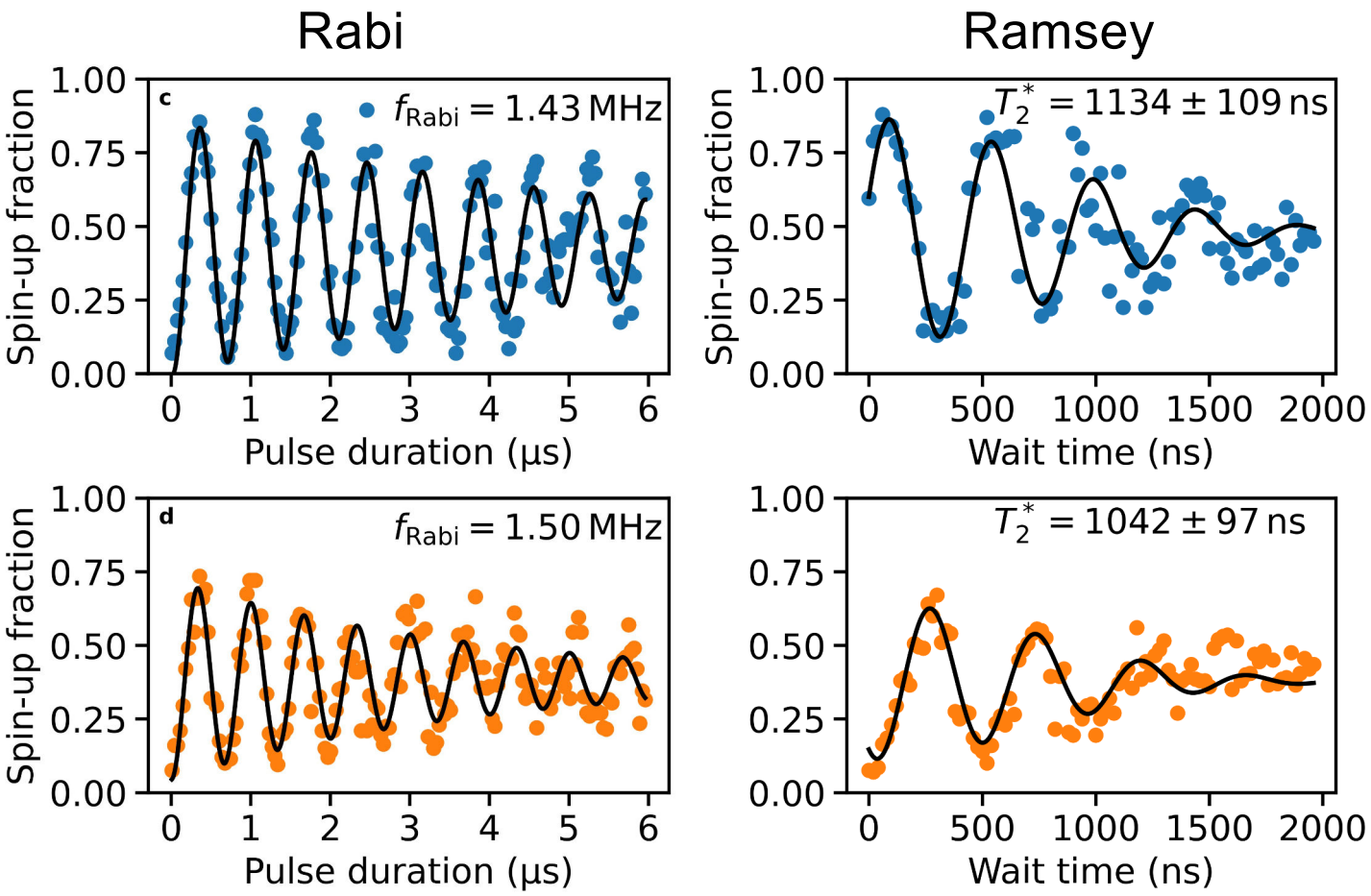

Isotopically purified Si:

$T_2^* = 120\ \mu s$

Veldhorst *et al., Nature Nanotech 9* (2014)

Single qubit operations

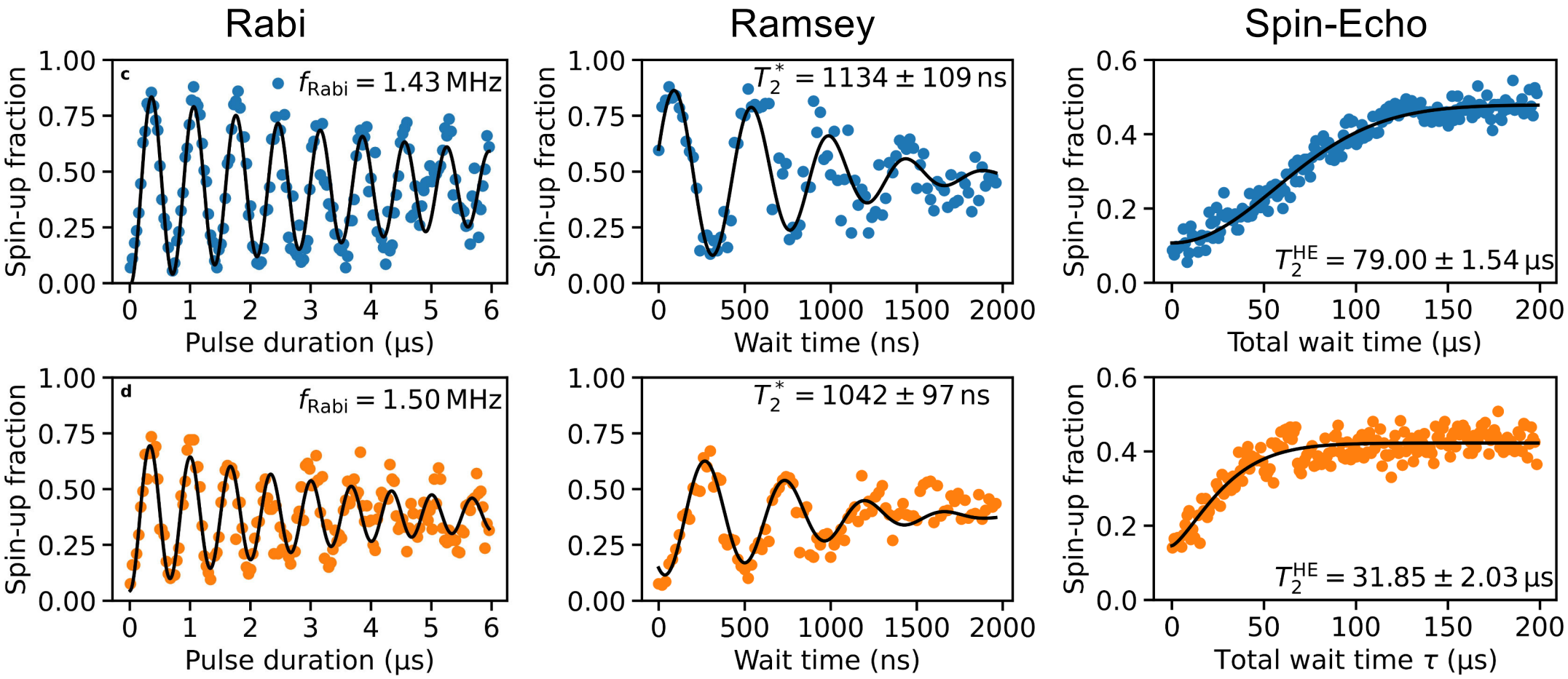

Exchange coupling of two spins

$H_1 = g\,\mu_B\,\boldsymbol{B_1}\cdot\boldsymbol{S_1}$ $\quad$ $H_2 = g\,\mu_B\,\boldsymbol{B_2}\cdot\boldsymbol{S_2}$

With Eigenstates: $|\downarrow\rangle_1, |\uparrow\rangle_1, |\downarrow\rangle_2, |\uparrow\rangle_2$

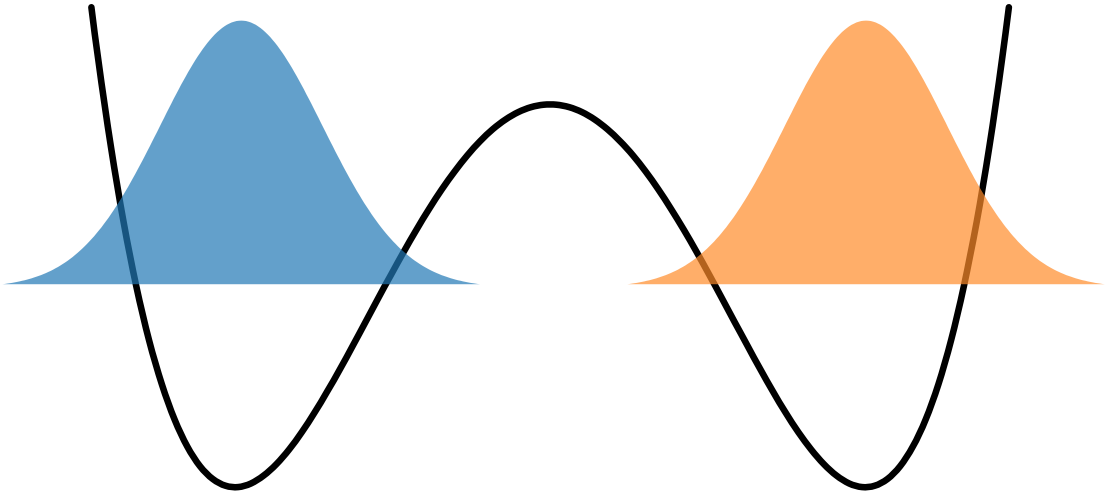

Exchange coupling of two spins

$H_1 = g\,\mu_B\,\boldsymbol{B_1}\cdot\boldsymbol{S_1}$ $\quad$ $H_2 = g\,\mu_B\,\boldsymbol{B_2}\cdot\boldsymbol{S_2}$

With Eigenstates: $|\downarrow\rangle_1, |\uparrow\rangle_1, |\downarrow\rangle_2, |\uparrow\rangle_2$

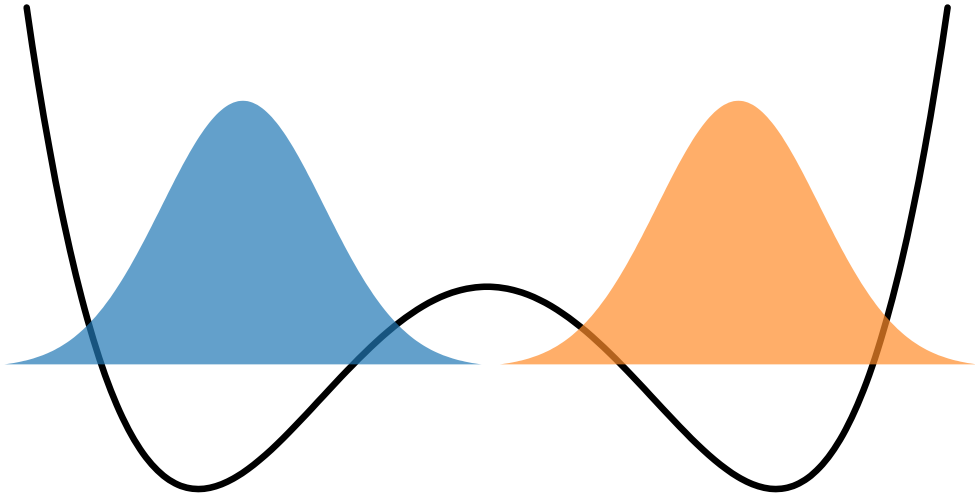

Exchange coupling of two spins

$$H = g\mu_B \boldsymbol{B_1} \cdot \boldsymbol{S_1} + g\mu_B \boldsymbol{B_2} \cdot \boldsymbol{S_2} + h\,J\left(\boldsymbol{S_1} \cdot \boldsymbol{S_2} - \frac{1}{4}\right)$$

With Eigenstates: $|\downarrow\downarrow\rangle$, $|\downarrow\uparrow\rangle$, $|\uparrow\downarrow\rangle$, $|\uparrow\uparrow\rangle$

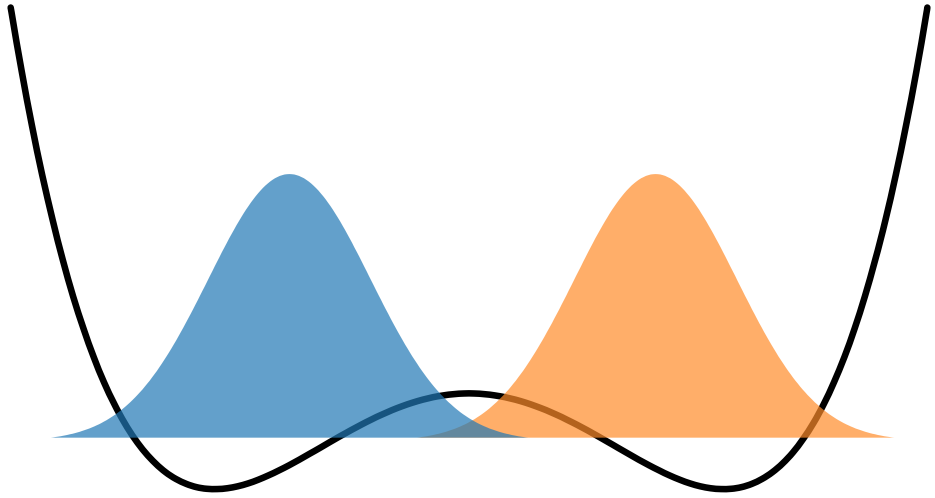

Loss and DiVincenzo, *Phys. Rev. A 57* (1998)

Veldhorst *et al., Nature 526* (2015)

Exchange coupling of two spins

$$H = g\mu_B \boldsymbol{B_1} \cdot \boldsymbol{S_1} + g\mu_B \boldsymbol{B_2} \cdot \boldsymbol{S_2} + h\,J\left(\boldsymbol{S_1} \cdot \boldsymbol{S_2} - \frac{1}{4}\right)$$

With Eigenstates: |↓↓⟩, |↓↑⟩, |↑↓⟩, |↑↑⟩

$$J = \frac{t_0^2}{U - \varepsilon - \Delta E_z/2} + \frac{t_0^2}{U + \varepsilon - \Delta E_z/2}$$

t_0	Tunnel coupling between dots
ΔE_z	Zeeman energy difference in between both dots
U	Charging energy of one dot
ε	Energy detuning between both dots

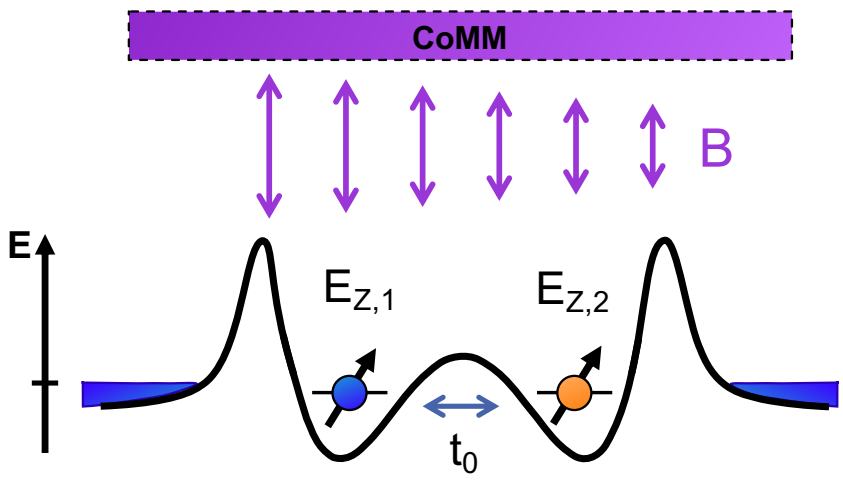

Exchange coupling of two spins

$$H = g\mu_B \boldsymbol{B_1} \cdot \boldsymbol{S_1} + g\mu_B \boldsymbol{B_2} \cdot \boldsymbol{S_2} + h\,J\left(\boldsymbol{S_1} \cdot \boldsymbol{S_2} - \frac{1}{4}\right)$$

With Eigenstates: |↓↓⟩, |↓↑⟩, |↑↓⟩, |↑↑⟩

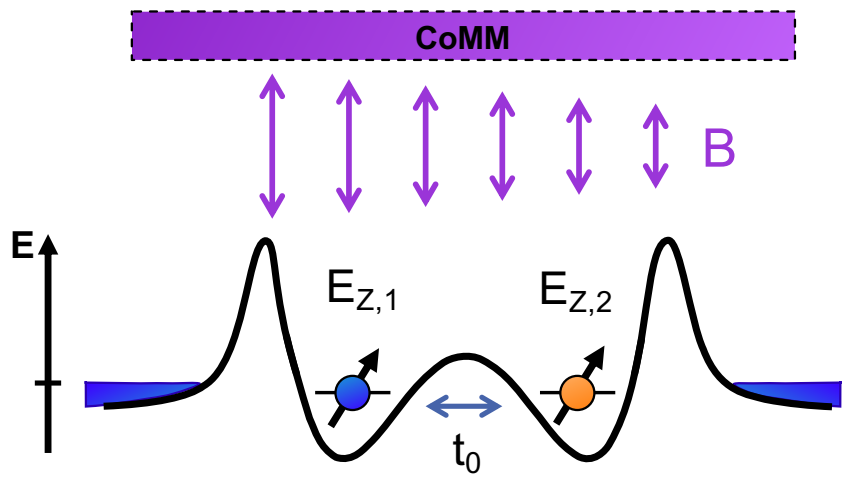

$$J = \frac{t_0^2}{U - \varepsilon - \Delta E_z/2} + \frac{t_0^2}{U + \varepsilon - \Delta E_z/2}$$

t_0	Tunnel coupling between dots
ΔE_z	Zeeman energy difference in between both dots
U	Charging energy of one dot
ε	Energy detuning between both dots

$$\varepsilon' = \frac{\varepsilon}{U}$$

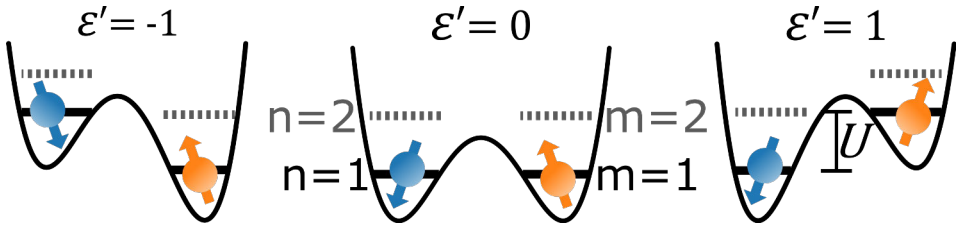

Exchange coupling of two spins

$$H = g\mu_B \boldsymbol{B_1} \cdot \boldsymbol{S_1} + g\mu_B \boldsymbol{B_2} \cdot \boldsymbol{S_2} + h\,J\left(\boldsymbol{S_1} \cdot \boldsymbol{S_2} - \frac{1}{4}\right)$$

With Eigenstates: $|\downarrow\downarrow\rangle$, $|\downarrow\uparrow\rangle$, $|\uparrow\downarrow\rangle$, $|\uparrow\uparrow\rangle$

$$J = \frac{t_0^2}{U - \varepsilon - \Delta E_z/2} + \frac{t_0^2}{U + \varepsilon - \Delta E_z/2}$$

t_0	Tunnel coupling between dots
ΔE_z	Zeeman energy difference in between both dots
U	Charging energy of one dot
ε	Energy detuning between both dots

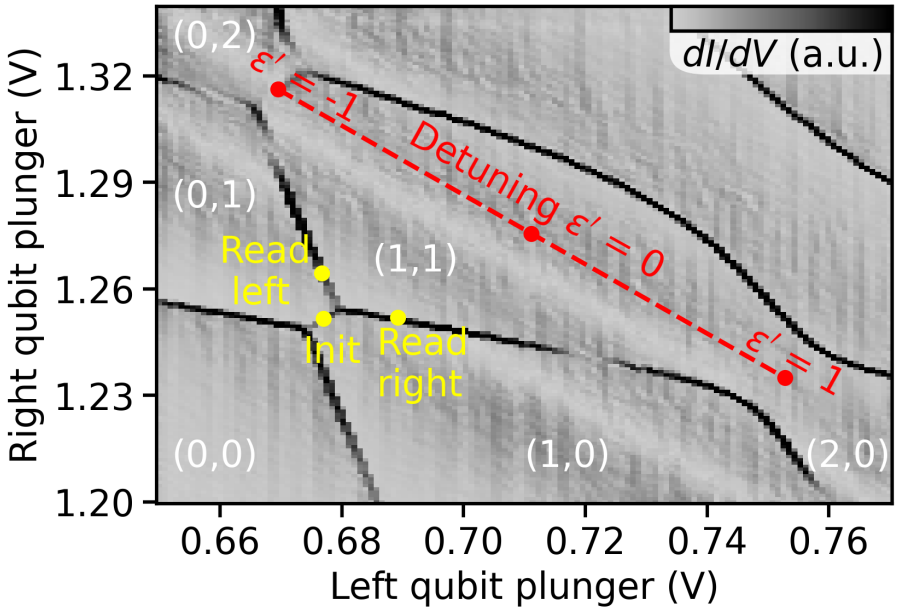

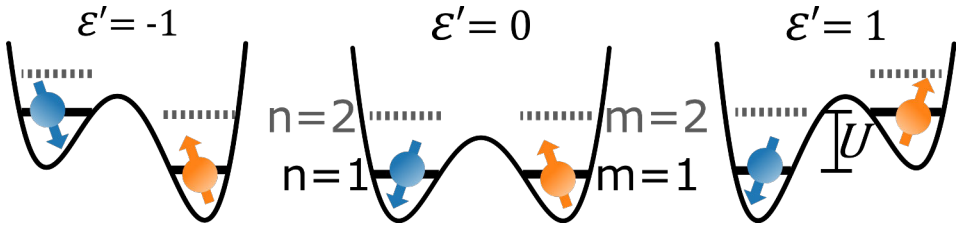

Exchange coupling of two spins

$$H = g\mu_B \boldsymbol{B_1} \cdot \boldsymbol{S_1} + g\mu_B \boldsymbol{B_2} \cdot \boldsymbol{S_2} + h\,J\left(\boldsymbol{S_1} \cdot \boldsymbol{S_2} - \frac{1}{4}\right)$$

With Eigenstates: $|\downarrow\downarrow\rangle$, $|\downarrow\uparrow\rangle$, $|\uparrow\downarrow\rangle$, $|\uparrow\uparrow\rangle$

$$J = \frac{t_0^2}{U - \varepsilon - \Delta E_z/2} + \frac{t_0^2}{U + \varepsilon - \Delta E_z/2}$$

t_0	Tunnel coupling between dots
ΔE_z	Zeeman energy difference in between both dots
U	Charging energy of one dot
ε	Energy detuning between both dots

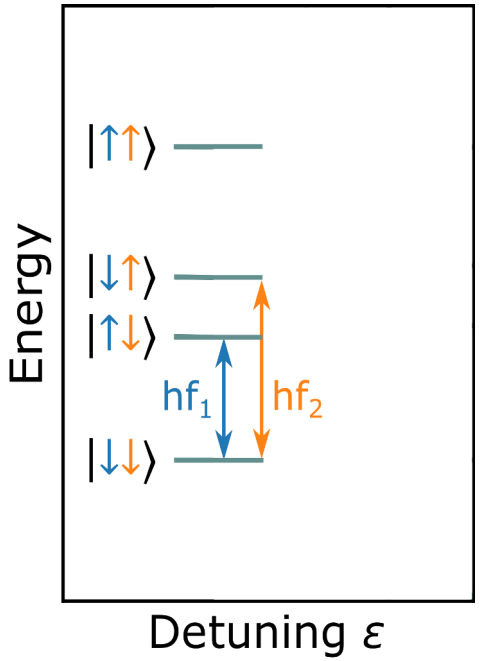

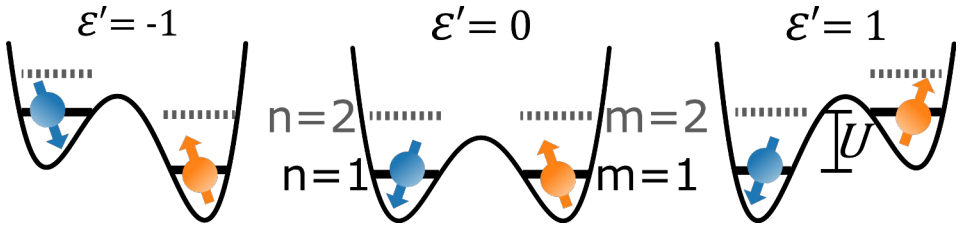

Exchange coupling of two spins

$$H = g\mu_B \boldsymbol{B_1} \cdot \boldsymbol{S_1} + g\mu_B \boldsymbol{B_2} \cdot \boldsymbol{S_2} + h\,J\left(\boldsymbol{S_1} \cdot \boldsymbol{S_2} - \frac{1}{4}\right)$$

With Eigenstates: $|\downarrow\downarrow\rangle$, $|\downarrow\uparrow\rangle$, $|\uparrow\downarrow\rangle$, $|\uparrow\uparrow\rangle$

$$J = \frac{t_0^2}{U - \varepsilon - \Delta E_z/2} + \frac{t_0^2}{U + \varepsilon - \Delta E_z/2}$$

t_0	Tunnel coupling between dots
ΔE_z	Zeeman energy difference in between both dots
U	Charging energy of one dot
ε	Energy detuning between both dots

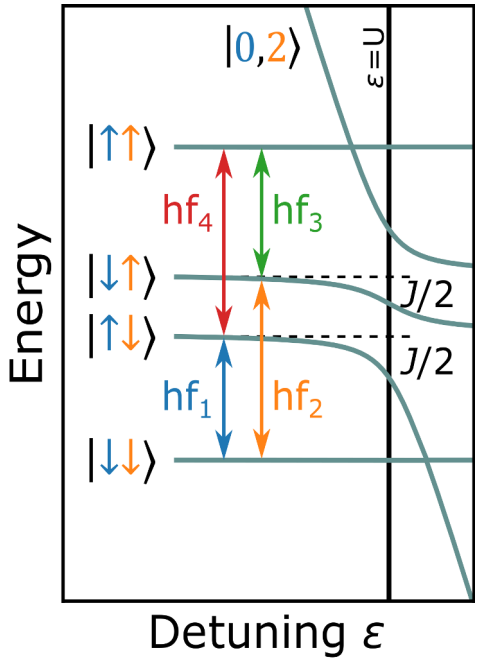

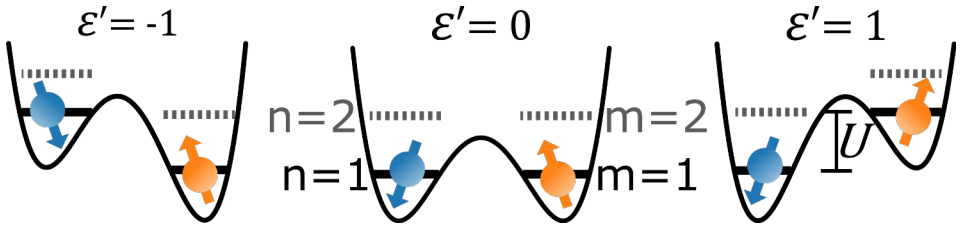

Exchange coupling of two spins

$$H = g\mu_B \boldsymbol{B_1} \cdot \boldsymbol{S_1} + g\mu_B \boldsymbol{B_2} \cdot \boldsymbol{S_2} + h\,J\left(\boldsymbol{S_1} \cdot \boldsymbol{S_2} - \frac{1}{4}\right)$$

With Eigenstates: $|\downarrow\downarrow\rangle$, $|\downarrow\uparrow\rangle$, $|\uparrow\downarrow\rangle$, $|\uparrow\uparrow\rangle$

$$J = \frac{t_0^2}{U - \varepsilon - \Delta E_z/2} + \frac{t_0^2}{U + \varepsilon - \Delta E_z/2}$$

t_0	Tunnel coupling between dots
ΔE_z	Zeeman energy difference in between both dots
U	Charging energy of one dot
ε	Energy detuning between both dots

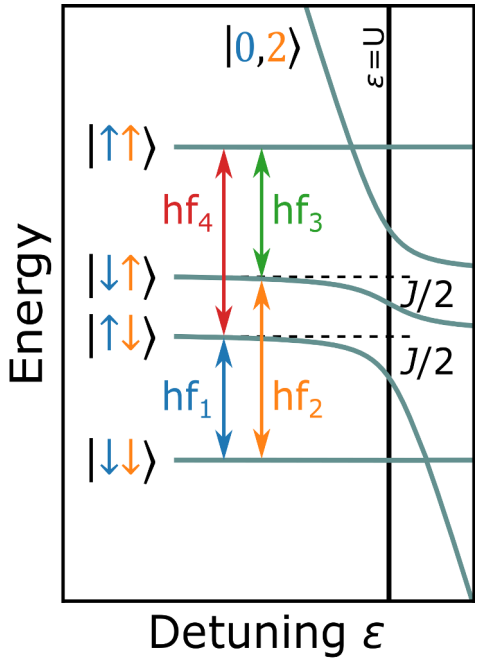

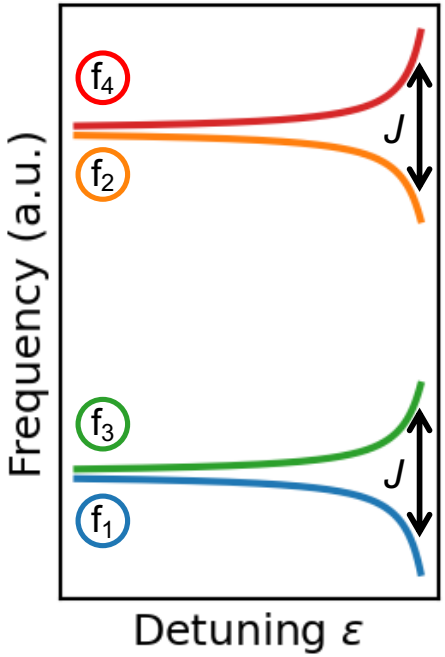

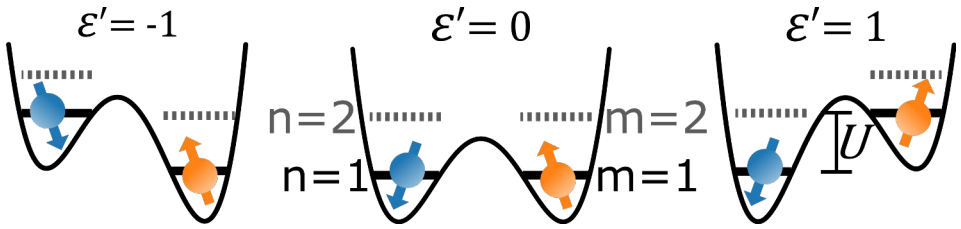

Exchange spectroscopy

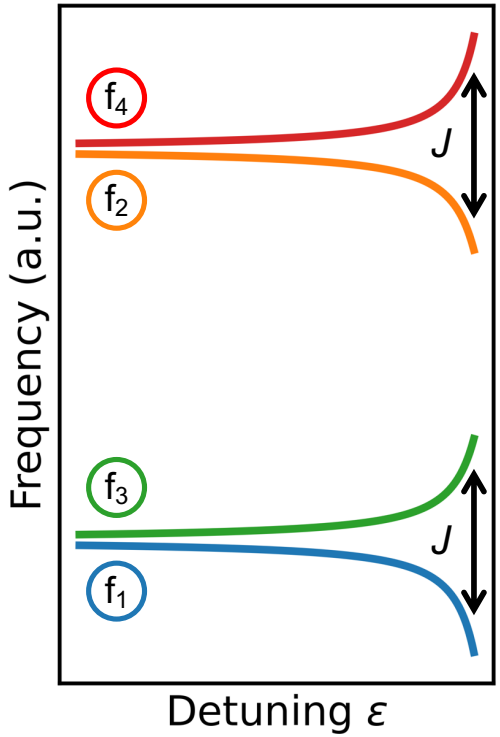

Right qubit = Target qubit

Left qubit = Target qubit

Exchange spectroscopy

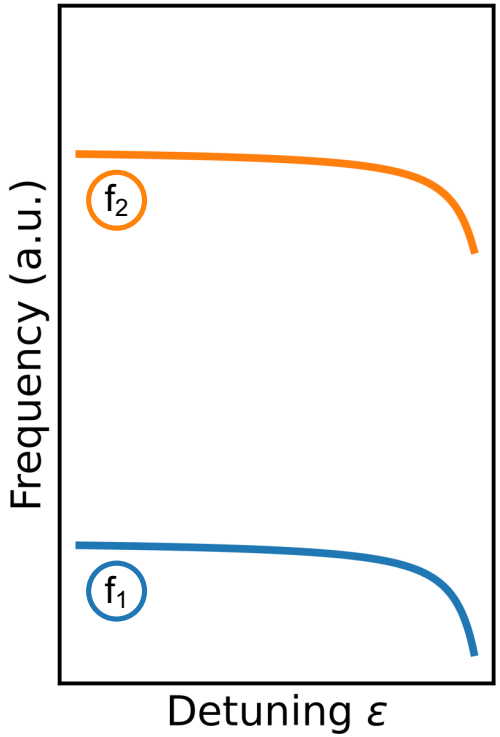

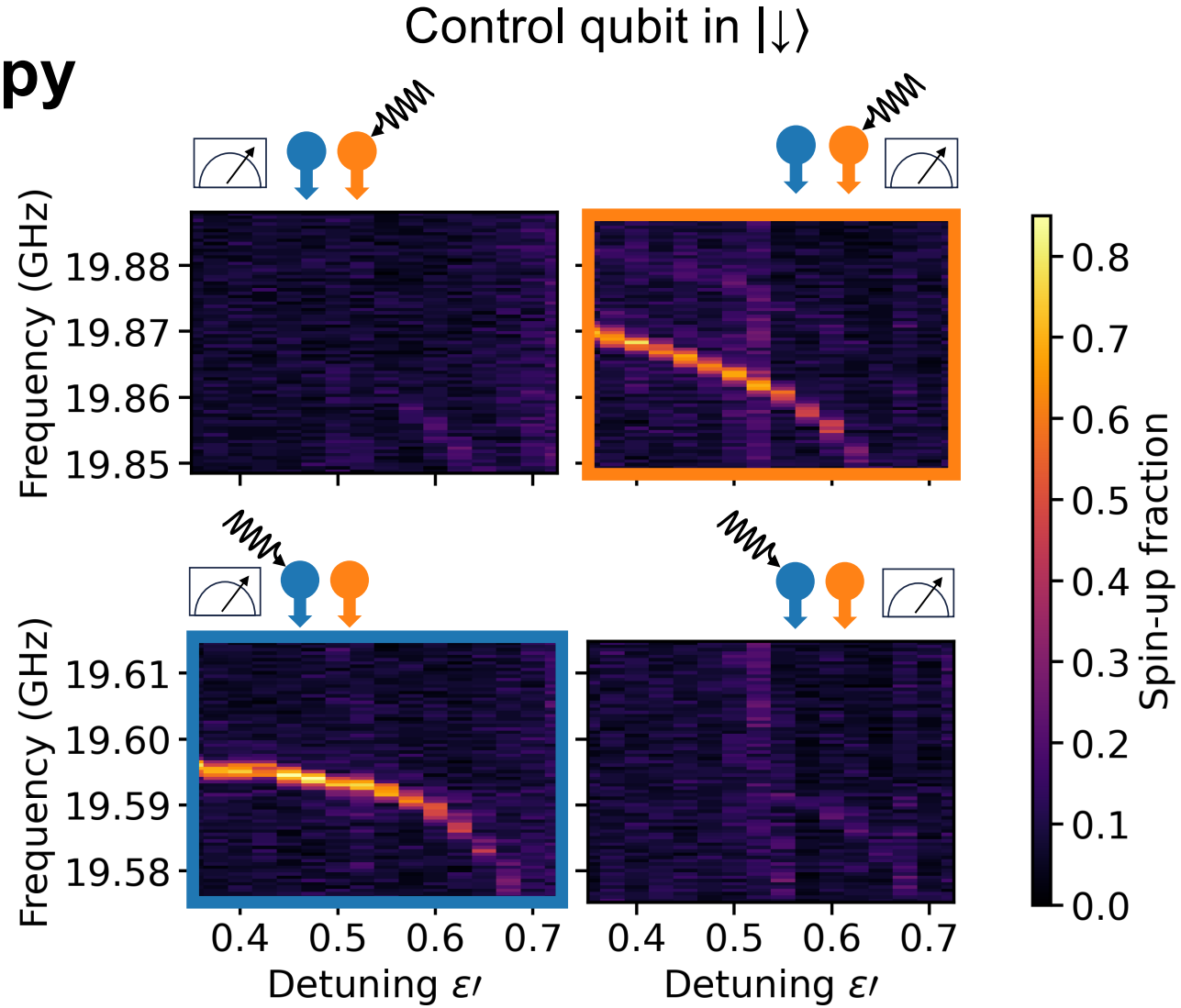

Exchange spectroscopy

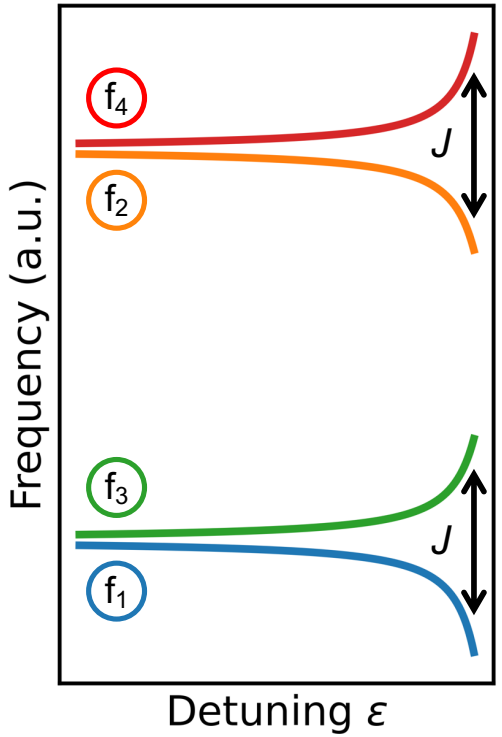

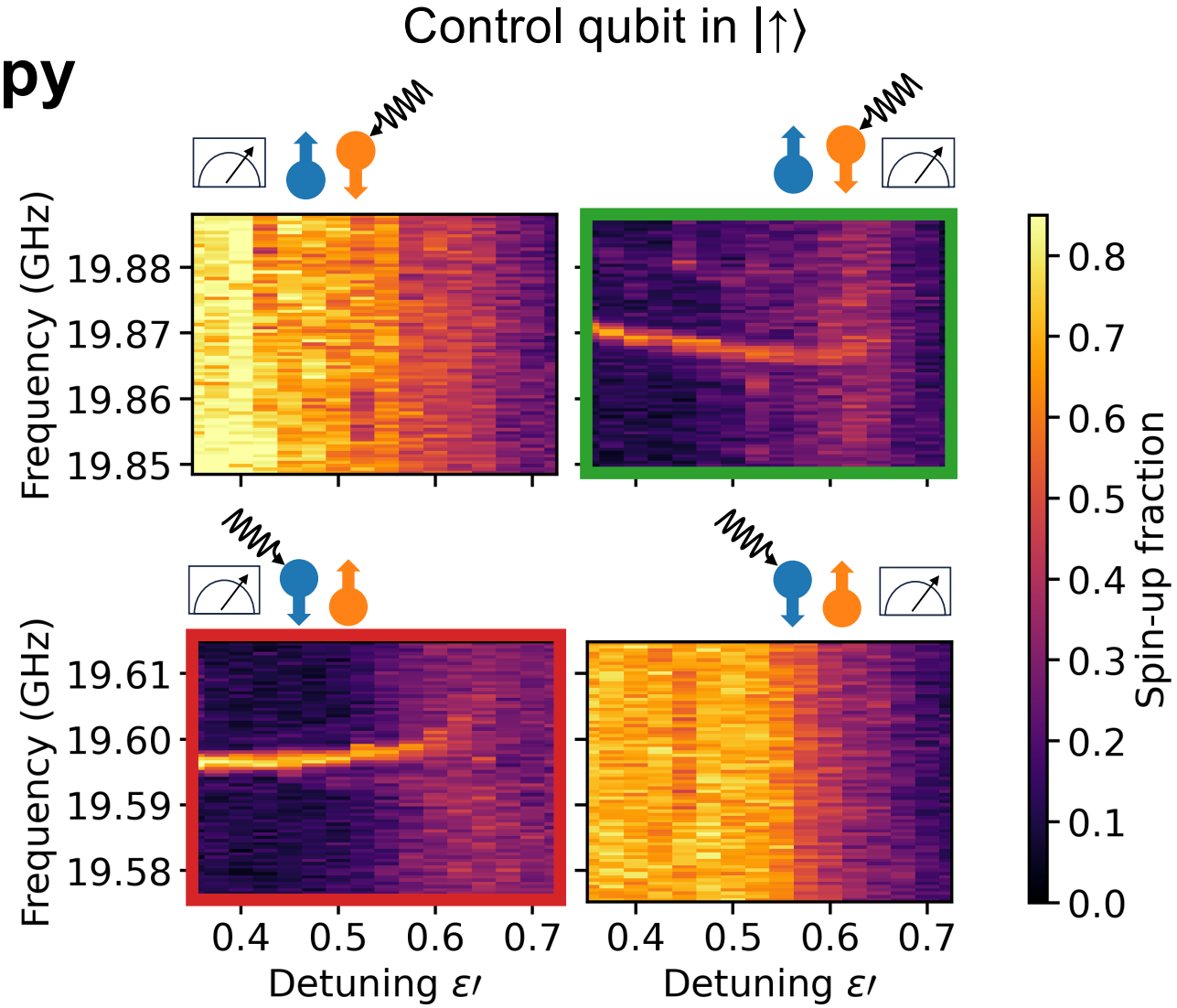

Controllable exchange coupling

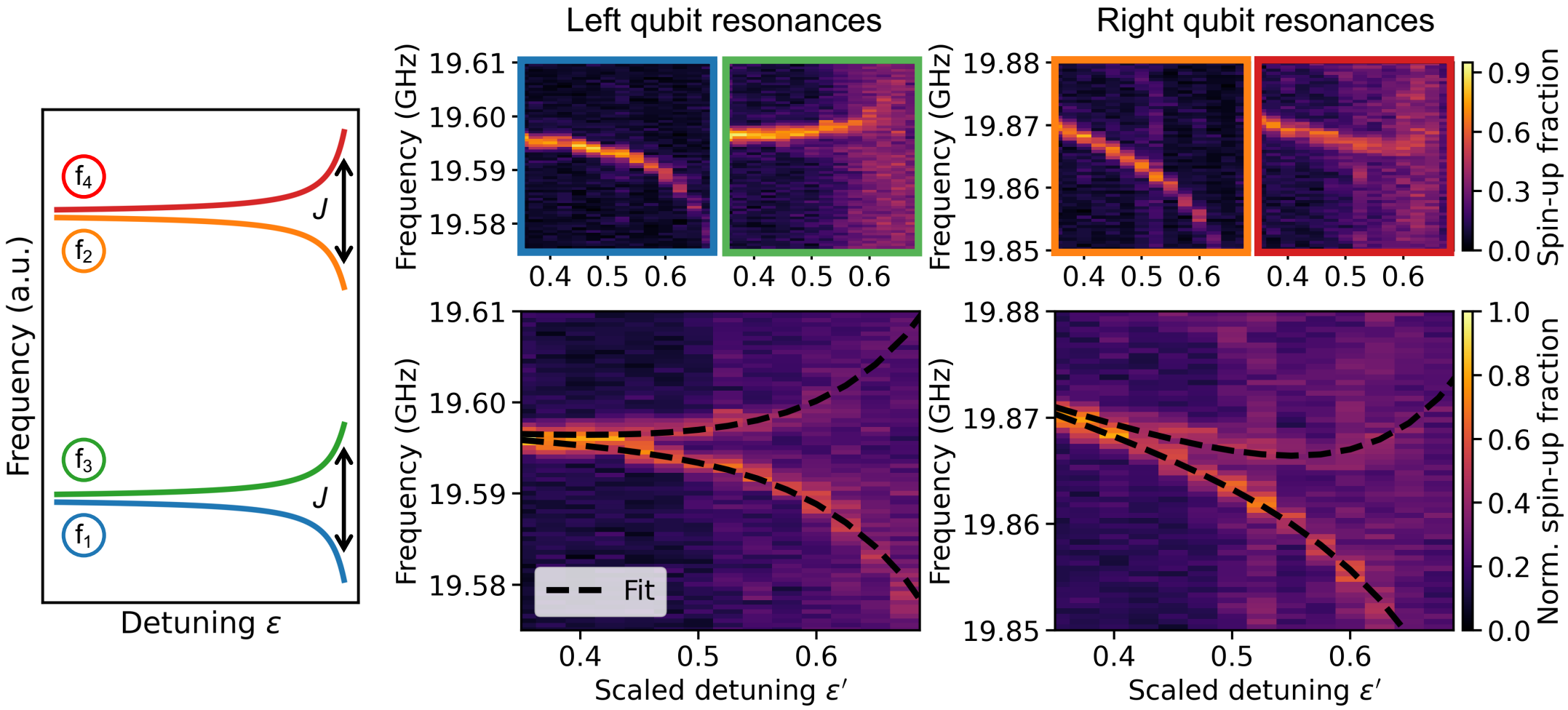

Controllable exchange coupling

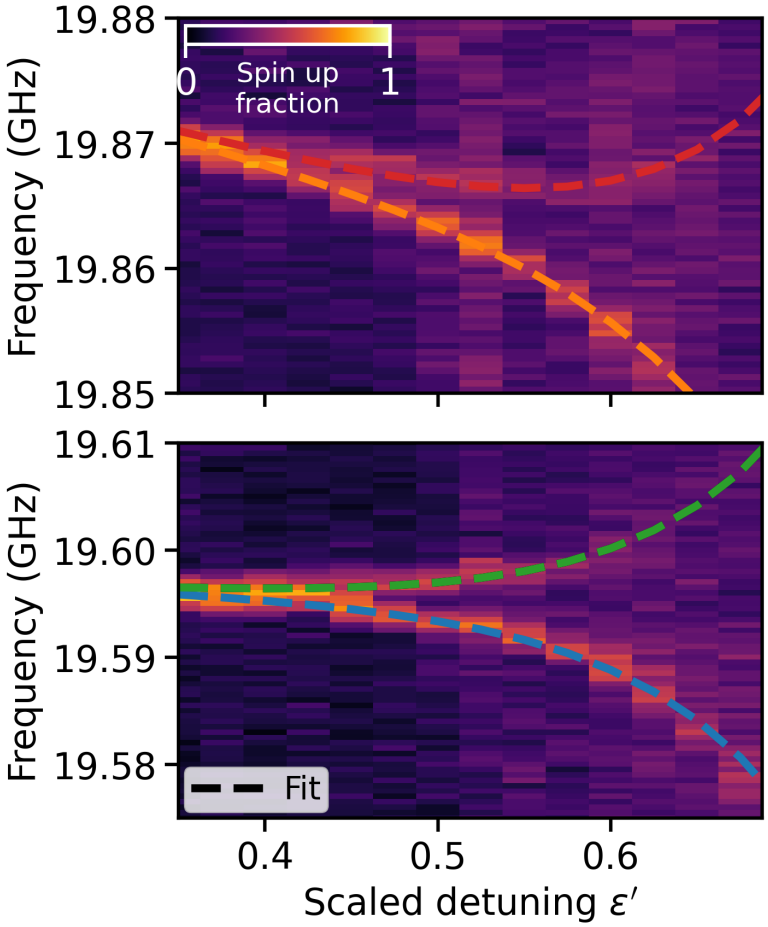

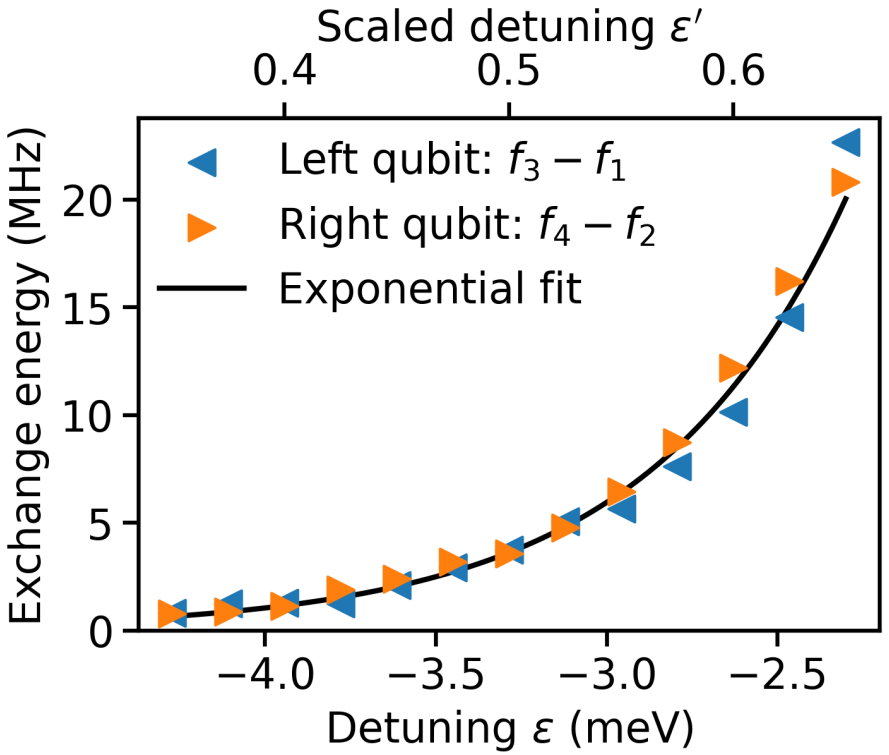

Conditional resonances

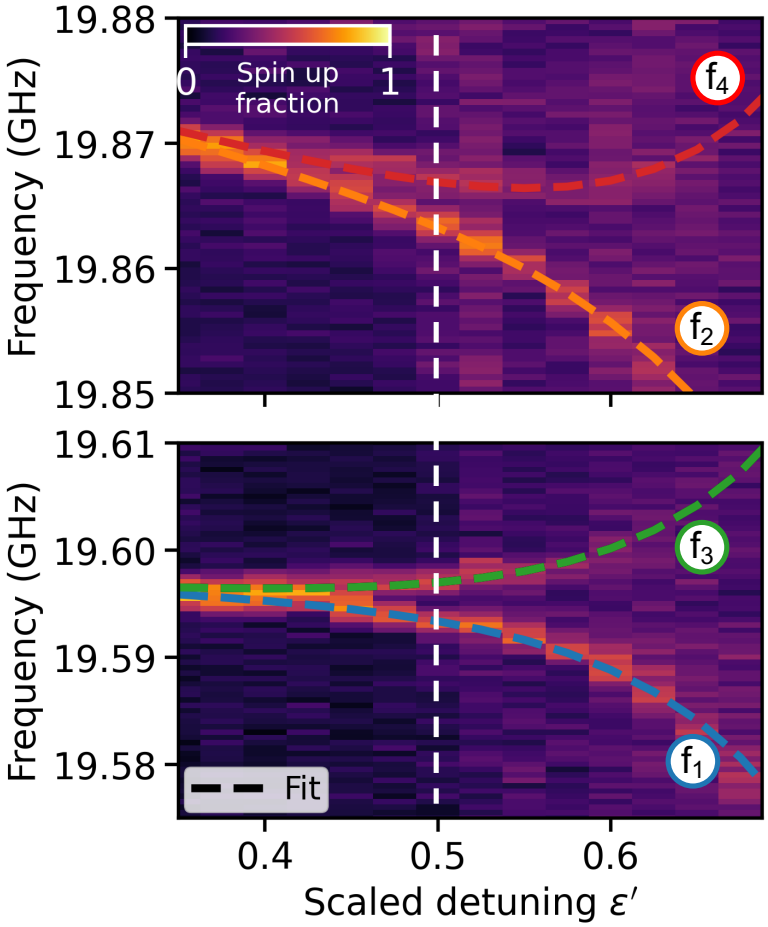

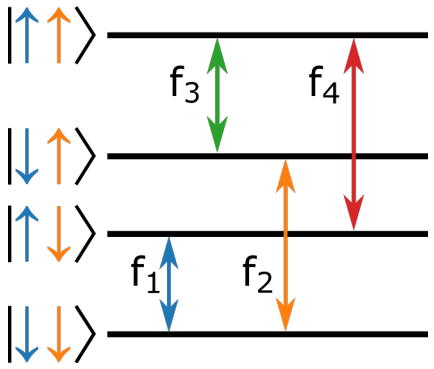

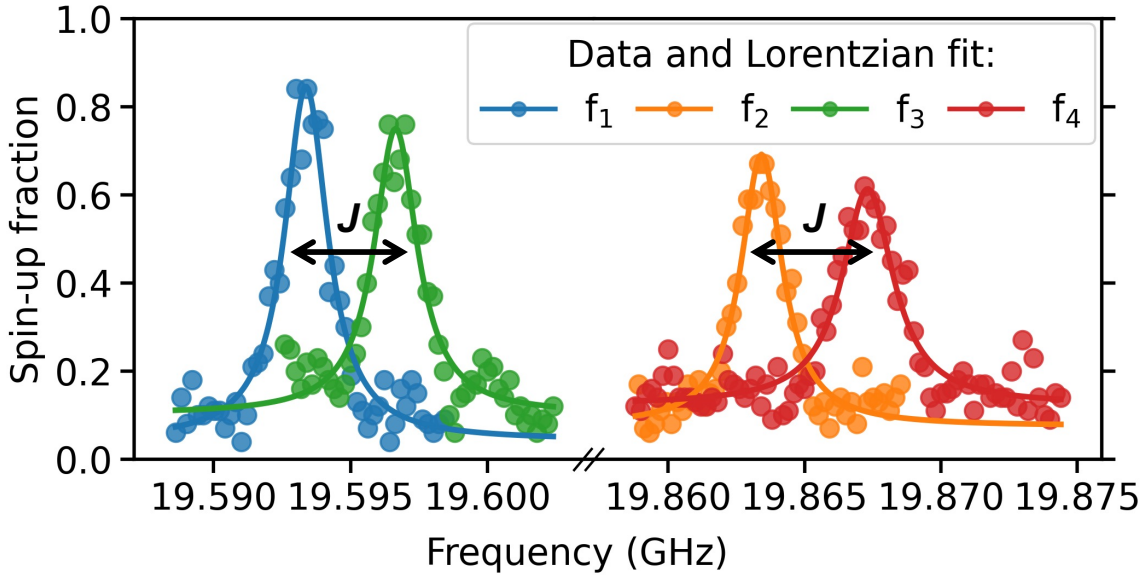

Conditional rotations (CROT)

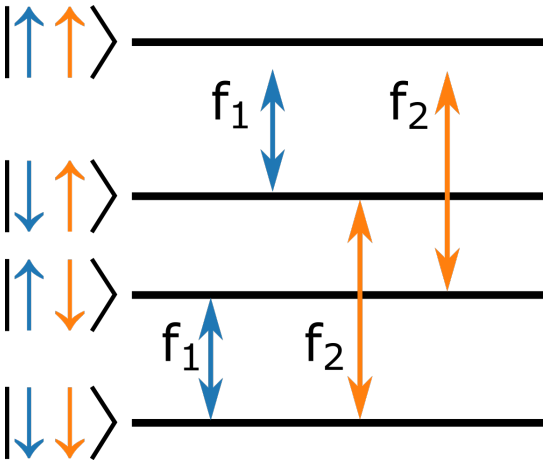

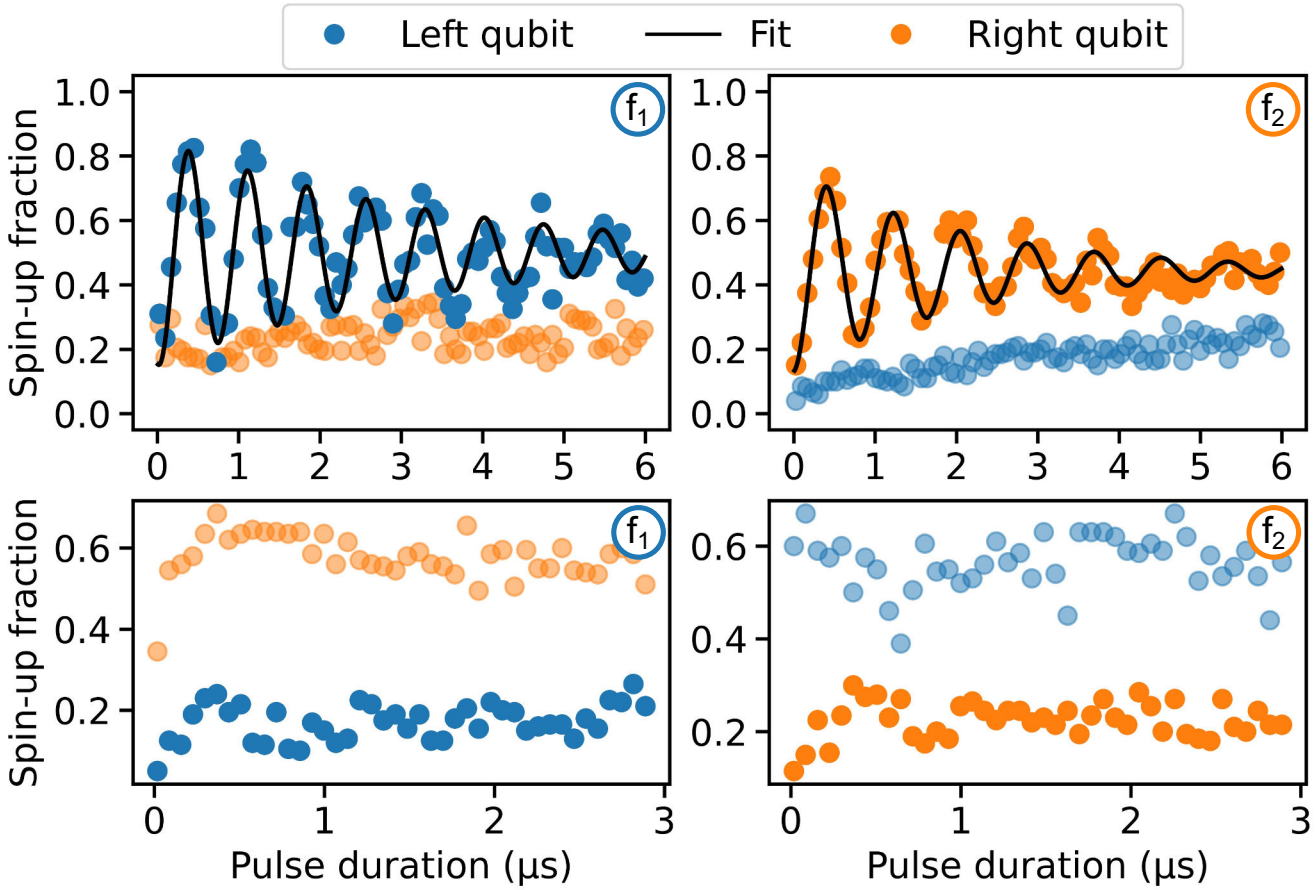

Conditional rotations (CROT)

Resonant CNOT gate!

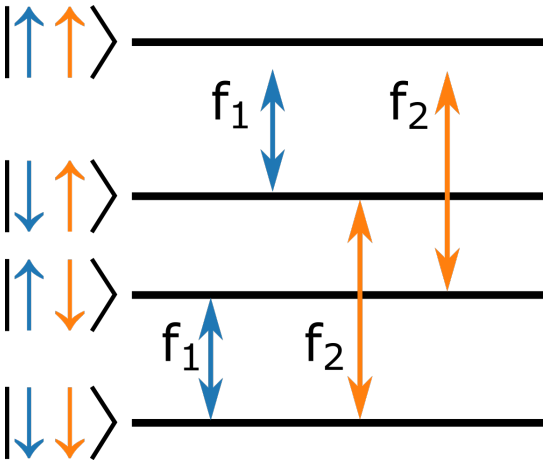

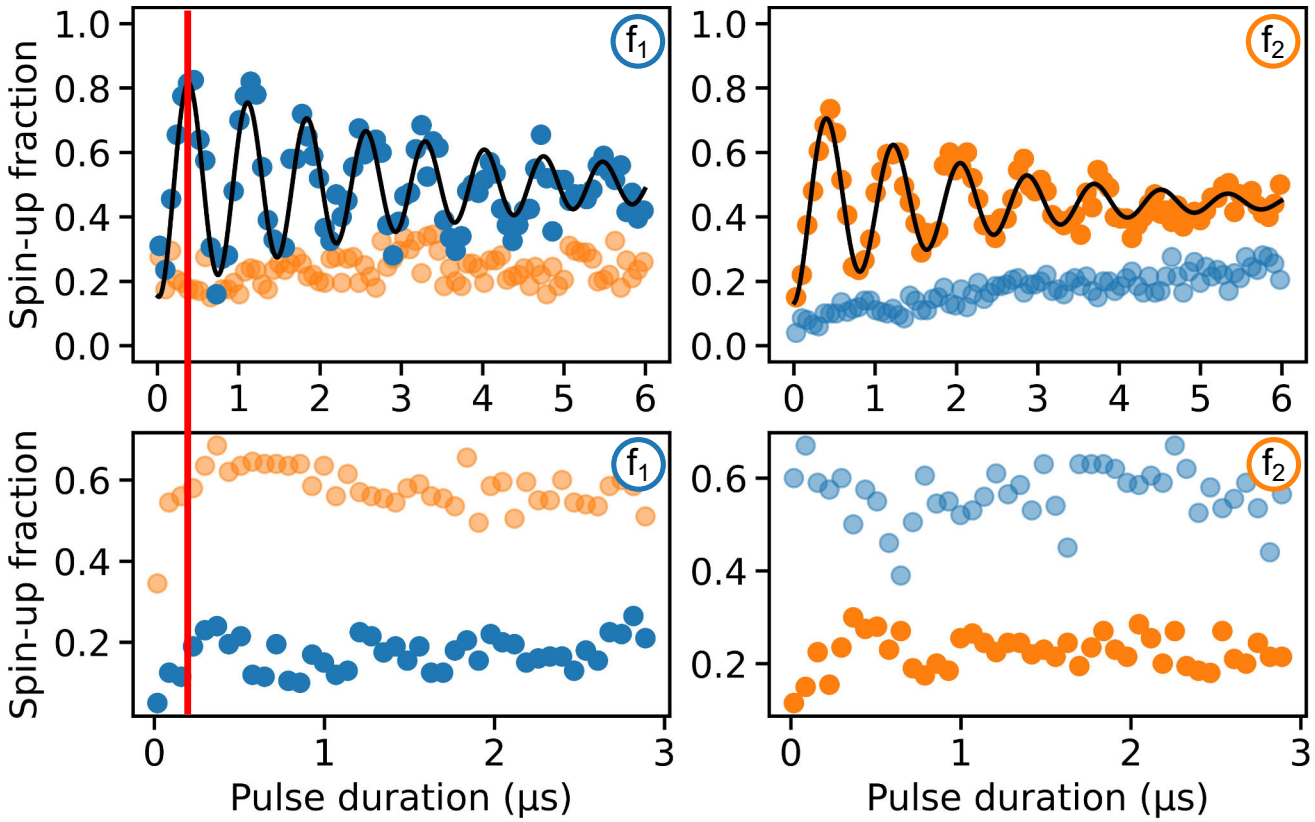

CROT with dynamical control qubit evolution

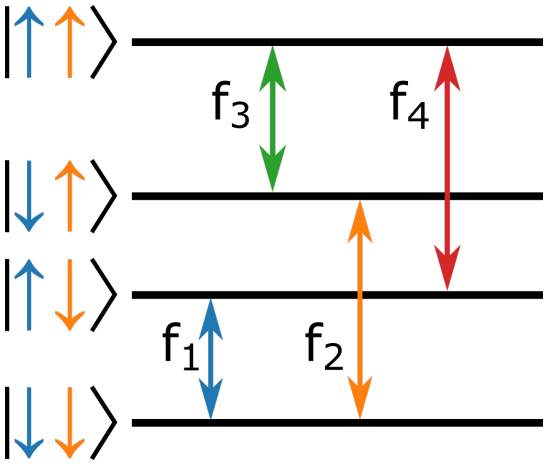

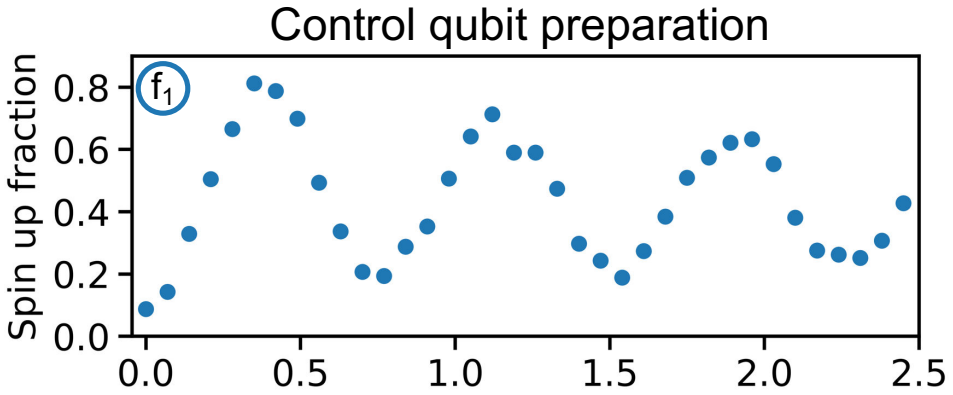

CROT with dynamical control qubit evolution

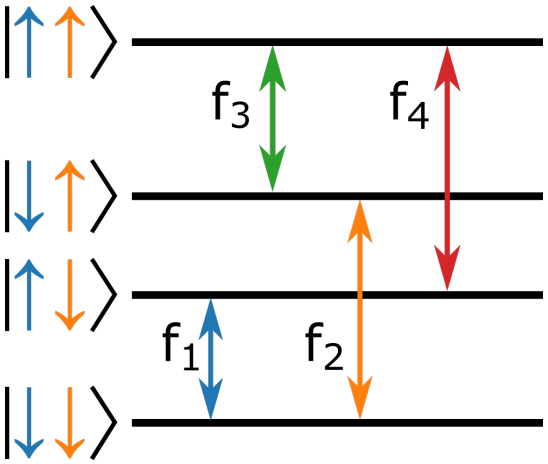

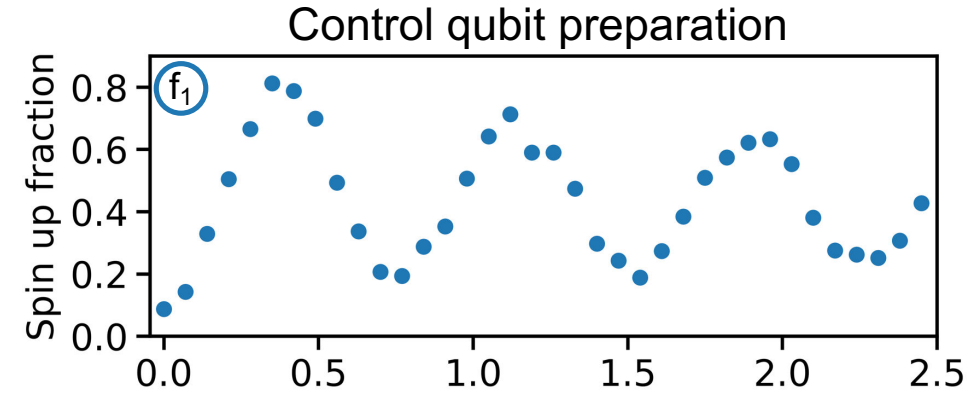

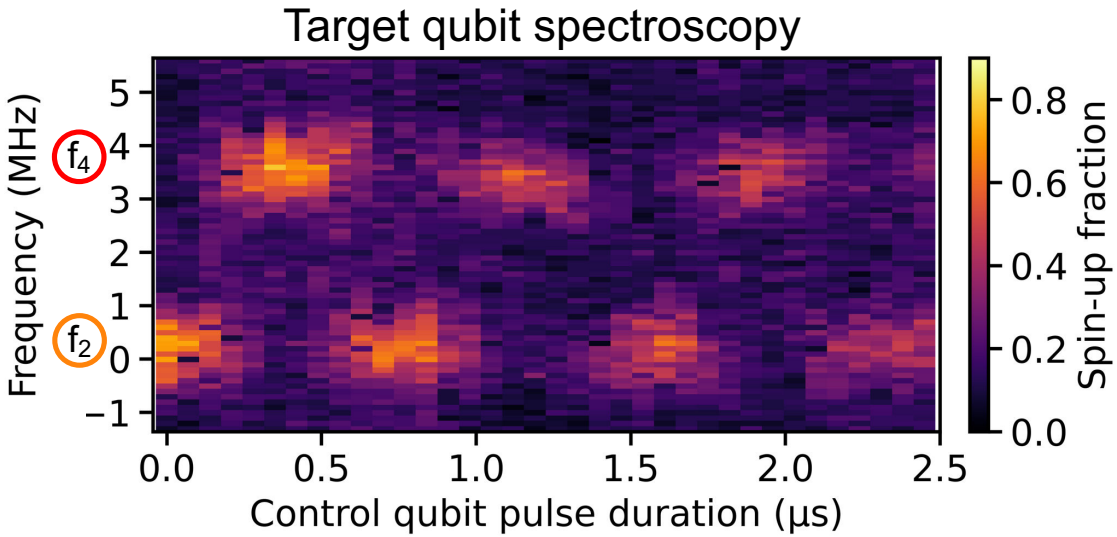

Coherent Two-Qubit Control in Industrial Si/SiGe Spin Qubits

☑ Tunable exchange interaction

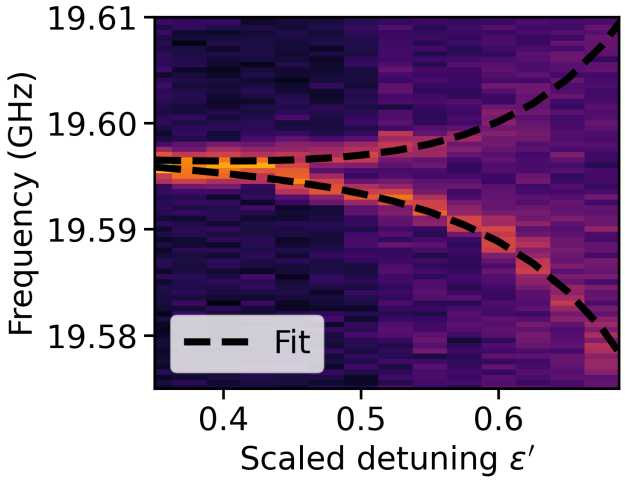

☑ Conditional two-qubit rotations

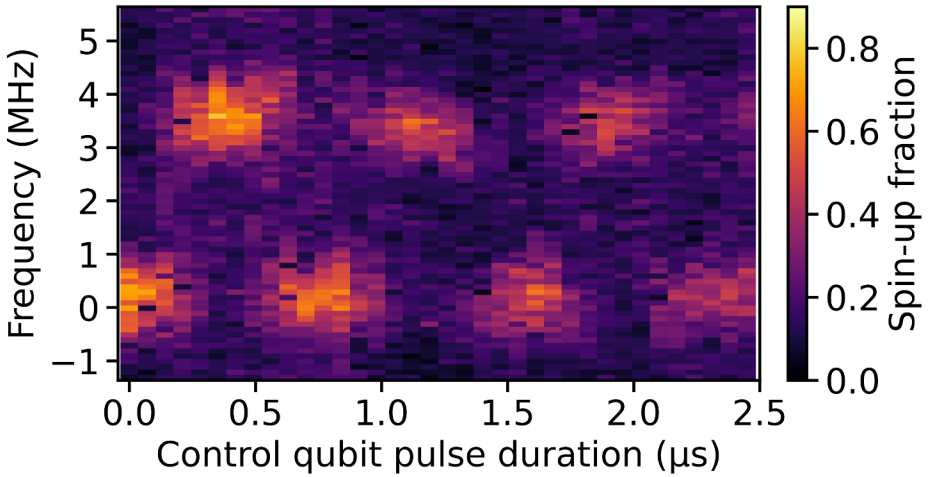

Industrial semiconductor processing is capable of multi-qubit quantum device fabrication

Viktor Adam, AG Wernsdorfer

Backup

Si/SiGe heterostructure

Simplified schematic

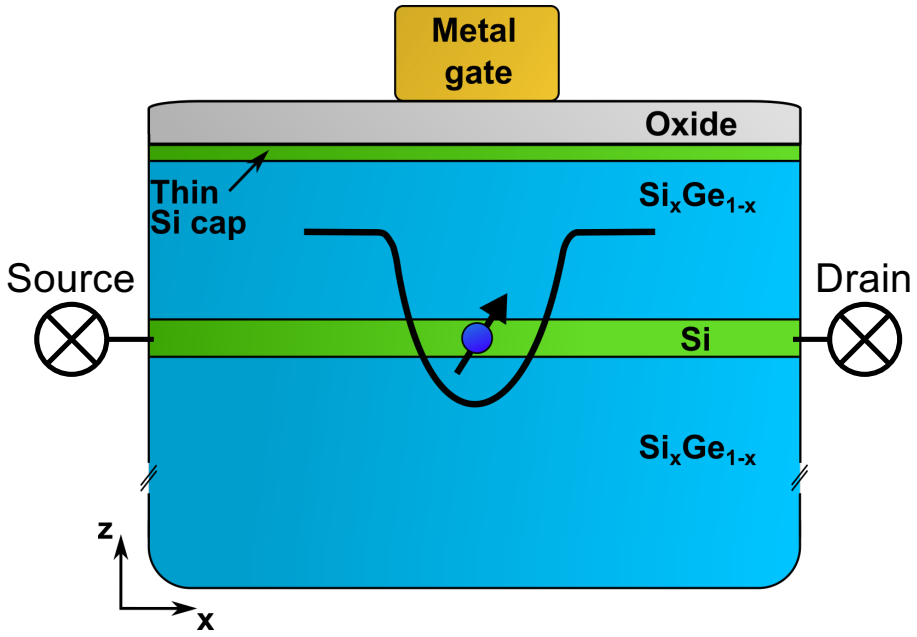

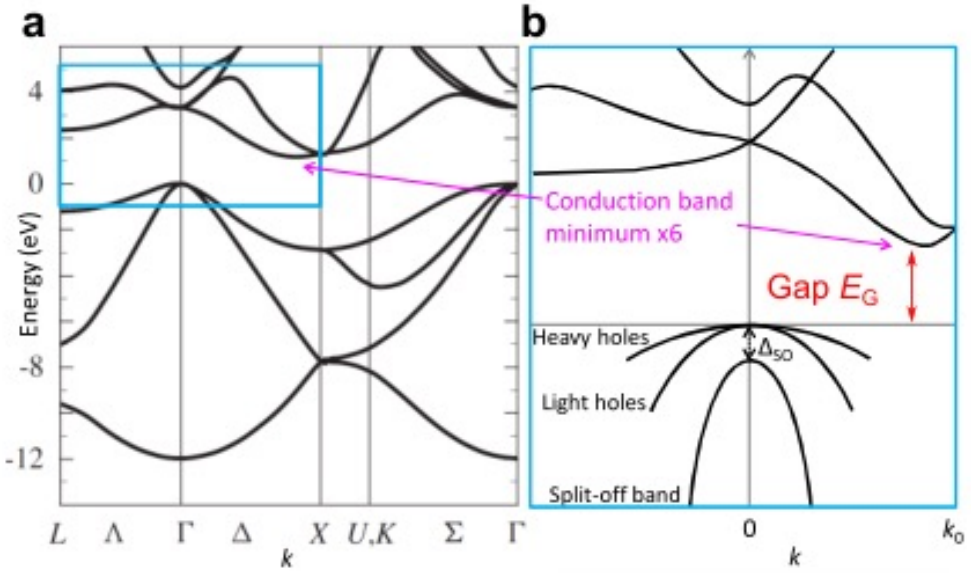

Cryogenic setup

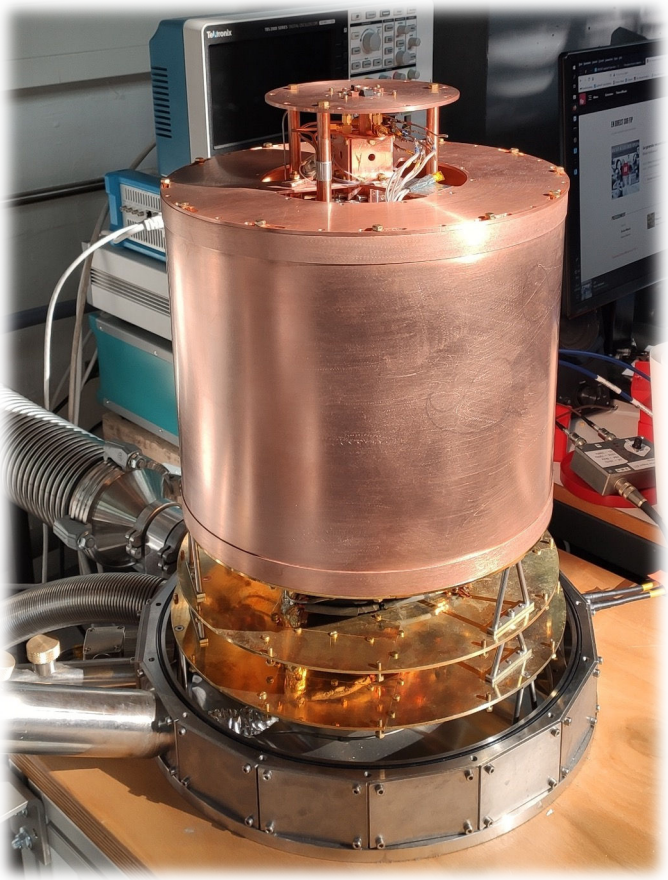

Qinu-type cryostat XL
“Obelix” 2021

Cooldown to < 100 mK
in 5.5 h

Base temperature < 30 mK

48 filtered DC lines

6 RF lines

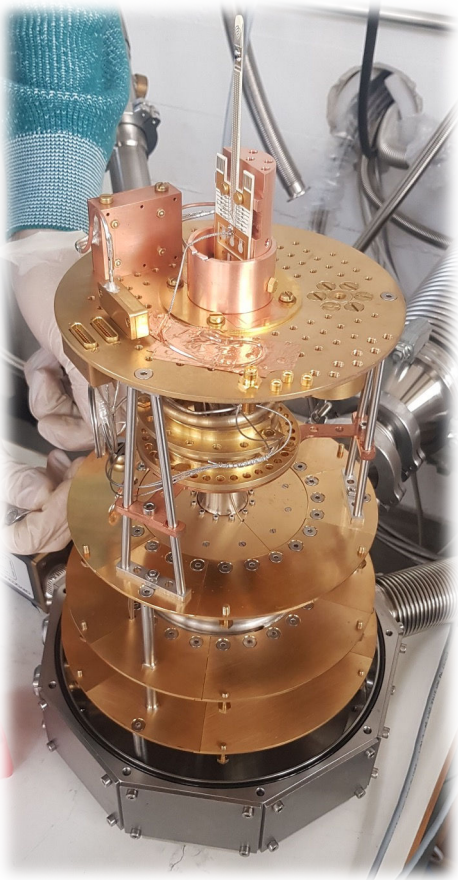

Qinu-type cryostat L
“Idefix” 2023

Cooldown to < 100 mK
in 3.5 h

Base temperature < 40 mK

54 filtered DC lines

13 RF lines

Our setup at KIT

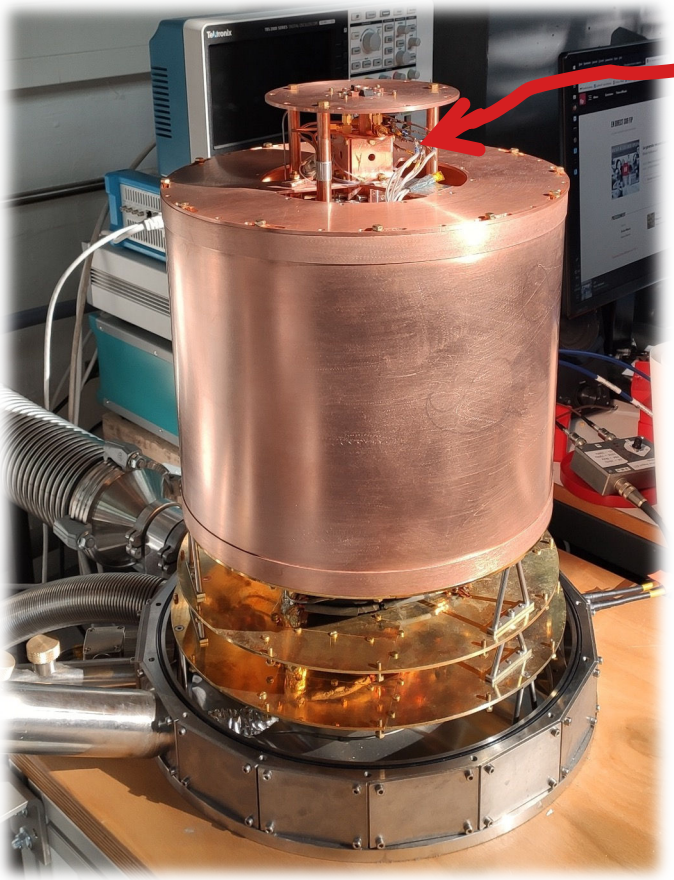

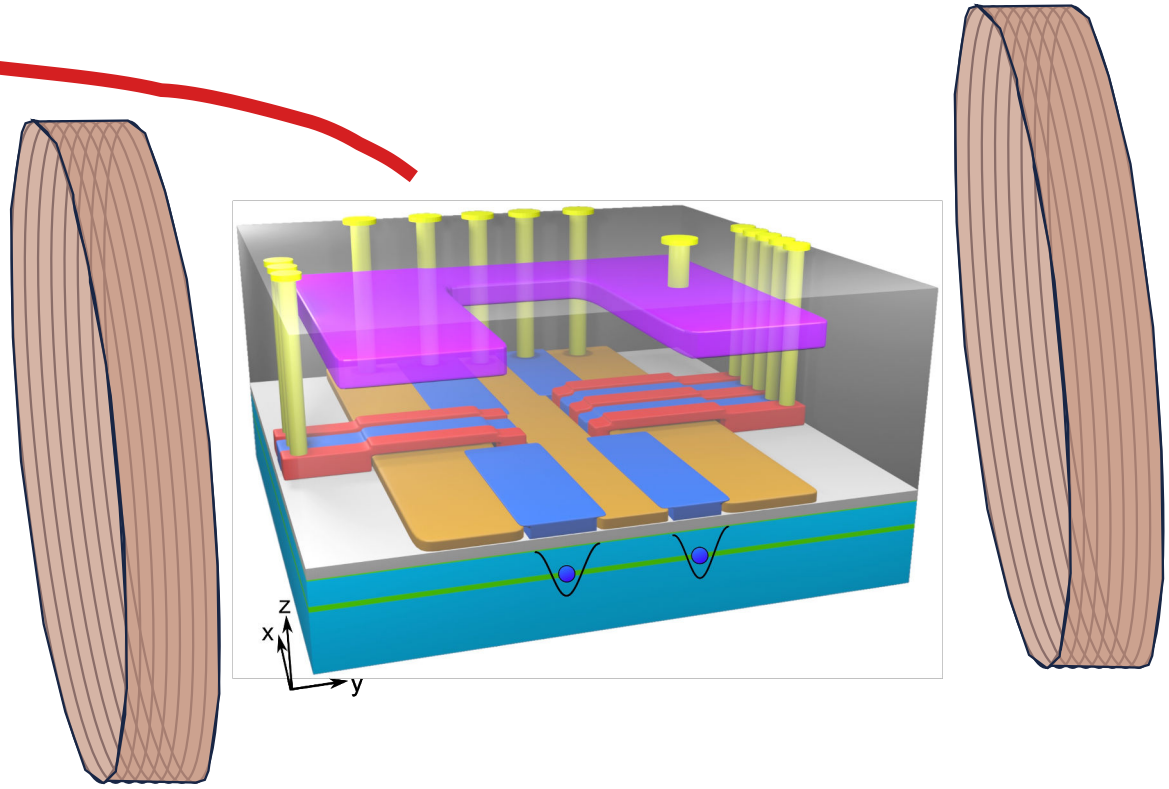

Table top cryostat Version L

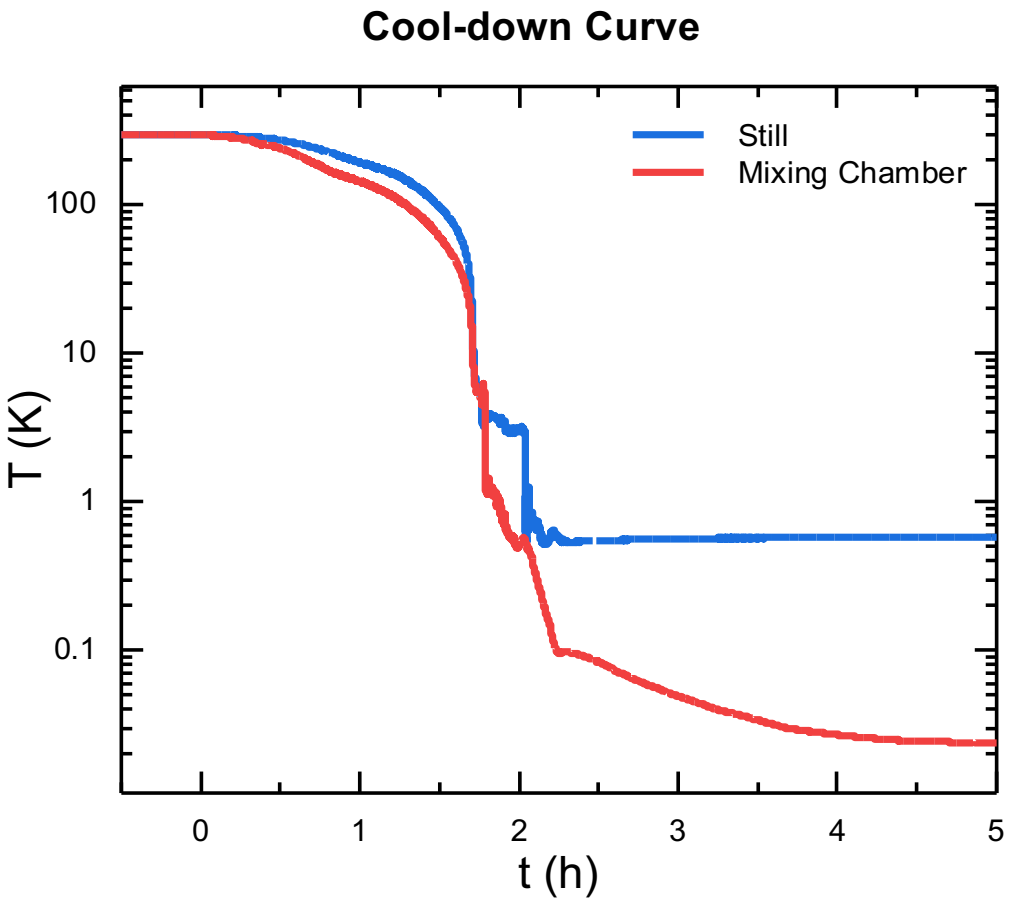

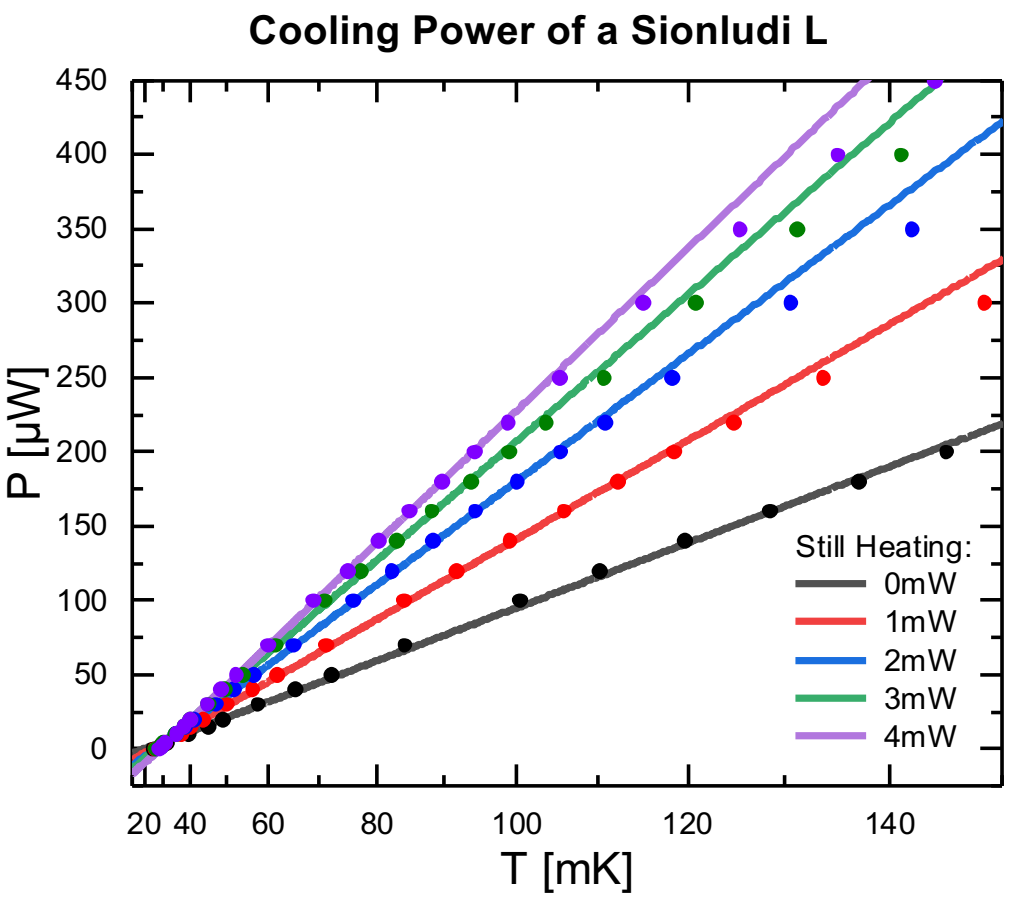

Two-qubit Si/SiGe device from imec

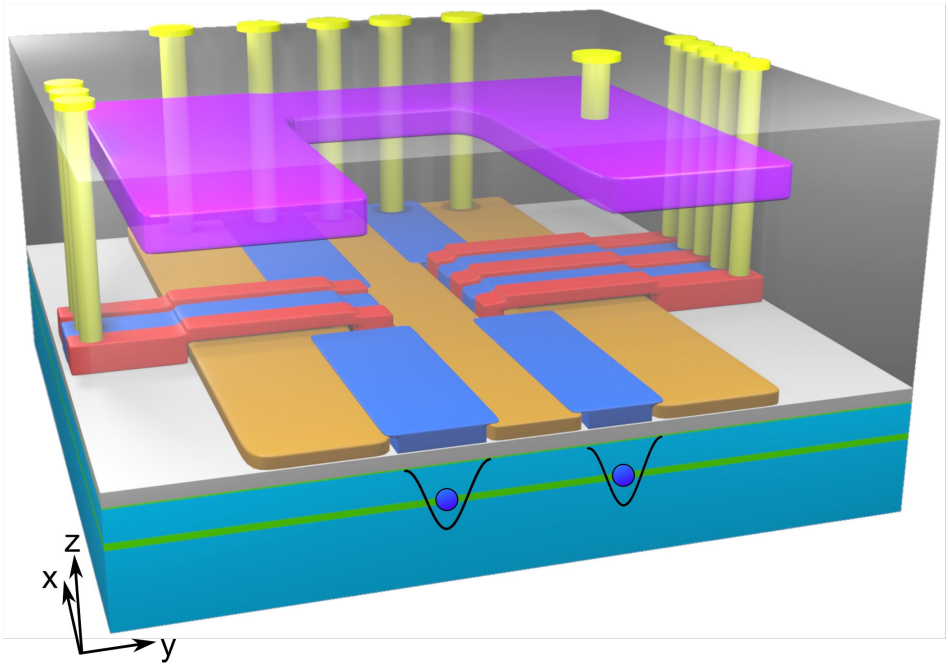

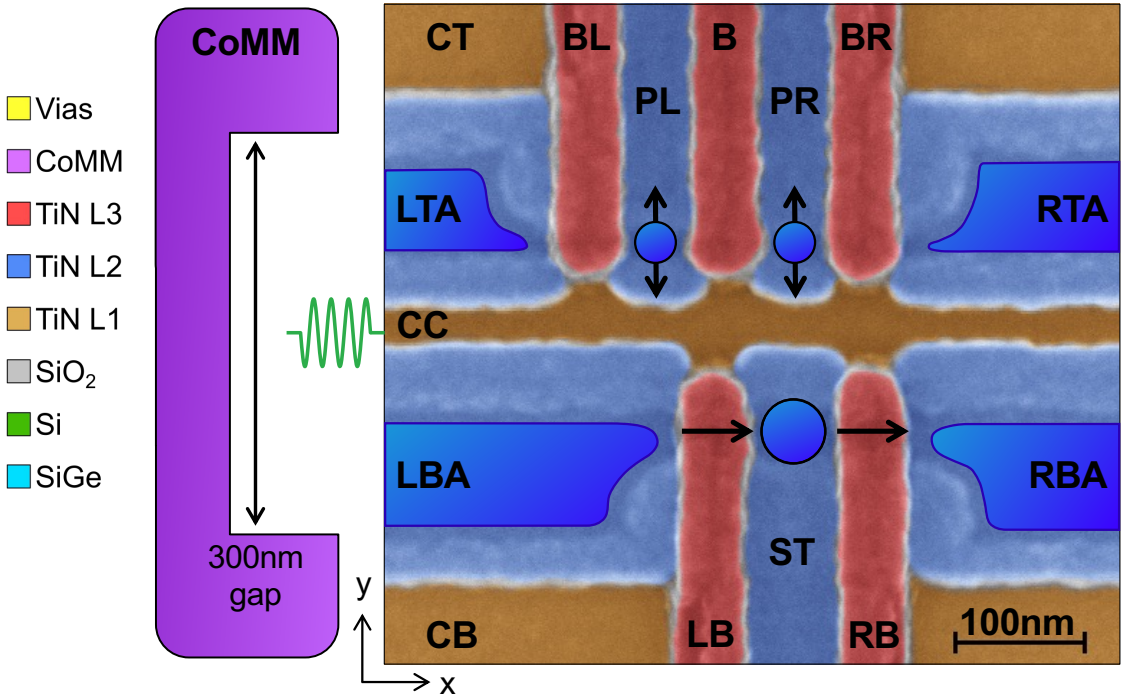

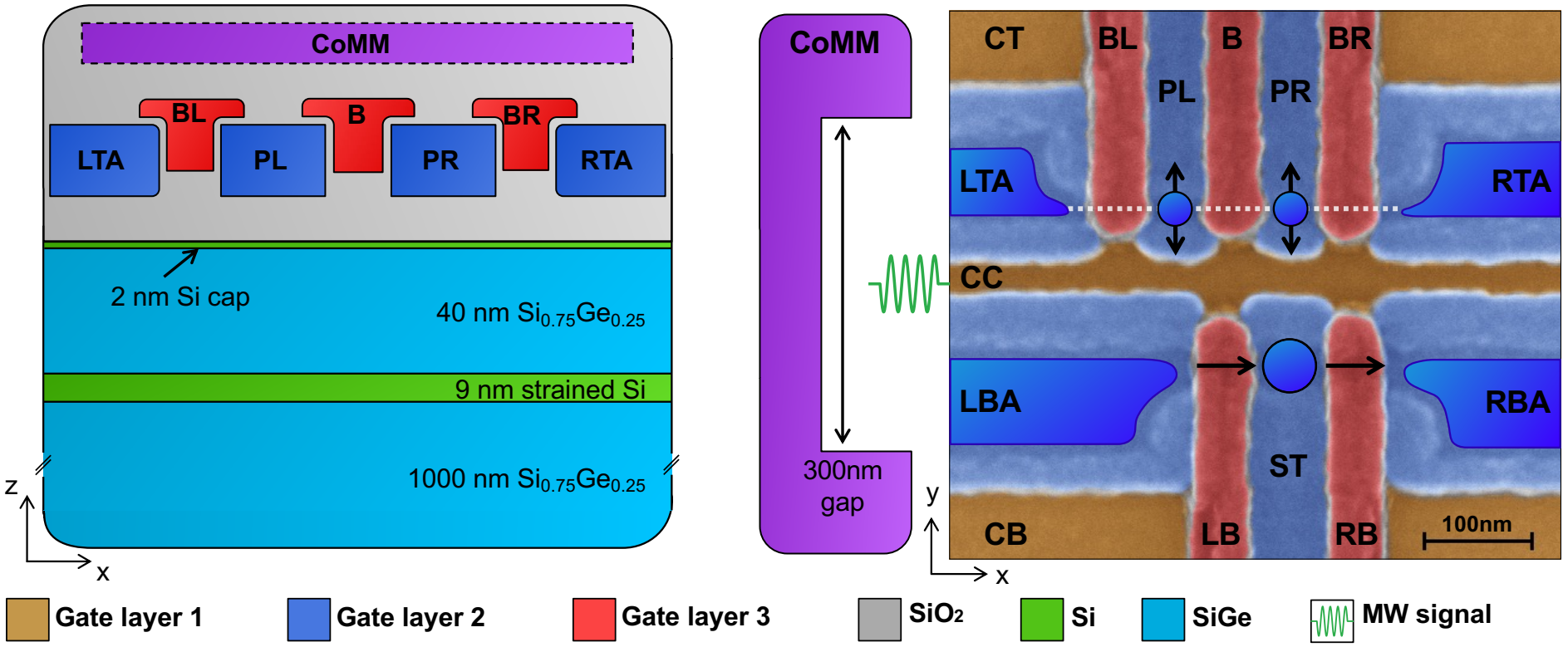
CoMM
BL
B
BR
LTA
PL
PR
RTA
2 nm Si cap
40 nm Si0.75Ge0.25
9 nm strained Si
1000 nm Si0.75Ge0.25
z
x
CoMM
300nm
gap
y
x
CT
BL
B
BR
PL
PR
LTA
RTA
CC
LBA
RBA
ST
CB
LB
RB
100nm
Gate layer 1
Gate layer 2
Gate layer 3
SiO2
Si
SiGe
MW signal

Charge noise

4 points to extract charge noise

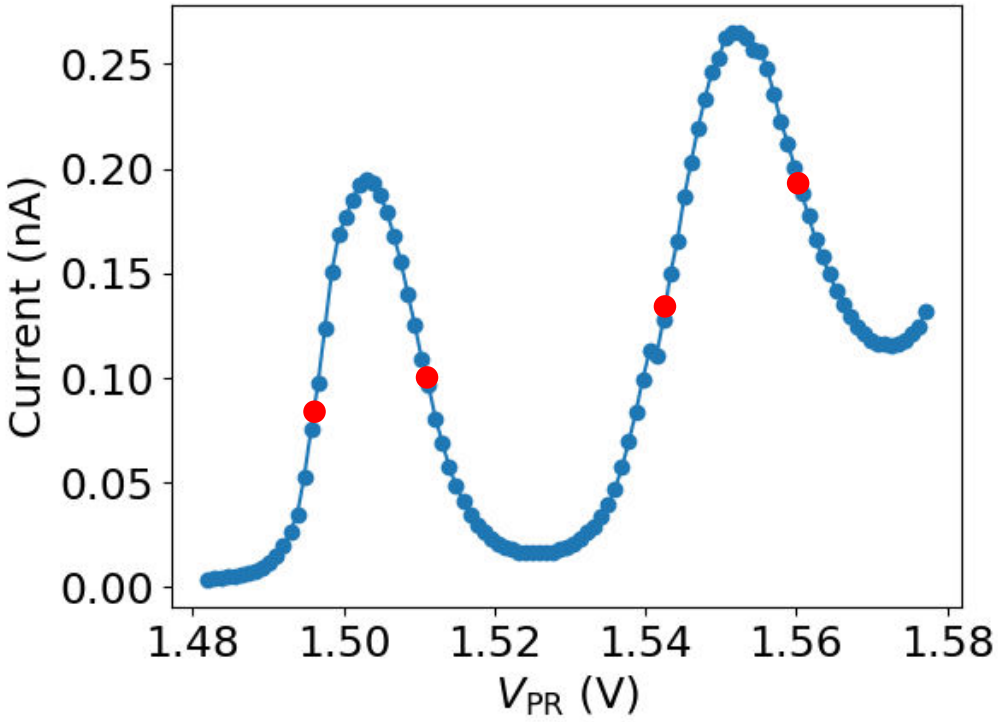

FFT from 5 min timetrace

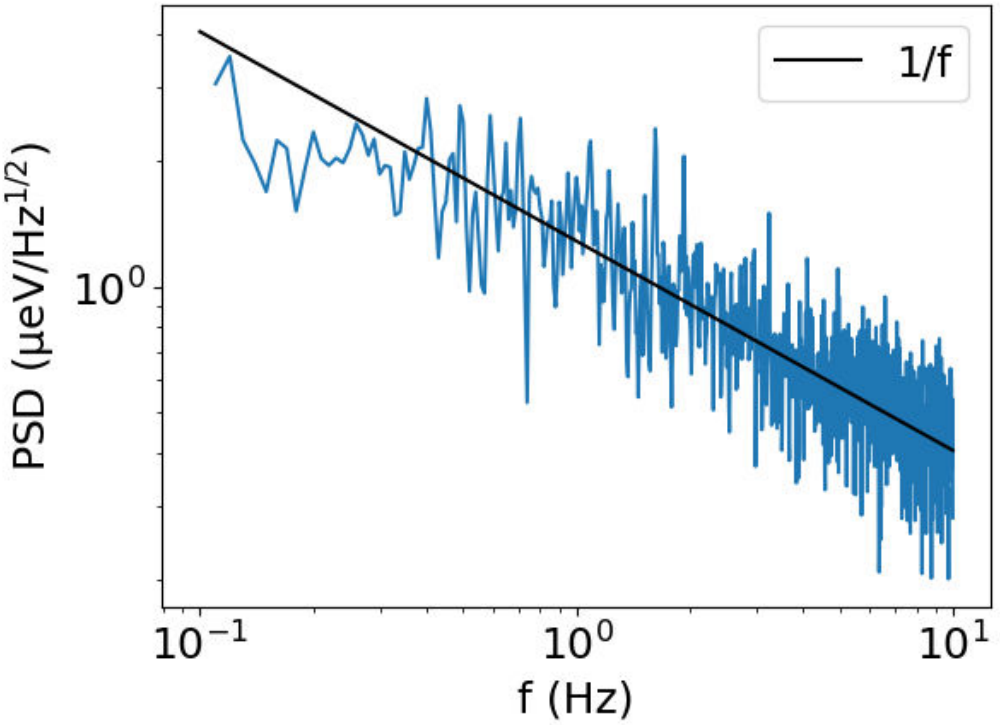

Mean 1Hz noise: $(\mathbf{1.36 \pm 0.07})\ \boldsymbol{\mu eV/\sqrt{Hz}}$

Also see: Elsayed, A. et al. (2024) Low charge noise quantum dots with industrial CMOS manufacturing.

Silicon based heterostructures for quantum computing

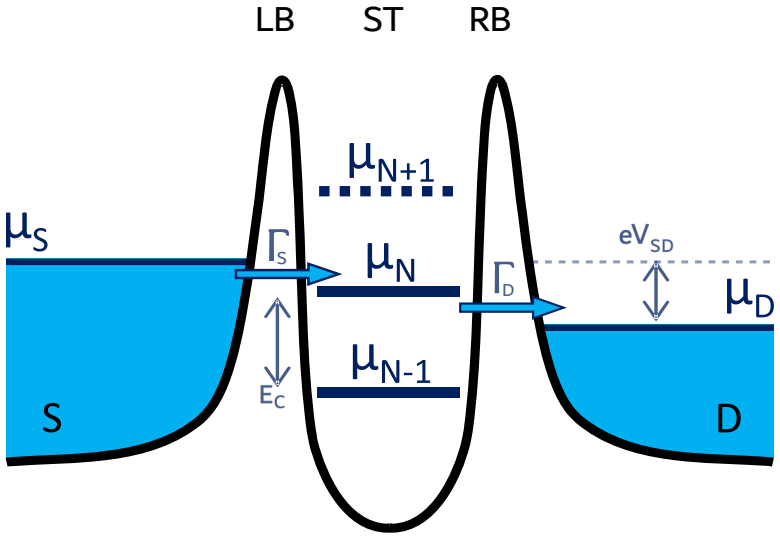

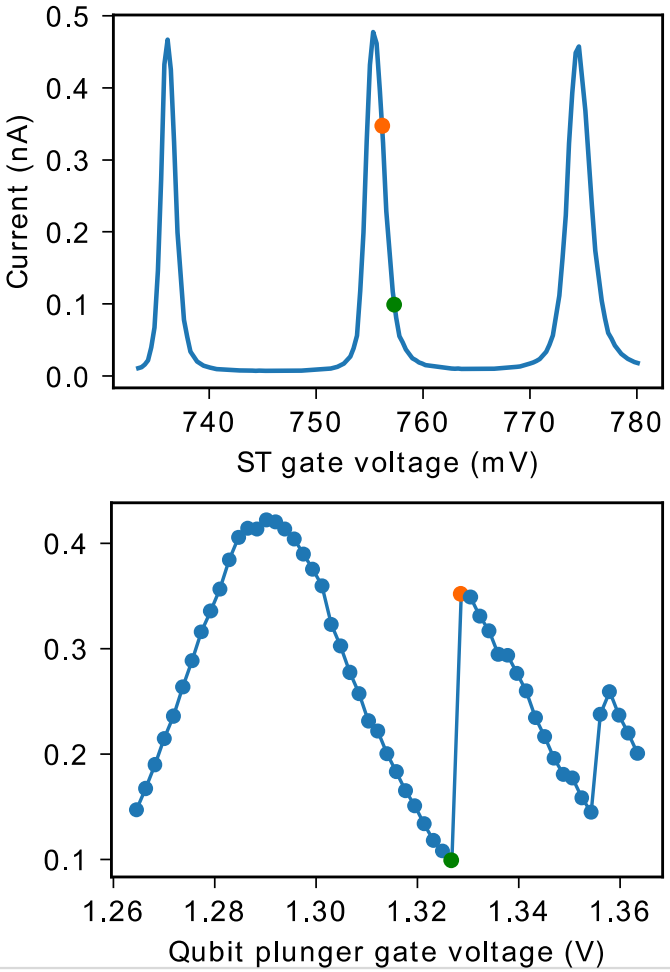

Spin to charge conversion

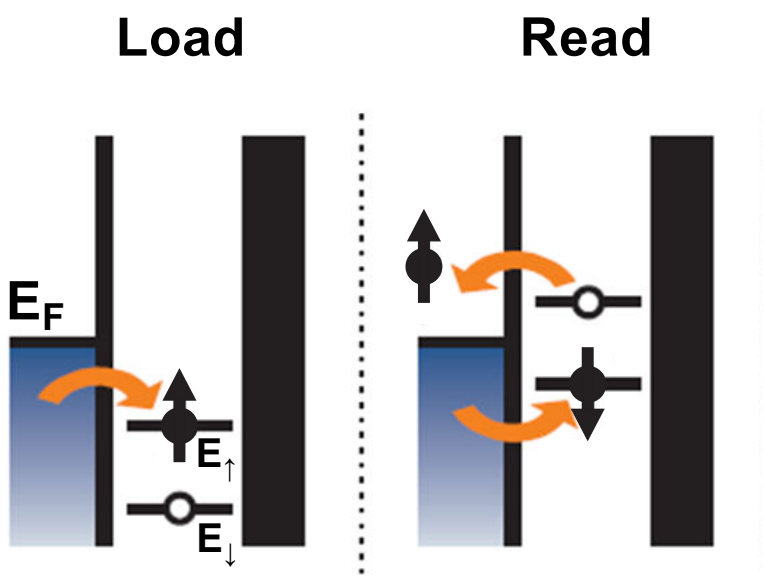

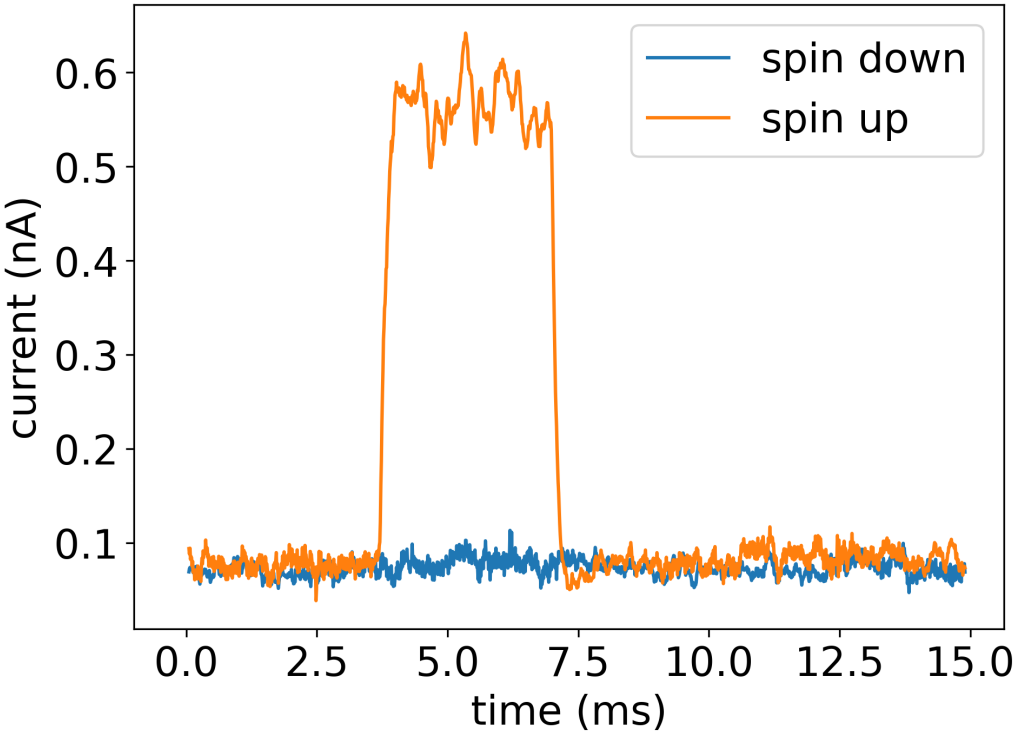

[Elzerman et al. 2004, Nature]

Spin to charge conversion

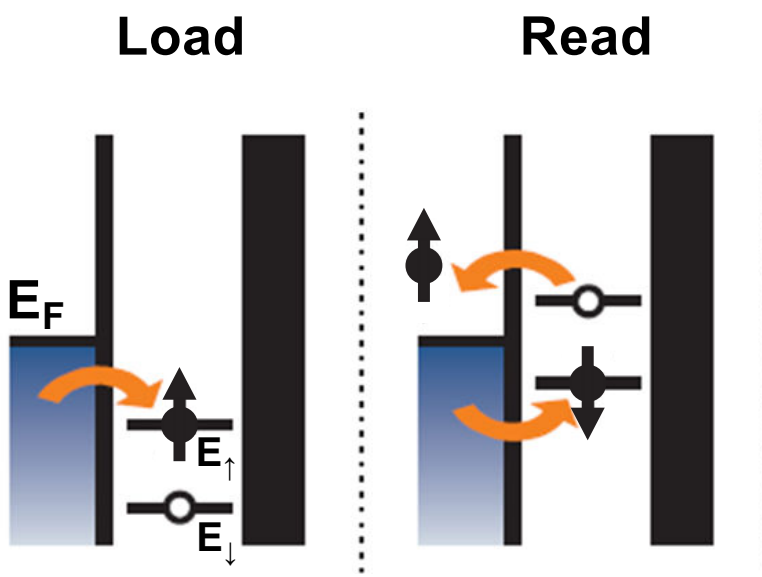

[Elzerman et al. 2004, Nature]

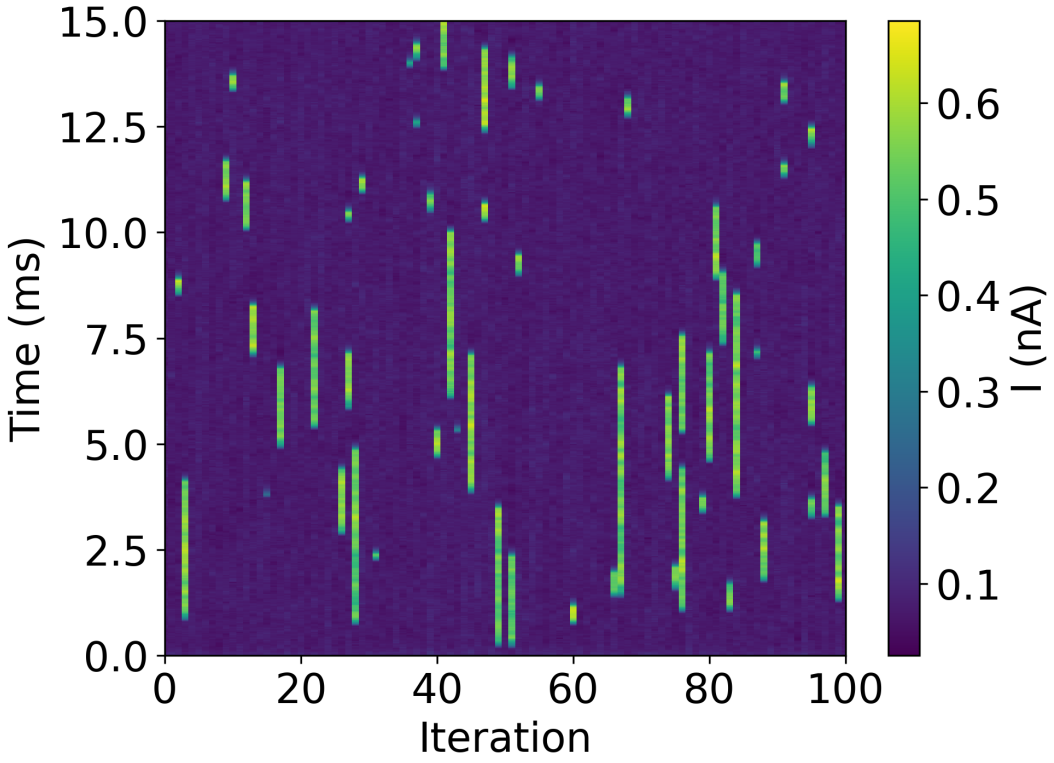

100 single shot measurements

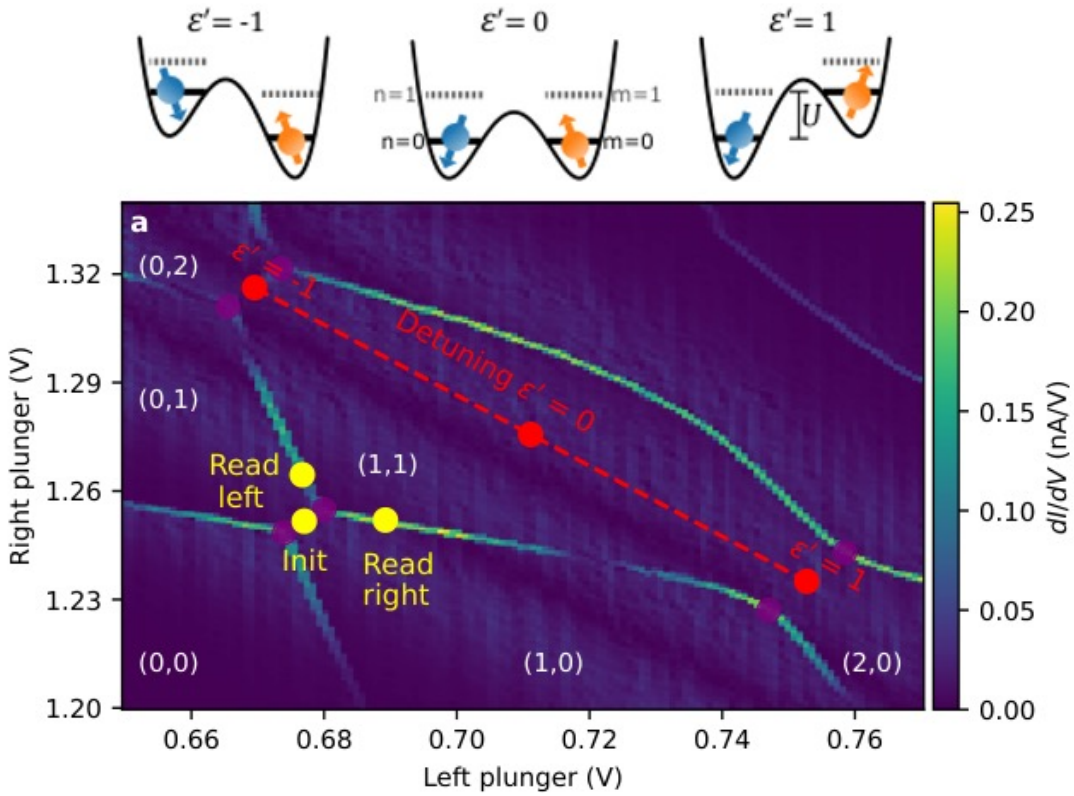
ε′ = -1
ε′ = 0
ε′ = 1
n=1
n=0
m=1
m=0
U
a
(0,2)
(0,1)
(0,0)
(1,1)
(1,0)
(2,0)
Read left
Init
Read right
Detuning ε′ = 0
ε′ = -1
ε′ = 1
Right plunger (V)
Left plunger (V)
dI/dV (nA/V)
1.32
1.29
1.26
1.23
1.20
0.66
0.68
0.70
0.72
0.74
0.76
0.25
0.20
0.15
0.10
0.05
0.00

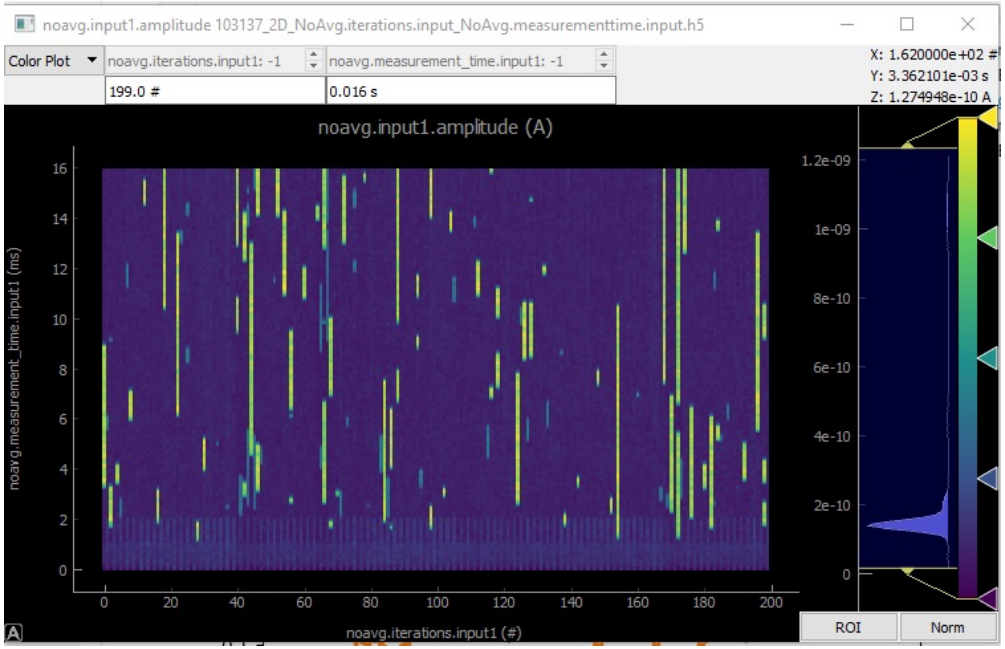
noavg.input1.amplitude 103137_2D_NoAvg.iterations.input_NoAvg.measurementtime.input.h5
Color Plot
noavg.iterations.input1: -1
noavg.measurement_time.input1: -1
199.0 #
0.016 s
X: 1.620000e+02 #
Y: 3.362101e-03 s
Z: 1.274948e-10 A
noavg.input1.amplitude (A)
noavg.measurement_time.input1 (ms)
noavg.iterations.input1 (#)
ROI
Norm

Two individually addressable spin qubits

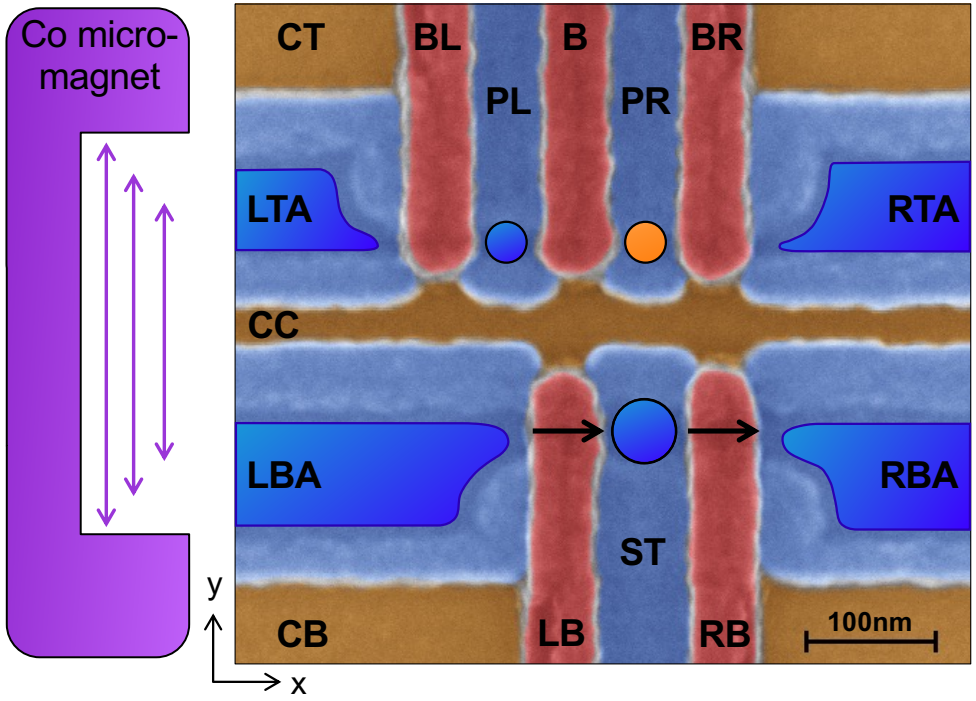

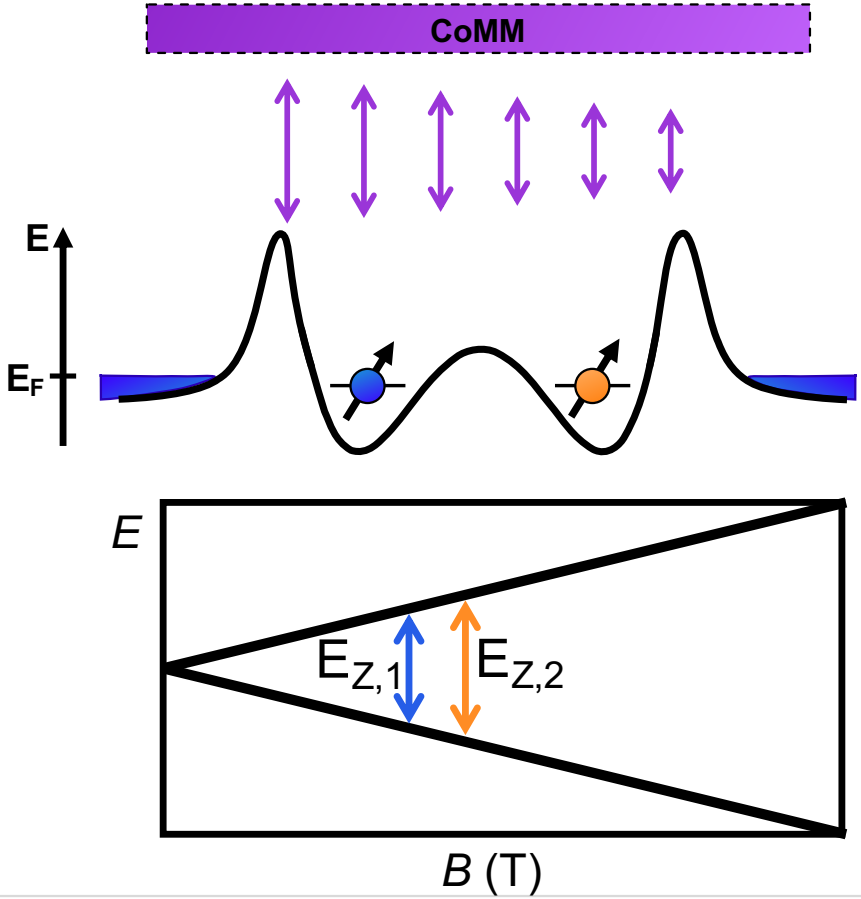

Single qubit operations

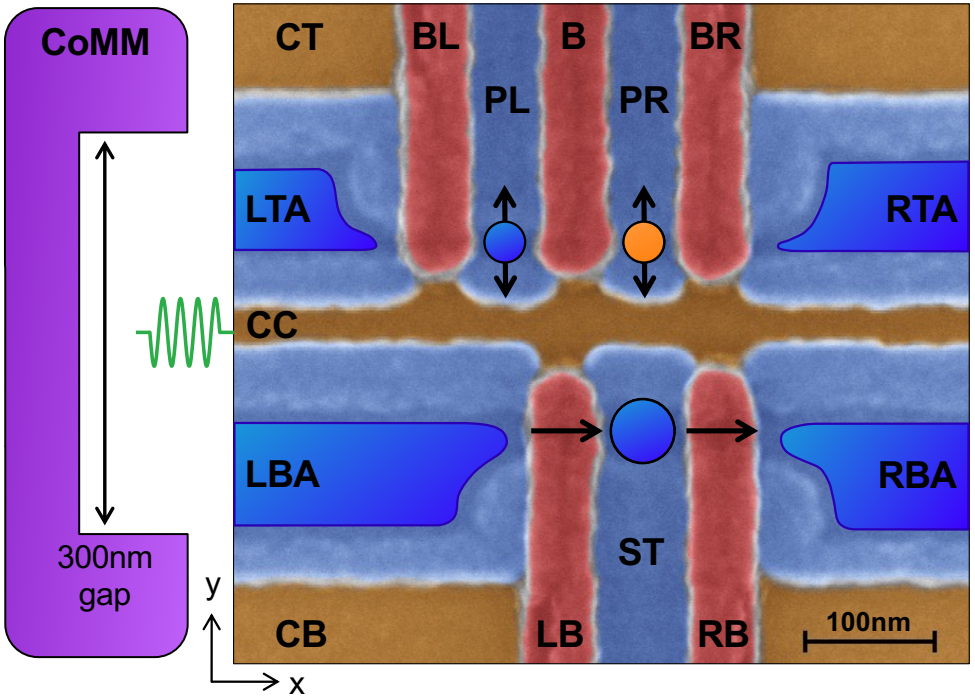

Parameter	Left Qubit	Right Qubit
Maximum visibility (%)	90	74
Rabi frequency f_{Rabi} (MHz)	1.43	1.50
Rabi coherence time $T_{2,\mathrm{Rabi}}$ (µs)	6.17 ± 0.88	3.79 ± 0.50
Ramsey coherence time T_2^* (µs)	1.13 ± 0.11	1.04 ± 0.10
Hahn-echo coherence time T_2^{HE} (µs)	79.00 ± 1.54	31.85 ± 2.03
Hahn-echo exponent β	2.02 ± 0.11	1.38 ± 0.16

Semiconductor based qubits

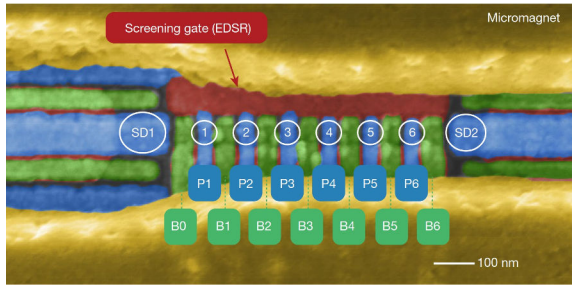

[Philips, et al., Nature 609, 919–924 (2022)]

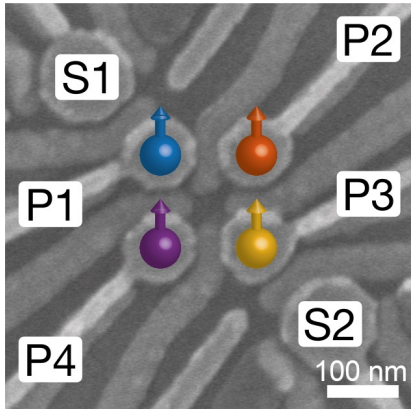

[Hendrickx, et al., Nature 591, 580–585 (2021)]

- Two qubit gate fidelity > 99%

  [Noiri, A. et al., *Nature* **601**, 338–342 (2022)]

- Two qubit logic at 1.1 K

  [Petit, L et al., *Nature* **580**, 355–359 (2020)]

- High Qubit density in 2D grids

  [Hendrickx, et al., Nature 591, 580–585 (2021)]

- CMOS compatible

  [Maurand, R. et al., Nat Commun 7, 13575 (2016)]

Shuttling
Cryo-CMOS

Cobalt micromagnet

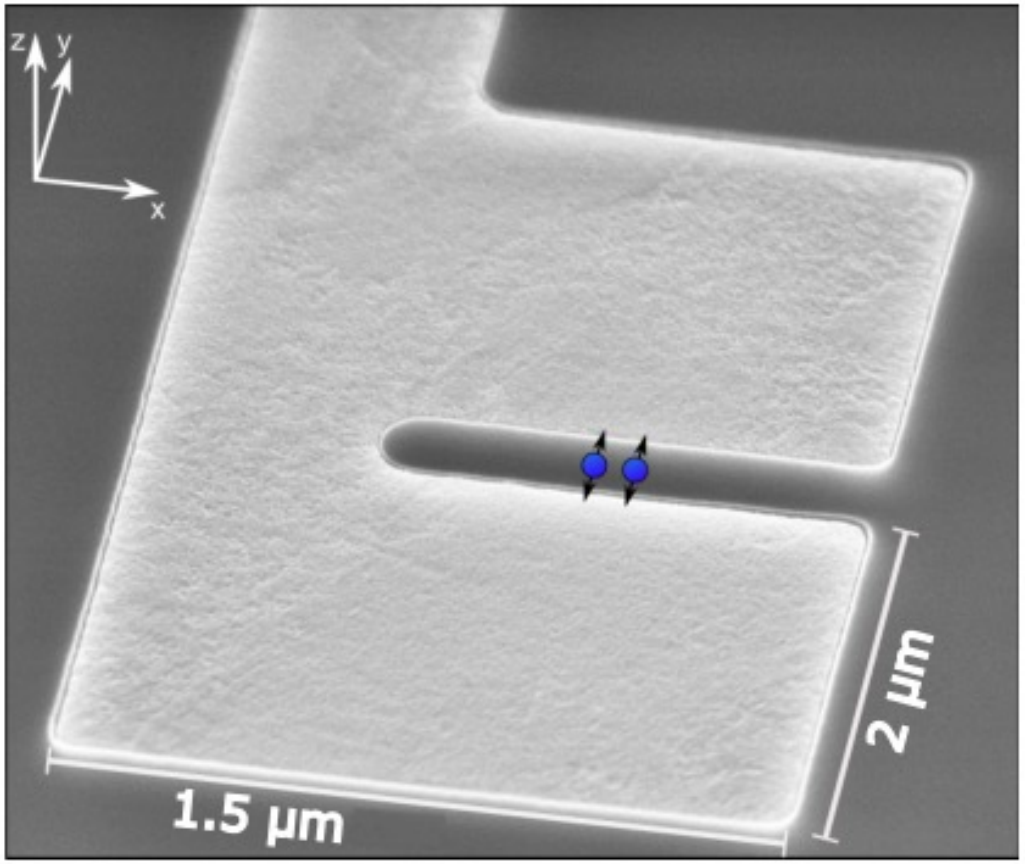

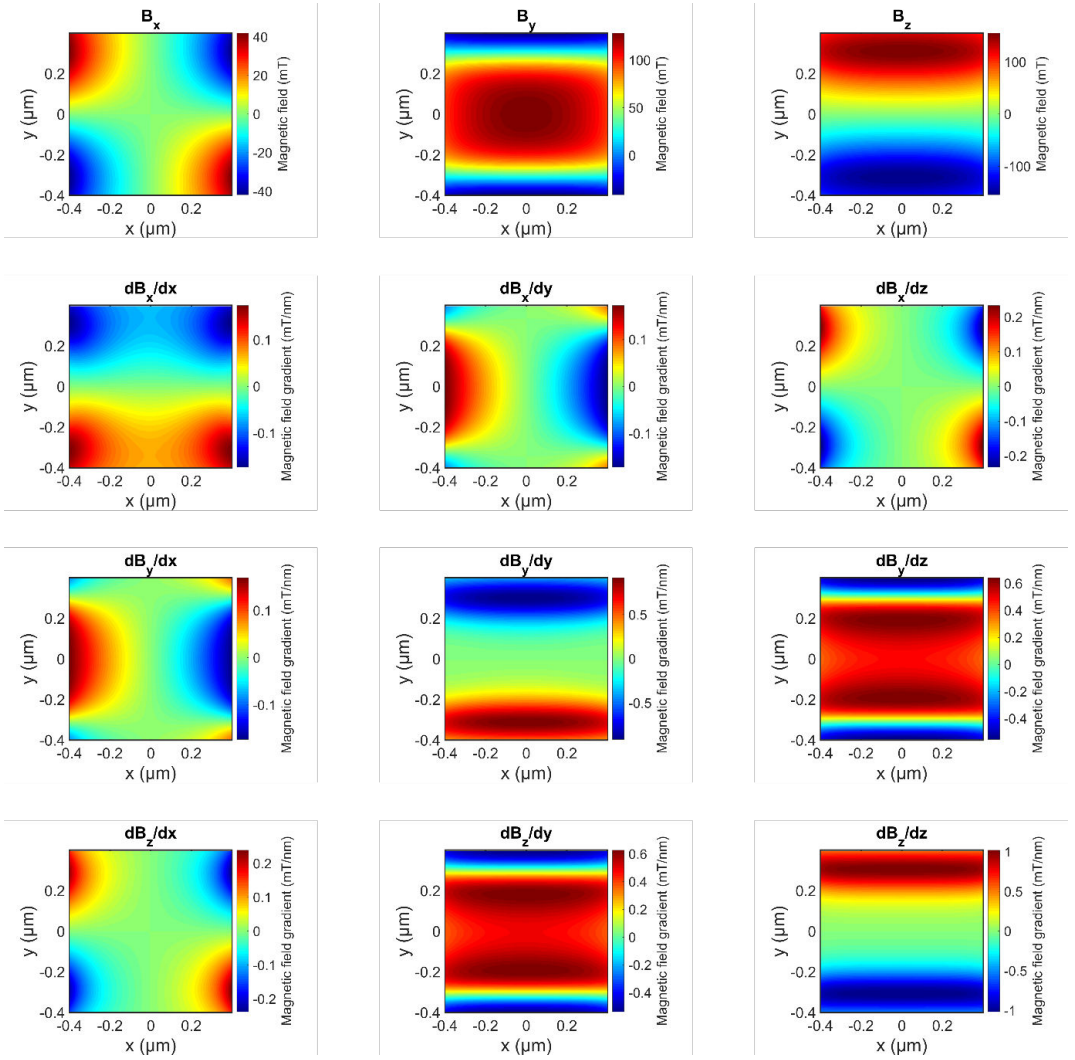

Stuyck *et al., Appl. Phys. Lett.* 119 (2021)

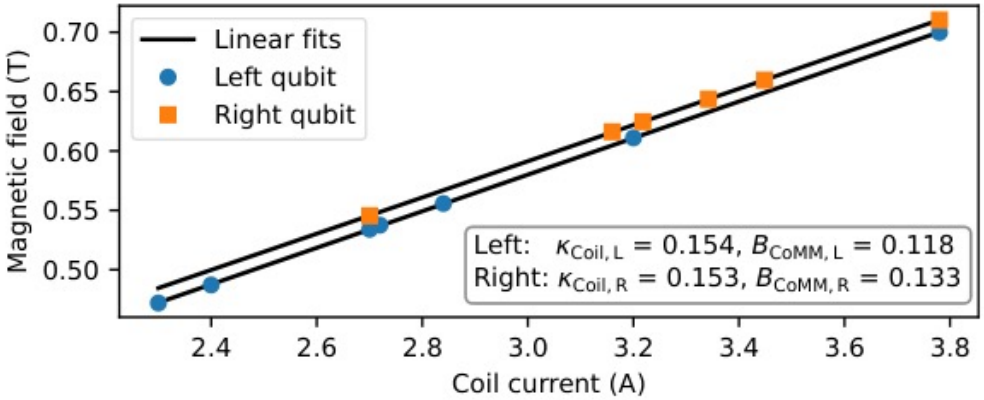
Linear fits
Left qubit
Right qubit
Left: $\kappa_{\mathrm{Coil,L}} = 0.154$, $B_{\mathrm{CoMM,L}} = 0.118$
Right: $\kappa_{\mathrm{Coil,R}} = 0.153$, $B_{\mathrm{CoMM,R}} = 0.133$
Magnetic field (T)
Coil current (A)

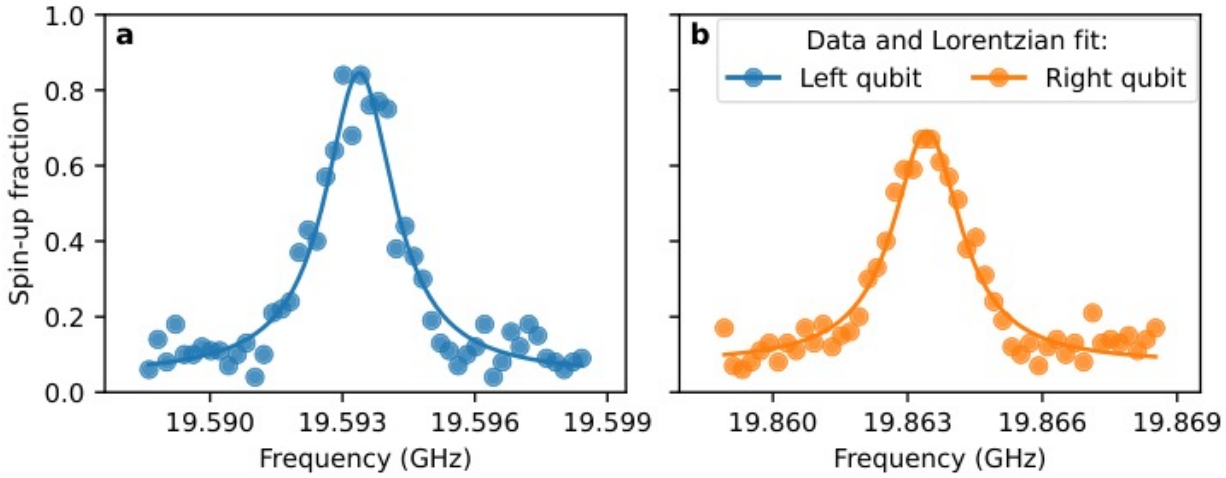
a
b
Data and Lorentzian fit:
Left qubit
Right qubit
Spin-up fraction
Frequency (GHz)
Frequency (GHz)

Sequential two-qubit control and readout

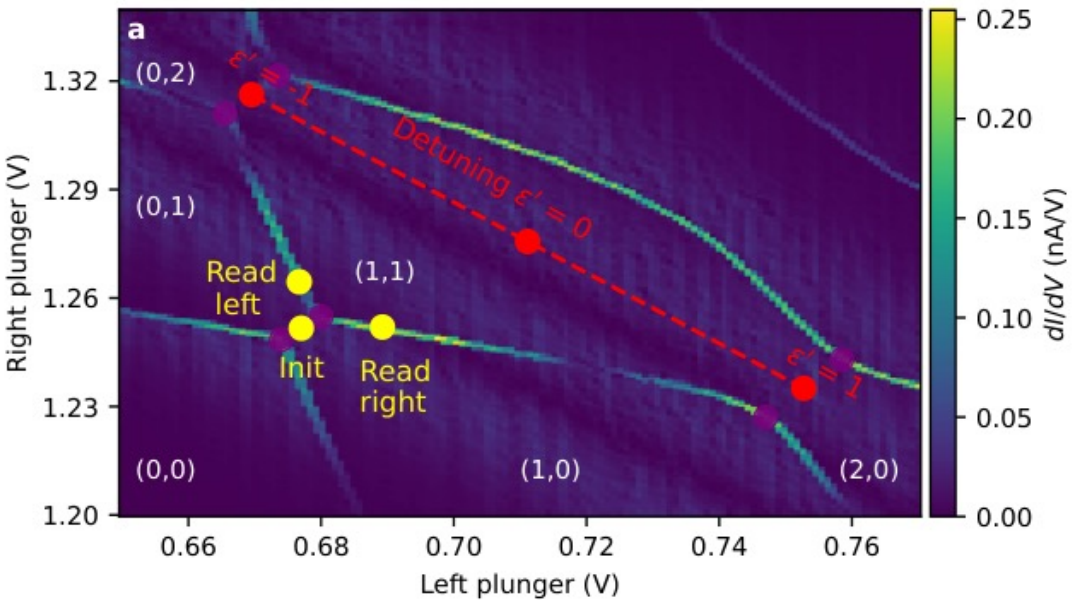

Measurement sequence:

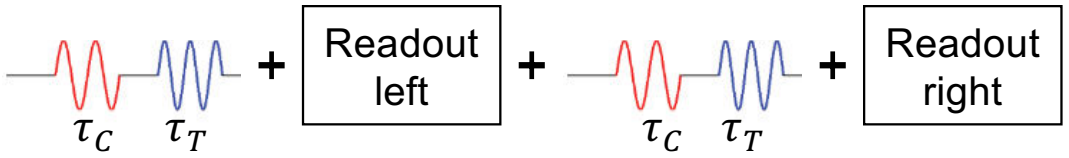

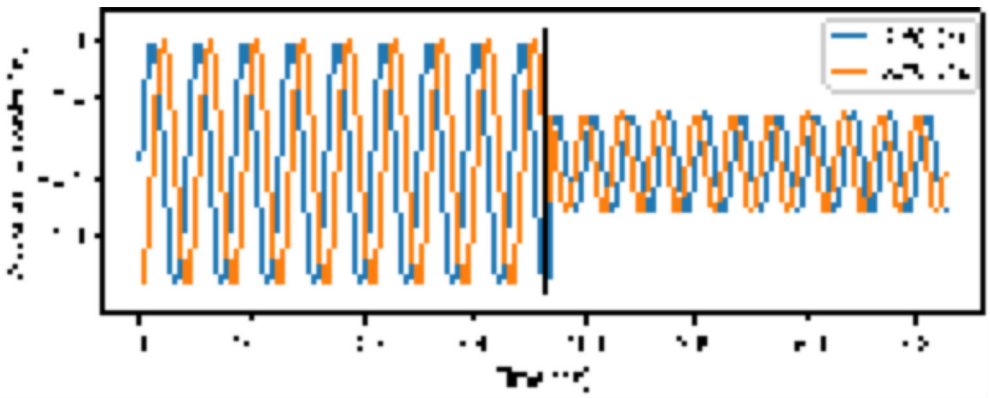

Exchange coupling of two spins

$$H_1 = g\mu_B \boldsymbol{B_1} \cdot \boldsymbol{S_1} + g\mu_B \boldsymbol{B_2} \cdot \boldsymbol{S_2} + hJ\left(\boldsymbol{S_1} \cdot \boldsymbol{S_2} - \frac{1}{4}\right)$$

With Eigenstates: $|\downarrow\downarrow\rangle$, $|\downarrow\uparrow\rangle$, $|\uparrow\downarrow\rangle$, $|\uparrow\uparrow\rangle$

$$H = \begin{pmatrix} \overline{E}_z & 0 & 0 & 0 \\ 0 & \Delta E_z/2 - J/2 & J/2 & 0 \\ 0 & J/2 & -\Delta E_z/2 - J/2 & 0 \\ 0 & 0 & 0 & -\overline{E}_z \end{pmatrix} \begin{pmatrix} |\downarrow\downarrow\rangle \\ |\downarrow\uparrow\rangle \\ |\uparrow\downarrow\rangle \\ |\uparrow\uparrow\rangle \end{pmatrix}$$

$$J = \frac{t_0^2}{U - \varepsilon - \Delta E_z/2} + \frac{t_0^2}{U + \varepsilon - \Delta E_z/2}$$

t_0	Tunnel coupling between dots
ΔE_z	Zeeman energy difference in between both dots
U	Charging energy of one dot
ε	Energy detuning between both dots

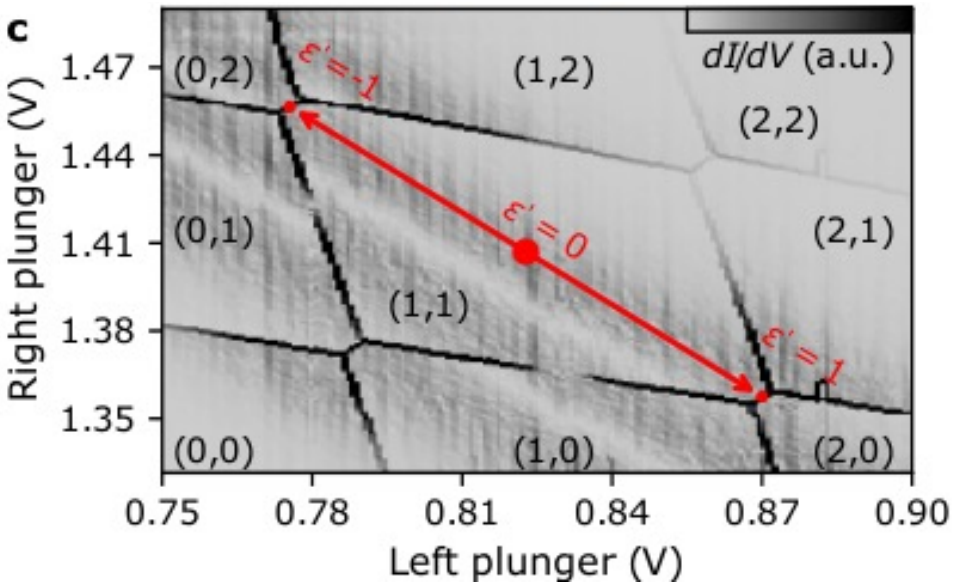

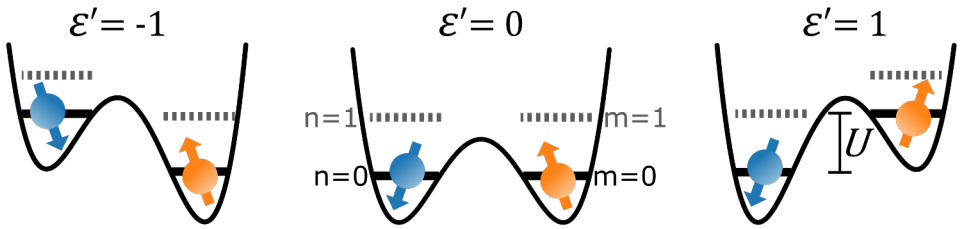

Exchange coupling of two spins

$$H_1 = g\mu_B \boldsymbol{B_1} \cdot \boldsymbol{S_1} + g\mu_B \boldsymbol{B_2} \cdot \boldsymbol{S_2} + h\,J\left(\boldsymbol{S_1} \cdot \boldsymbol{S_2} - \frac{1}{4}\right)$$

With Eigenstates: $|\downarrow\downarrow\rangle$, $|\downarrow\uparrow\rangle$, $|\uparrow\downarrow\rangle$, $|\uparrow\uparrow\rangle$

$$H = \begin{pmatrix} \overline{E}_z & 0 & 0 & 0 \\ 0 & \Delta E_z/2 - J/2 & J/2 & 0 \\ 0 & J/2 & -\Delta E_z/2 - J/2 & 0 \\ 0 & 0 & 0 & -\overline{E}_z \end{pmatrix} \begin{pmatrix} |\downarrow\downarrow\rangle \\ |\downarrow\uparrow\rangle \\ |\uparrow\downarrow\rangle \\ |\uparrow\uparrow\rangle \end{pmatrix}$$

$$J = \frac{t_0^2}{U - \varepsilon - \Delta E_z/2} + \frac{t_0^2}{U + \varepsilon - \Delta E_z/2}$$

t_0	Tunnel coupling between dots
ΔE_z	Zeeman energy difference in between both dots
U	Charging energy of one dot
ε	Energy detuning between both dots

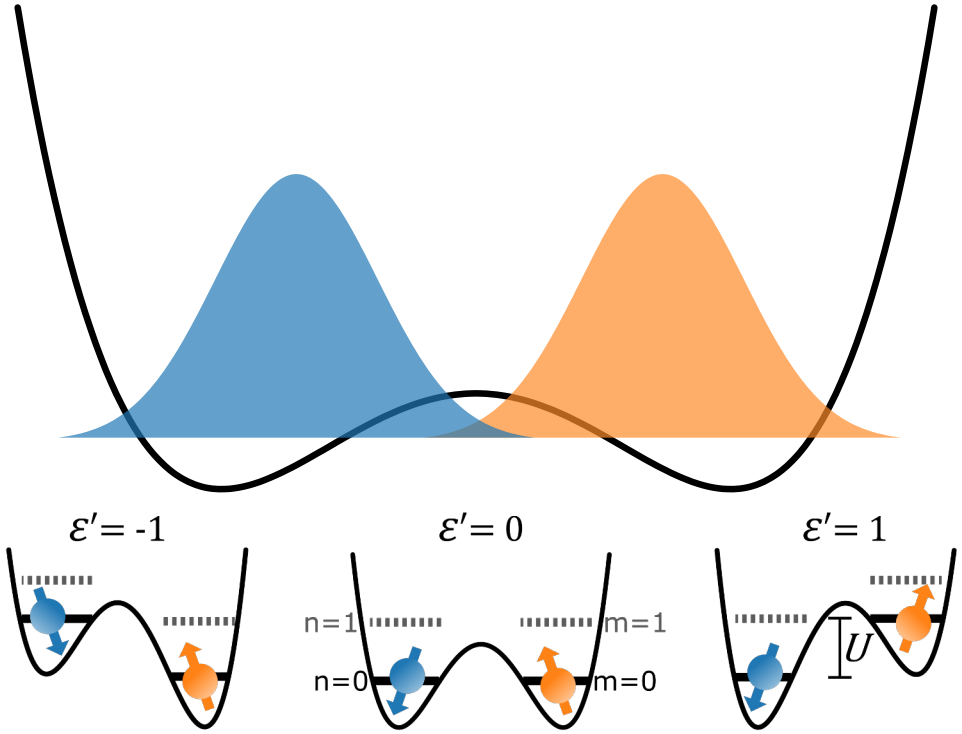

Two Qubit gates

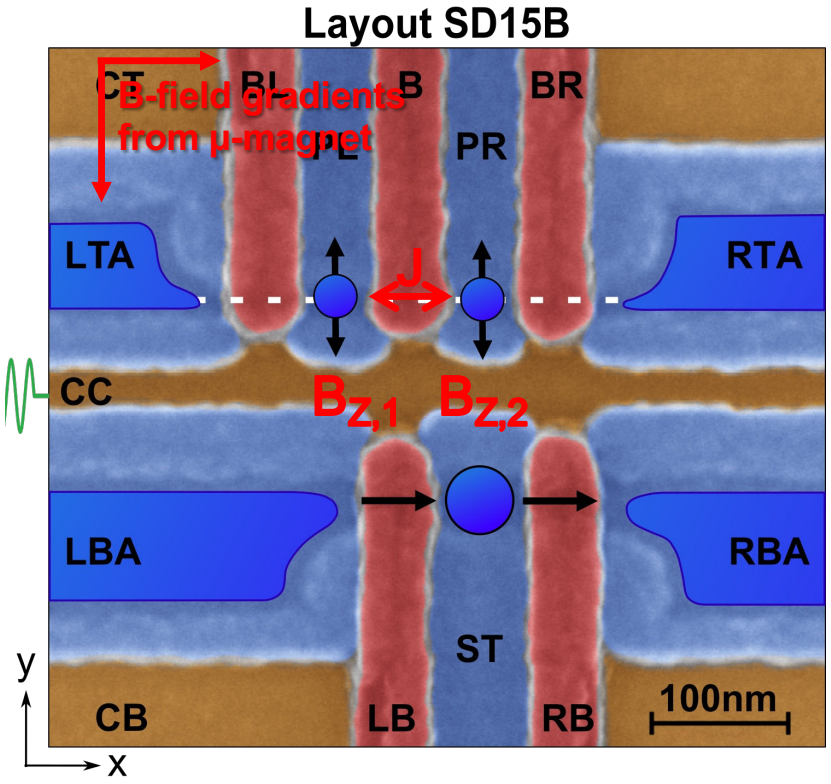

$$H = g\mu_B \mathbf{B}_1 \cdot \mathbf{S}_1 \qquad H = g\mu_B \mathbf{B}_2 \cdot \mathbf{S}_2$$

With Eigenstates: $|\downarrow\rangle_1, |\uparrow\rangle_1, |\downarrow\rangle_2, |\uparrow\rangle_2$

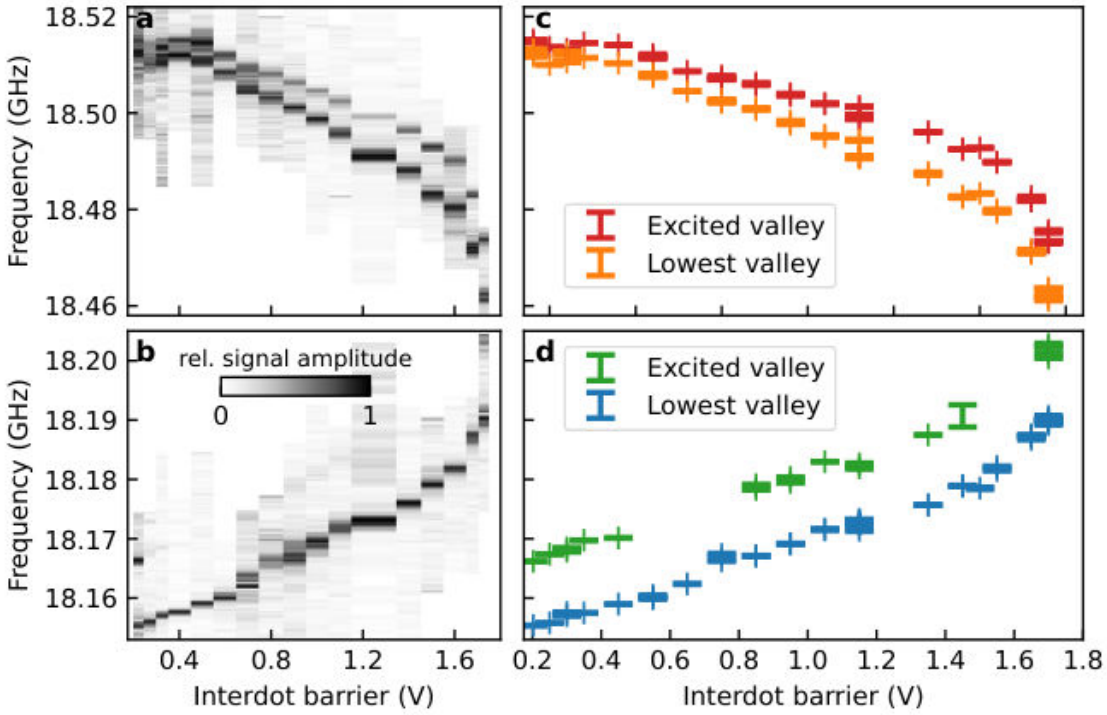

Exchange splitting

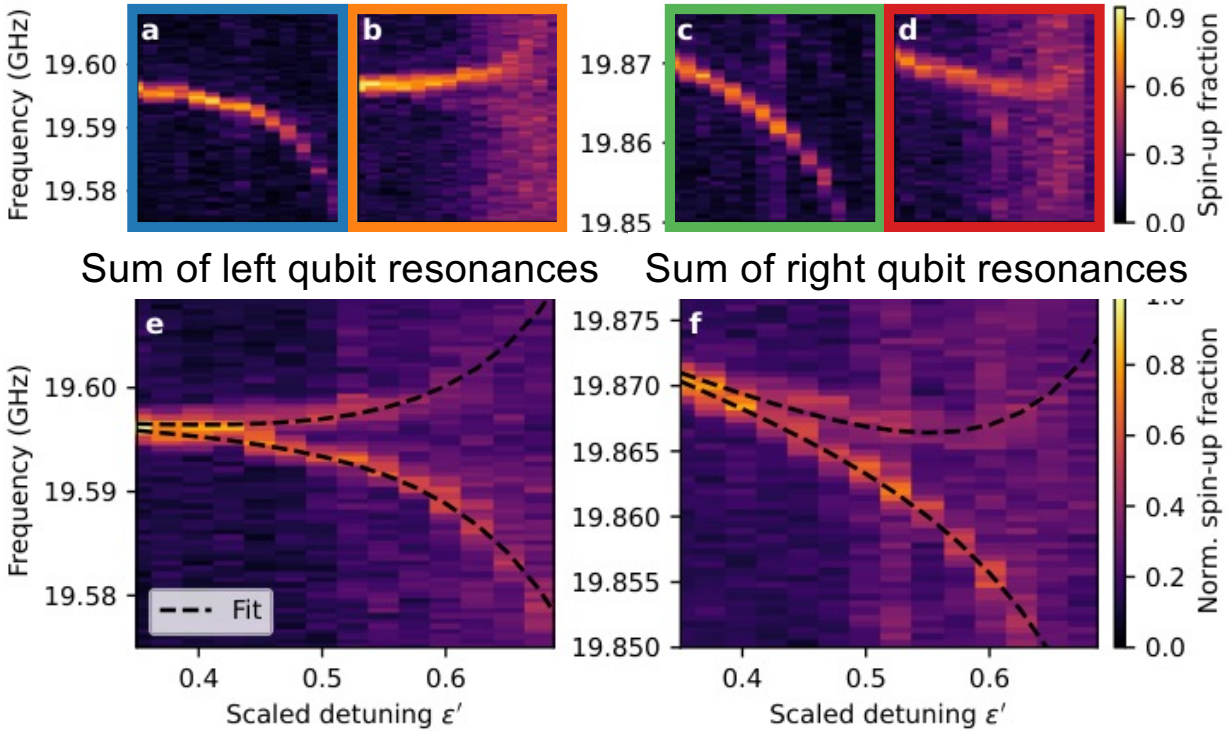

Single fit function for all curves:

$$f_{\mathrm{res}}(\varepsilon_{\mathrm{u}}) = f_0 + \alpha_{\mathrm{S}}\varepsilon_{\mathrm{u}} \pm \frac{J_0}{2}\exp\left(-\frac{\varepsilon_{\mathrm{u}}}{\varepsilon_0}\right)$$

Parameter	Fitted Value	Unit
$f_{0,\mathrm{L}}$	19.592 ± 0.000	GHz
$f_{0,\mathrm{R}}$	19.846 ± 0.000	GHz
$\alpha_{\mathrm{S,L}}$	-1.034 ± 0.138	MHz/meV
$\alpha_{\mathrm{S,R}}$	-5.672 ± 0.138	MHz/meV
J_0	1.083 ± 0.176	GHz
ε_0	0.576 ± 0.020	meV

Exchange coupling J

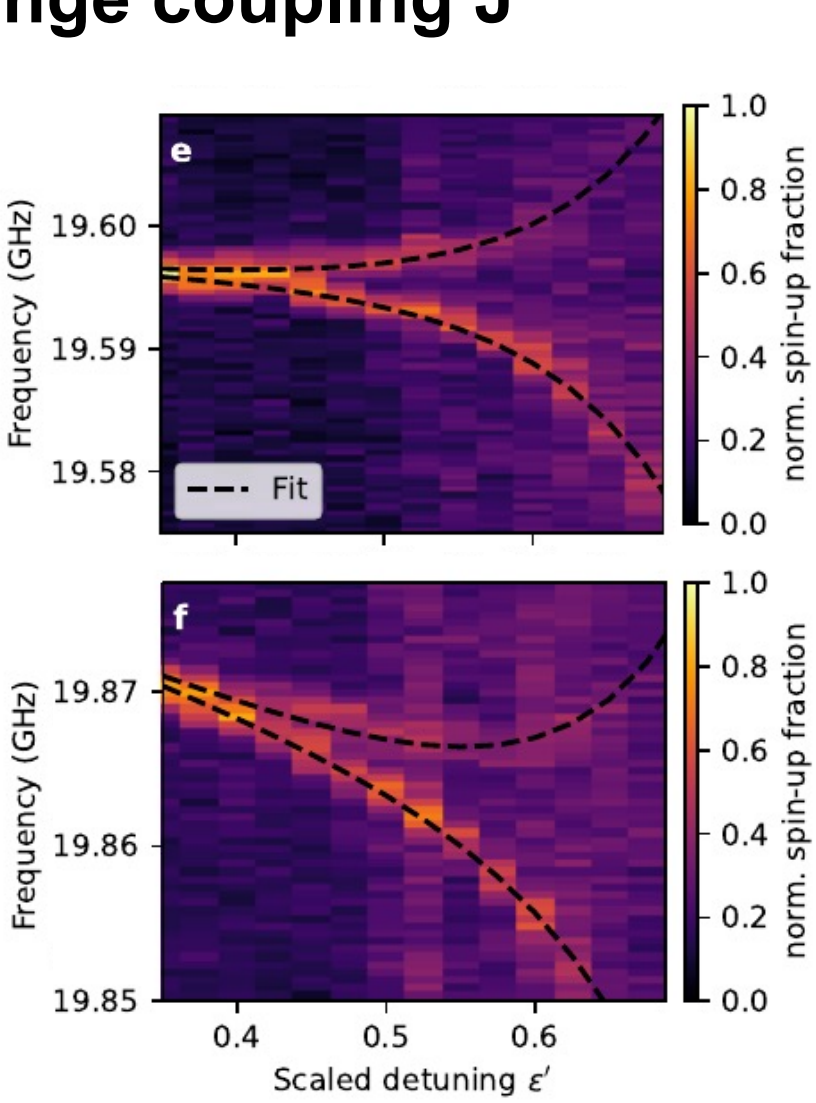

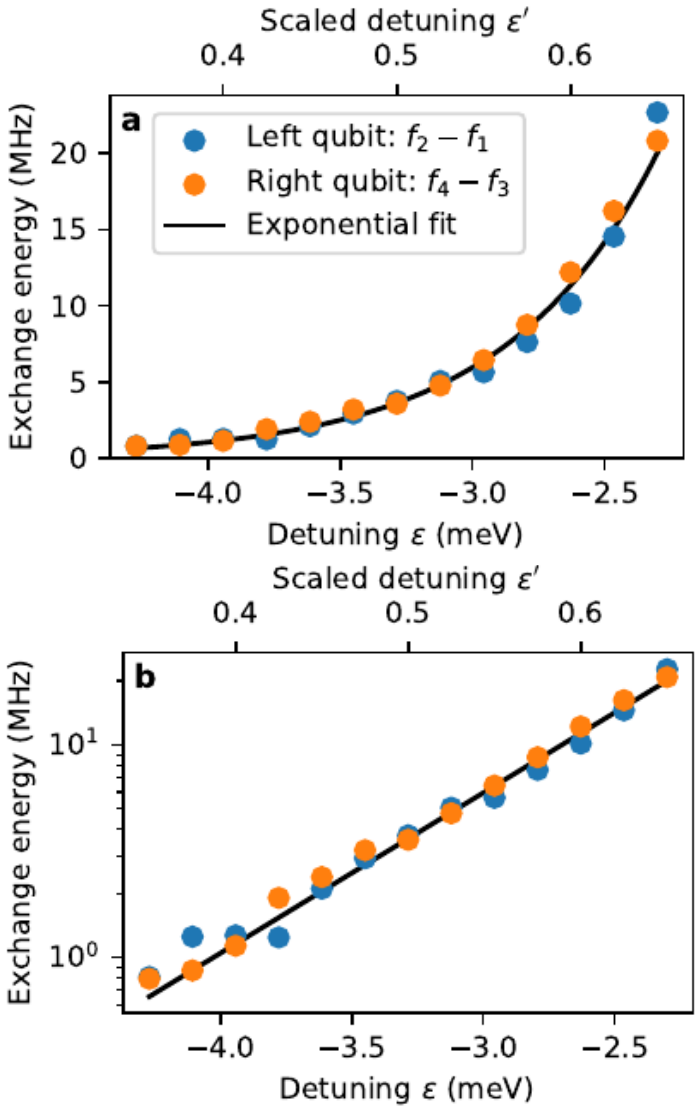

Lin scale

Log scale

Two Qubit gates

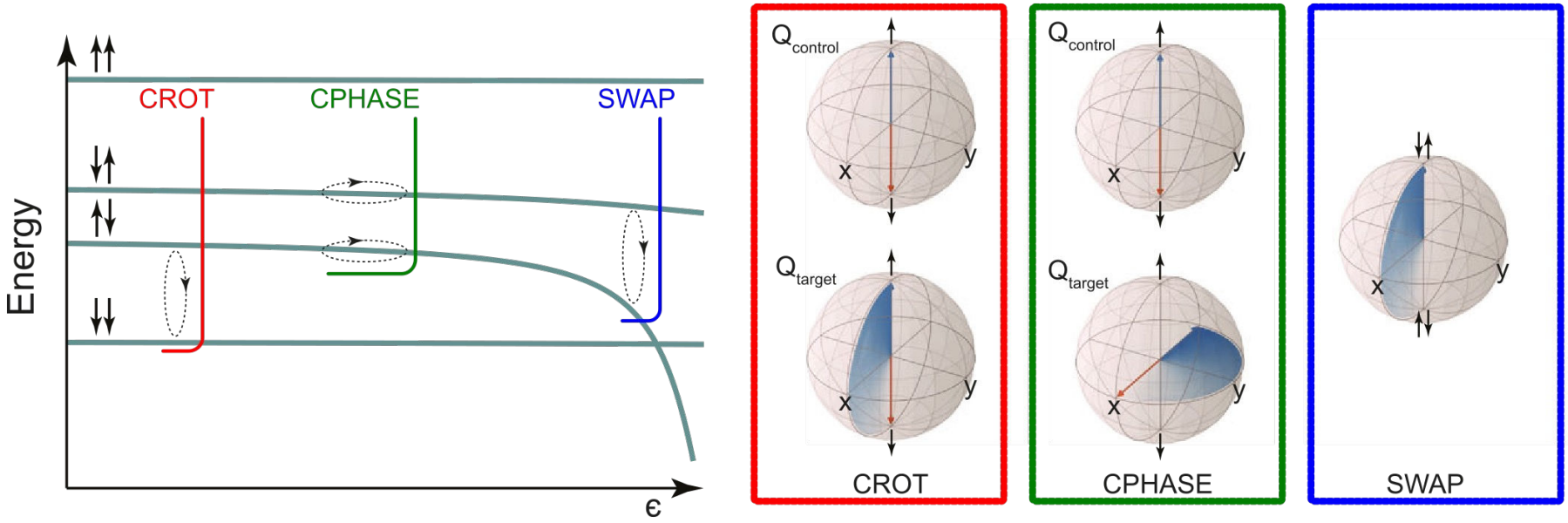

Xue, X. et al. (2022). *Quantum logic with spin qubits crossing the surface code threshold.*

Conditional rotations (CROT)

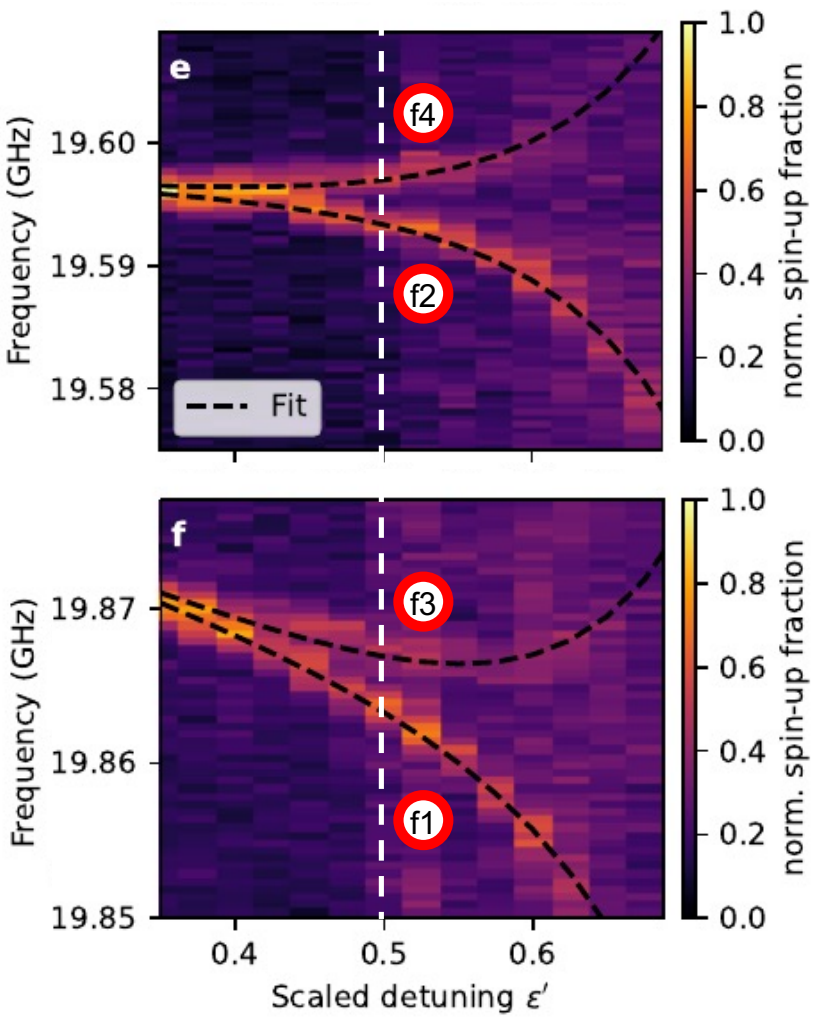

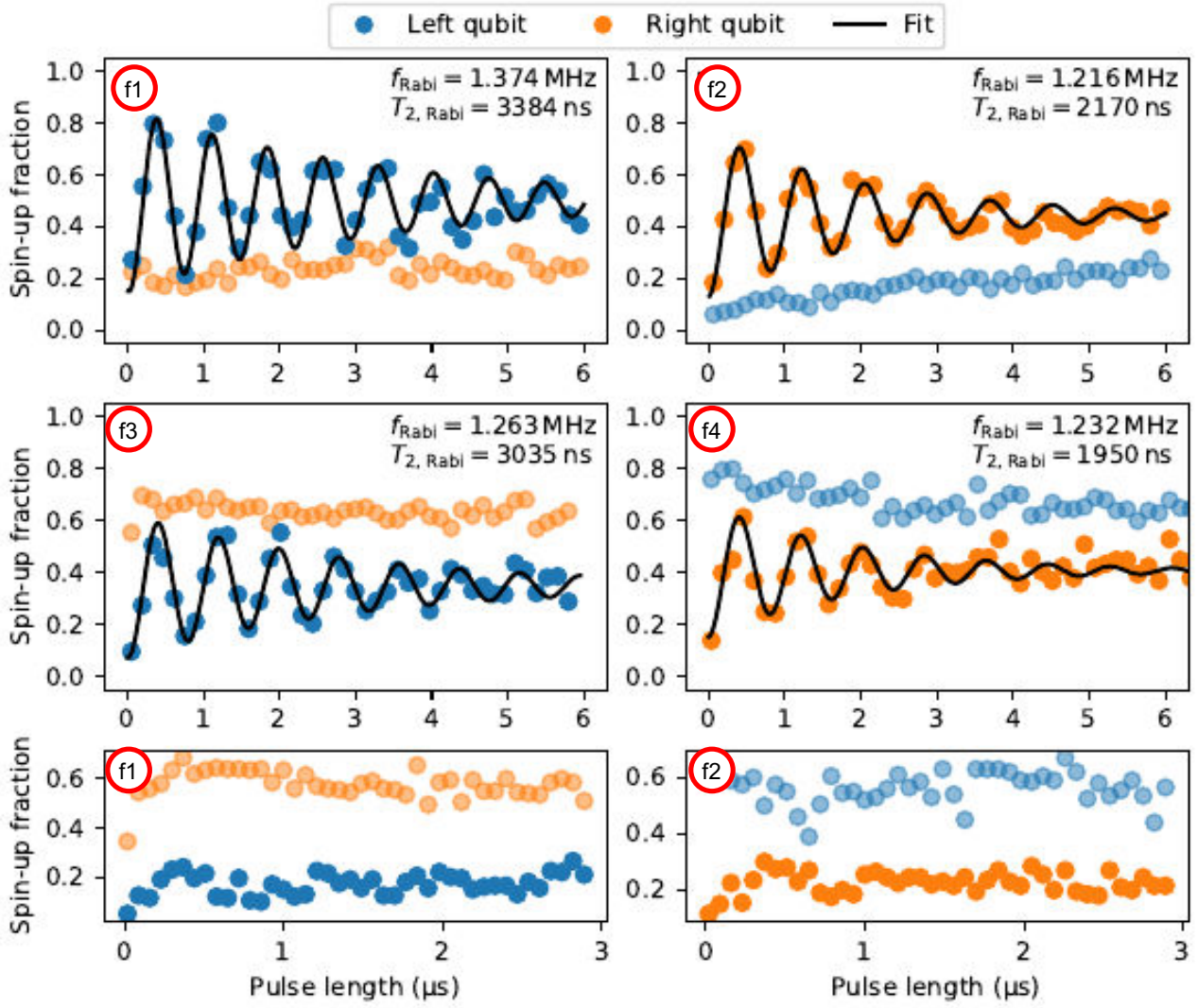

Viktor Adam, AG Wernsdorfer

Usable as non–demolishing readout!

CROT with dynamical condition

Rabi drive of first f3 and then f1 with different pulse durations before readout

Measurement Sequence:

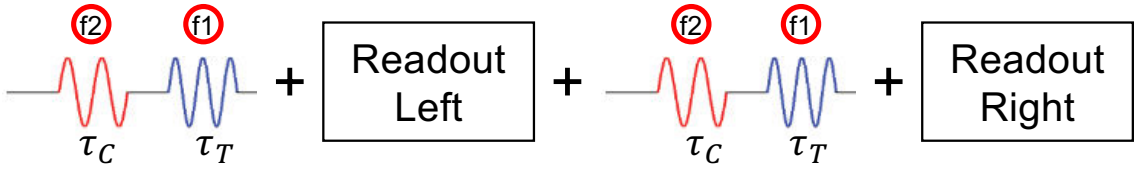

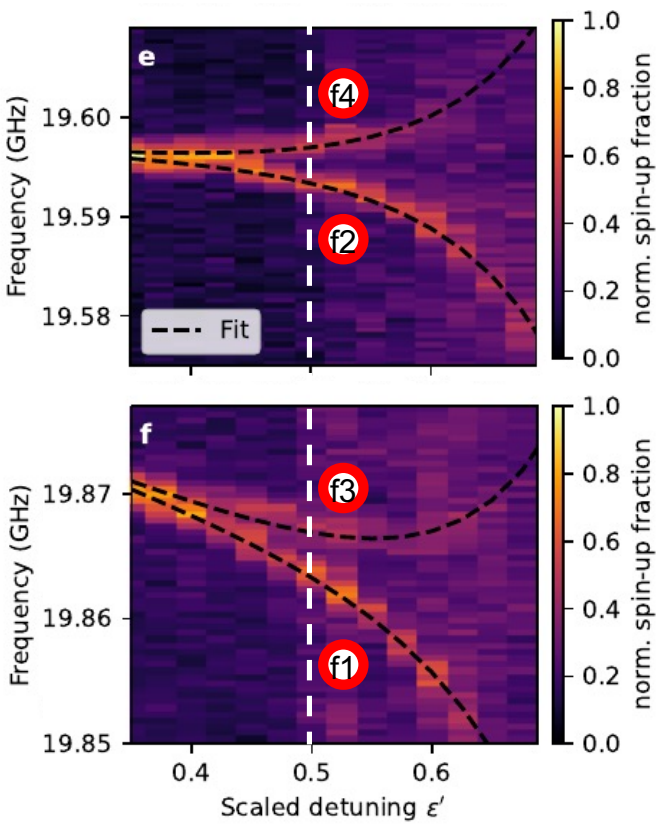

Zero detuning:
$\varepsilon' = 0$

Finite detuning:
$\varepsilon' = 0.5$

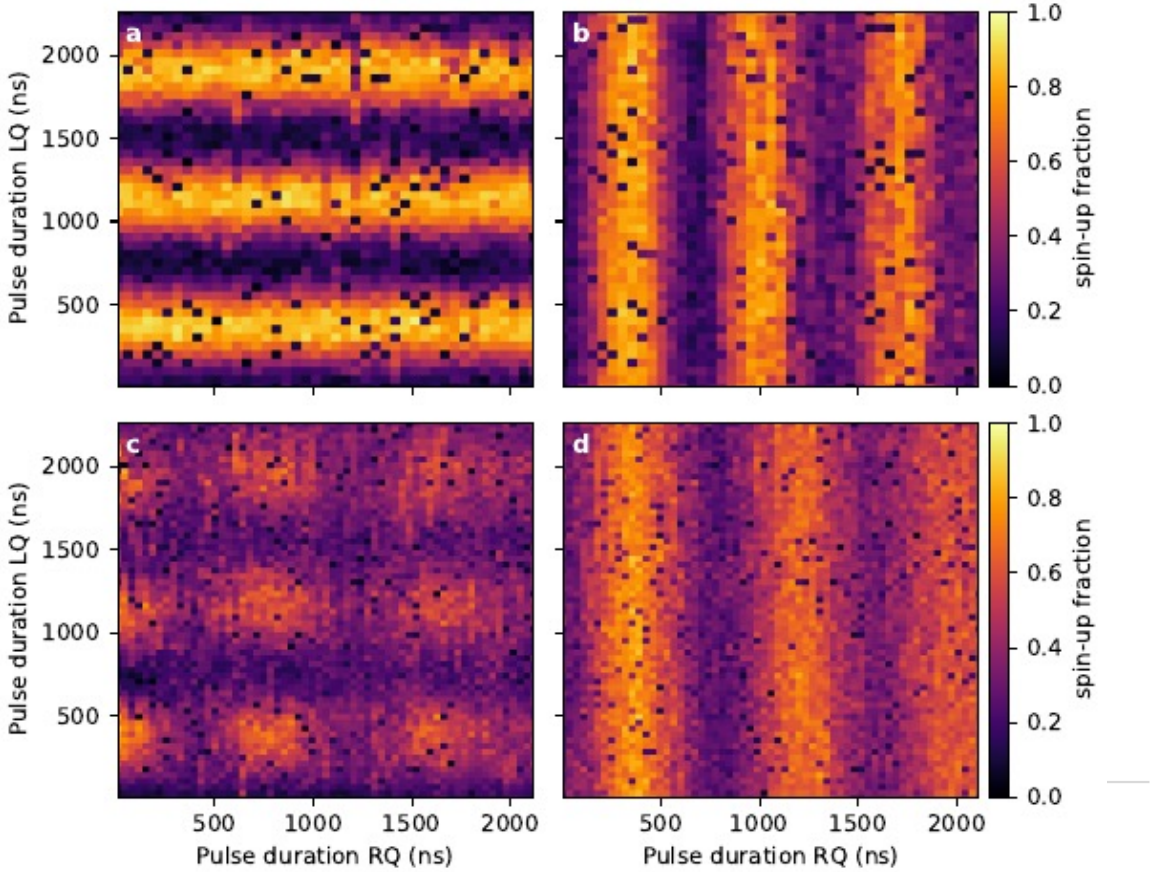

Another CROT with dynamical condition

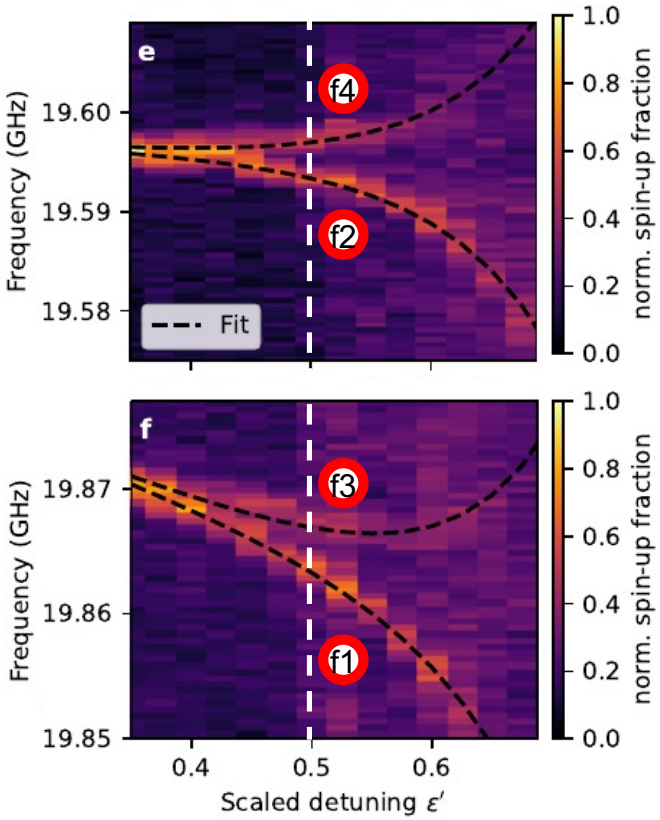

Rabi drive of first f1 and then pi-pulse target before readout

Measurement Sequence: